DEVELOPMENT OF A METHODOLOGY FOR SIZING AND ASSESSMENT OF WIND INTEGRATED ADVANCED ADIABATIC COMPRESSED AIR ENERGY STORAGE SYSTEM (AA-CAES)

A THESIS SUBMITTED TO
THE GRADUATE SCHOOL OF NATURAL AND APPLIED SCIENCES
OF
MIDDLE EAST TECHNICAL UNIVERSITY

BY

KORAY TAŞTANKAYA

IN PARTIAL FULLFILLMENT OF THE REQUIREMENTS
FOR
THE DEGREE OF MASTER OF SCIENCE
IN
MECHANICAL ENGINEERING

JANUARY 2014

Approval of the thesis:

DEVELOPMENT OF A METHODOLOGY FOR SIZING AND ASSESSMENT OF WIND INTEGRATED ADVANCED ADIABATIC COMPRESSED AIR ENERGY STORAGE SYSTEM (AA-CAES)

submitted by **KORAY TAŞTANKAYA** in partial fulfillment of the requirements for the degree of **Master of Science in Mechanical Engineering Department, Middle East Technical University** by,

Prof. Dr. Canan Özgen
Dean, Graduate School of **Natural and Applied Sciences** _____

Prof. Dr. Süha Oral
Head of Department, **Mechanical Engineering** _____

Assoc. Prof. Dr. İlker Tarı
Supervisor, **Mechanical Engineering Dept., METU** _____

Assoc. Prof. Dr. Derek K. Baker
Co-Supervisor, **Mechanical Engineering Dept., METU NCC** _____

Examining Committee Members:

Assist. Prof. Dr. Ahmet Yozgatlıgil
Mechanical Engineering Dept., METU _____

Assoc. Prof. Dr. İlker Tarı
Mechanical Engineering Dept.,METU _____

Assoc. Prof. Dr. Derek K. Baker
Mechanical Engineering Dept., METU NCC _____

Assoc. Prof. Dr. Oğuz Uzol
Aerospace Engineering Dept., METU _____

Assist. Prof. Dr. Metin Yavuz
Mechanical Engineering Dept., METU _____

Date: 31/01/2014

I hereby declare that all information in this document has been obtained and presented in accordance with academic rules and ethical conduct. I also declare that, as required by these rules and conduct, I have fully cited and referenced all material and results that are not original to this work.

Name, Last name: Koray Taştankaya

Signature:

ABSTRACT

DEVELOPMENT OF A METHODOLOGY FOR SIZING AND ASSESSMENT OF WIND INTEGRATED ADVANCED ADIABATIC COMPRESSED AIR ENERGY STORAGE SYSTEM (AA-CAES)

Taştankaya, Koray

M. Sc., Department of Mechanical Engineering

Supervisor: Assoc. Prof. Dr. İlker Tarı

Co-Supervisor: Assoc. Prof. Dr. Derek K. Baker

January 2014, 105 pages

Renewable energy usage has become widespread and gained world-wide importance lately. In order to get high quality power from renewable energy sources to the grid, bulk energy storage system will be required as a buffer, due to the intermittent nature of renewable energy. Advanced adiabatic compressed air energy storage (AA-CAES) technology is uniquely different from conventional energy storage techniques for renewable energy in that it captures and stores the heat generated during the compression cycle and releases this heat in the expansion cycle. In this thesis, a new method is developed for sizing and assessment of adiabatic compressed air energy storage system (AA-CAES) as a buffer for wind energy production taking into consideration the indeterminacy of the wind resource and variations in electrical demand. In this methodology, a specific place in which the wind farms and very large air storage cavern are located is selected for the system construction. For that specific place, the hourly electricity production for the wind farm is calculated according to wind speed taken from TMY2 data by using power output graph for

specific wind turbines. Additionally, hourly power consumption of the selected place is taken according to energy consumption data of the selected place. These generation and consumption values are compared and hourly energy storage and energy production algorithms are developed. For this method, components used during the energy production and storage process such as compressor, turbine and thermal energy storage tank are separately examined and modeled in MATLAB software platform. According to the energy production and storage algorithms, sizing of packed bed thermal energy storage tank and air storage cavern are studied by using a simplified packed bed thermal energy storage method, and this method is verified with experimental data in the open literature. In addition, several parametric studies related to the sizing and properties of the system components are performed and the effect of these to the system performance is evaluated. Finally, the total system efficiency is calculated and compared with existing AA-CAES concepts. To demonstrate this method, the power generations of DARES Datça wind farm according to TMY2 data and power consumption of Datça peninsula, which is calculated indirectly from total Aegean Region power consumption data, values are used as input values.

Keywords: Renewable energy storage, compressed air energy storage, advanced adiabatic compressed air energy storage, thermal energy storage

ÖZ

BASINÇLI HAVA İLE RÜZGÂR ENTEGRELİ GELİŞMİŞ ADİYABATİK ENERJİ DEPOLAMA SİSTEMİNİN BOYUTLANDIRMA VE DEĞERLENDİRME METODUNUN GELİŞTİRİLMESİ

Taştankaya, Koray
Yüksek Lisans, Makine Mühendisliği Bölümü
Tez Yöneticisi: Doç. Dr. İlker Tarı
Ortak Tez Yöneticisi: Doç. Dr. Derek K. Baker

Ocak 2014, 105 sayfa

Yenilenebilir enerji kaynakları kullanımı günden güne bütün dünyada hızlı bir şekilde önem kazanıp yaygınlaşmaktadır. Yenilenebilir enerji kaynaklarından yüksek kaliteli enerji elde etmek için kaynakların kesintili yapısını önleyecek, tampon görevi görecek büyük hacimli enerji depolama sistemi konulması gerekmektedir. Basınçlı hava ile gelişmiş adiyabatik enerji depolama sistemi diğer geleneksel yenilenebilir enerji depolama tekniklerinden farklı olarak sıkıştırma döngüsünde üretilen ısıyı tutarak depo eder ve genleşme döngüsünde geri verir. Bu tezde basitleştirilmiş dolgulu yatak ısı enerjisi depolama yöntemi ile oluşturulmuş basınçlı hava ile gelişmiş adiyabatik enerji depolama sisteminin parçalarının boyutlandırma ve değerlendirme metodu rüzgar enerjisi için geliştirilmiştir. Bu metoda rüzgâr santrallerinin ve büyük mağaraların bulunduğu sistem kurulumu için belirli bir bölge seçilmiştir. Bölgeye ait TMY2 verilerinden elde edilen rüzgar hızları kullanarak bölgede bulunan rüzgar türbinlerinin ürettiği elektrik saatlik bazda hesaplanmıştır. Ayrıca seçilen bölgeye ait elektrik tüketim verileri de alınarak ve elektrik üretim

verileri ile karşılaştırılarak enerji depolama ve enerji üretme algoritmaları geliştirilmiştir. Bu sistemde kullanılan kompresör, türbin ve ısı depolama tankı gibi birimler MATLAB yazılım ortamında modellenmiştir. Bu algoritmalara göre termal enerji depolama tankının ve hava depolama mağarasının boyutlandırılmasına basitleştirilmiş dolgulu yatak ısı enerjisi depolama sistemi metodu kullanılarak çalışılmıştır. Dolgulu yatak ısı enerjisi depolama yöntemi literatürde bulunan bir deney düzeneği ile doğrulanmıştır. Ek olarak, boyutlandırma ve sistem parçalarının özellikleri ile ilgili çeşitli parametrik çalışmalar incelenmiş ve bunların sistem performansına olan etkileri değerlendirilmiştir. Son olarak toplam sistem verimliliği hesaplanmış ve literatürde bulunan diğer sistem konseptleri ile karşılaştırılmıştır. Çalışmanın uygulamasının gösterimi için TMY2 datasını kullanılarak DARES Datça rüzgar santralinin elektrik üretim verileri ve Ege bölgesinin toplam enerji tüketiminden yola çıkılarak hesaplanan Datça enerji tüketimi girdi olarak kullanılmıştır.

Anahtar Kelimeler: Yenilenebilir enerji depolama, sıkıştırılmış hava ile enerji depoloma, basınçlı hava ile gelişmiş adiyabatik enerji depolama, ısı enerjisi depolama

To My Family…

ACKNOWLEDGEMENTS

First of all, I want to express my sincere appreciation to Dr. İlker Tarı, Dr. Derek Baker and Dr. Oğuz Uzol for their supervision and helpful critics throughout the progress of my thesis study.

I would like to thank Dr. Merih Aydınalp Köksal for her valuable contribution to my thesis.

I would like to express my special thanks to my colleague Furkan Lüleci, I would not have been able to accomplish this task without his invaluable contributions. I also would like to thank my big boss Mustafa Karasan, my chief İsmail Güler for their support, patience and friendship.

I also want to thank my friends Selçuk Öksüz, Çağrı Balıkcı and Ahmet Enes Taş for valuable comments about my study.

I would to declare my graces about dearest friends. I am grateful to and members of "Pikniçliker"' for their encouragement and support during my thesis. They have always shown great care for completing my studies.

And finally, I would like to thank my parents, sister, and Başak for their endless love, patience and support.

TABLE OF CONTENTS

ABSTRACT ..... **V**

ÖZ ..... **VII**

ACKNOWLEDGEMENTS ..... **X**

TABLE OF CONTENTS ..... **XI**

LIST OF FIGURES ..... **XIV**

LIST OF TABLES ..... **XVIII**

LIST OF ABBREVIATIONS ..... **XIX**

CHAPTERS

1 INTRODUCTION **1**

1.1 Background 1

1.2 Energy Storage 5

1.2.1 Pumped Hydro Energy Storage 5

1.2.2 Thermal Energy Storage (TES) 6

1.2.3 Compressed Air Energy Storage (CAES) 8

1.3 Survey of Studies Regarding AA-CAES 11

1.4 Motivation of the Study 12

1.5 Objective of the Study 14

1.6 The Organization of the Study 15

2 THEORY FOR AA-CAES MODEL **17**

2.1 Introduction 17

2.2 Compression Stage 18

2.3 Thermal Energy Storage Stage 20

2.3.1 Model of Simplified Packed Bed Thermal Energy Storage System 21

2.3.2 Verification of Simplified Packed Bed Thermal Energy Storage System 26

2.3.2.1 Experimental Set-up 26

2.3.2.2 Packed Bed TES Tank, Storage Filler Material and HTF Properties 27
2.3.2.3 Test Procedures 28
2.3.2.4 Experimental Results 29
2.3.2.5 Packed Bed Thermal Energy Storage Simplified Model Results 31
2.3.2.6 Comparison of Simplified Model Results and Experimental Results 33
2.3.3 Pressure Drop In the Packed Bed Thermal Energy Storage System 35
2.4 Air Storage Stage 36
2.5 Expansion Stage 37
2.6 Conclusion 39

3 METHODOLOGY FOR SIZING AND ASSESSING OF WIND INTEGRATED AA-CAES 41

3.1 Introduction 41
3.2 Site Selection 42
3.3 Wind Speed Information and Wind Turbine Power Calculation 44
3.3.1 Wind Speed Information 44
3.3.2 Wind Turbine Power Calculation 45
3.4 The Comparison of Energy Production and Energy Demand of a Selected Site 46
3.5 Determination of Size of Packed Bed Thermal Energy Storage Tank 47
3.6 Determination of the Minimum Volume of the Air Storage Cavern 53
3.7 Pressure Limits and Size of Air Storage Cavern 56
3.8 System Performance Metric 57
3.9 The Assessment of System Design Parameters 58
3.9.1 Effects of the Size of the Thermal Energy Storage Tank 58
3.9.2 Effects of the Volume of the Air Storage Cavern 58
3.9.3 Effects of the Air Turbine Operation Temperature on System Performance 59
3.9.4 Effects of the Air Mass Flow Rate that Goes To Turbine on System Performance 59
3.9.5 Effects of the Initial Fullness Ratio of Air Storage Cavern on System Performance 60
3.10 Conclusion 60

4 CASE STUDY: APPLICATION OF METHODOLOGY TO DATÇA PENINSULA 61

4.1 Site Selection for AA-CAES Model 61
4.2 Power Calculation of Wind Farm 62
4.2.1 Wind Speed Information of Datça 62
4.2.2 Power Production of DARES Wind Farm 63

4.3 Comparison of Energy Production of DARES Wind Farm and Datça Peninsula Energy Demand Data 65
4.4 Determination of the Size of the Packed Bed TES and Air Storage Cavern 68
4.4.1 Determination of the Size Estimation of the Packed Bed TES 68
4.4.2 Determination of Minimum Volume Estimation of the Air Storage Cavern for Datça 73
4.5 The Assessment of Pressure Limits and Size of the Air Storage Cavern 74
4.5.1 The Assessment of Minimum Capacity of Air Storage Cavern (min.cap) 75
4.5.2 The Assessment of Maximum Capacity of Air Storage Cavern (max.cap) 79
4.5.3 The Assessment of Lack of Storage (L.O.S) 82
4.6 The Assessment of System Design Parameters 84
4.6.1 Size of the Packed Bed Thermal Energy Storage System Effect 85
4.6.1.1 Changes in the Length of Packed Bed 85
4.6.1.2 Changes in the Radius of Packed Bed 86
4.6.2 Changes in the Air Mass Flow Rate of the Turbine 87
4.6.3 Change in the Volume of Air Storage Cavern 89
4.6.4 Changes in Minimum Turbine Operating Temperature 90
4.6.5 Changes in the Initial Fullness of Air Storage Cavern 91

5 SUMMARY AND CONCLUSIONS 93

5.1 Summary of the Study 93
5.2 Conclusions 94
5.3 Future Works 96

REFERENCES 97

APPENDICES

A METHODOLOGY FOR SIZING TES TANK FLOW CHART 101

B METHODOLOGY FOR SIZING MINIMUM VOLUME OF THE AIR STORAGE CAVERN FLOW CHART 103

C METHODOLOGY FOR ASSESSING AA-CAES SYSTEM FLOW CHART 105

LIST OF FIGURES

FIGURES

Figure 1.1 World power generation source [2] 1

Figure 1.2 Growth of fuel inputs to power [2] 3

Figure 1.3 Primary energy consumption in Turkey 2009 [5] 3

Figure 1.4 Share of power generation from renewable energy [2] 4

Figure 1.5 Pumped hydro energy storage system [9] 6

Figure 1.6 Thermal energy storage types [10] 7

Figure 1.7 Compressed air energy storage system [12] 8

Figure 1.8 Isothermal CAES system [14] 10

Figure 1.9 Scheme of AA-CAES system [15] 11

Figure 2.1 AA-CAES system schematic diagram [24] (M/G = Motor/Generator) 17

Figure 2.2 Packed bed thermal energy storage system [27] 22

Figure 2.3 Schematic of experimental setup [29] 26

Figure 2.4 The experimental results for heat charging period [29] 29

Figure 2.5 The experimental results for heat discharging period [29] 30

Figure 2.6 Simplified model results for heat charging 31

Figure 2.7 Simplified model results for heat discharging 32

Figure 2.8 Comparison of experimental results and model results for heat charging process 33

Figure 2.9 Comparison of experimental results and model results heat discharging process 35

Figure 3.1 Density of cavern distribution in Turkey [36] 43
Figure 3.2 Enercon E-82 wind turbine power curve [37] 46
Figure 3.3 Wind integrated AA-CAES working principle..... 47
Figure 3.4 Temperature distribution for R=1m..... 49
Figure 3.5 Temperature distribution for R=2m..... 50
Figure 3.6 Temperature distribution for R=3m..... 51
Figure 3.7 Temperature distribution for R=4m..... 51
Figure 3.8 Temperature distribution for R=5m..... 52
Figure 3.9 Temperature distribution of the packed bed for 10 kg/s air mass flow rate 54
Figure 3.10 Temperature distribution of the packed bed for 20 kg/s air mass flow rate 54
Figure 3.11 Temperature distribution of the packed bed for 25 kg/s air mass flow rate 55
Figure 4.1 DARES Datça wind farm [38]..... 61
Figure 4.2 Hourly wind speed for Datça for a year..... 62
Figure 4.3 The hourly wind speed and corrected wind speed for January for Datça. 63
Figure 4.4 Enercon E-48 power vs. wind speed curve (f_{E-48}) [37] 64
Figure 4.5 Enercon E-44 power vs. wind speed curve (f_{E-44}) [37] 64
Figure 4.6 Hourly total power production for DARES Datça wind farm for January65
Figure 4.7 Hourly power consumption data for Datça Peninsula for January 66
Figure 4.8 Hourly power difference for Datça Peninsula for January 67
Figure 4.9 Pressure drop of air across the packed bed TES tank for different length and radius pairs 69
Figure 4.10 Volume of the TES tank for given length and radius pairs 70

Figure 4.11 Convective heat transfer coefficient for different length and radius pairs 71

Figure 4.12 HSNSD for calculation length and radius pairs of TES tank 72

Figure 4.13 The capability of power production of AA-CAES system according to given length and radius pairs in a year 73

Figure 4.14 The number of hours AA-CAES turbine cannot operate for 5 kg/s 76

Figure 4.15 Pressure variation of the air storage cavern ($5x10^4$ m^3) for 5 kg/s..... 77

Figure 4.16 Pressure variation of the air storage cavern (10^5 m^3) for 5 kg/s..... 78

Figure 4.17 The number of hours AA-CAES turbine cannot operate due to minimum capacity of the cavern in different mass flow rate 78

Figure 4.18 The number of hours cavern pressure is at max. for 20 kg/s 80

Figure 4.19 Max.cap vs. the volume of air storage cavern 81

Figure 4.20 Pressure change of the air storage cavern for a year for 10^5 m^3 volume 81

Figure 4.21 Pressure change of the air storage cavern for $3x10^5$ m^3 volume for a year 82

Figure 4.22 Effects of size of TES on air storage 83

Figure 4.23 The number of hours that system cannot compress the air into the cavern vs. volume of the cavern 84

Figure 4.24 Hourly system not satisfy the demand vs. length of TES tank 86

Figure 4.25 Hourly system not satisfy the demand vs. radius of TES tank 87

Figure 4.26 Hourly system not satisfy the demand vs. turbine air mass flow rate 88

Figure 4.27 Average air temperatures vs. mass flow rate of air..... 88

Figure 4.28 Hourly system not satisfy demand and min.cap vs. air storage cavern volume..... 89

Figure 4.29 Hourly system not satisfy demand vs. minimum turbine operation temperature..... 91

Figure 4.30 Hourly system not satisfy demand vs. initial fullness ratio of the tank .. 92

Figure A.1 Sizing TES tank flow chart 101

Figure B.1 Sizing minimum volume of air storage cavern flow chart 103

Figure C.1 General assessing methodology for AA-CAES 105

LIST OF TABLES

TABLES

Table 1 Packed Bed Storage Filler Properties [29] 27

Table 2 Heat Transfer Fluid (Xceltherm 600) Properties @300 K [30] 27

Table 3 Packed Bed Tank Properties [29] 28

Table 4 Test Conditions for Heat Charging and Discharging Period [29] 29

Table 5 System Design Parameters 58

Table 6 Technical Specifications of E-48 and E-44 [37] 63

Table 7 Properties of Air, Pebbles and TES Tank at 800 K 68

Table 8 Length and Radius Pairs 69

Table 9 Constant System Parameters 75

Table 10 System Performance Results 95

LIST OF ABBREVIATIONS

AA-CAES	Advanced Adiabatic Compressed Air Energy Storage
CAES	Compressed Air Energy Storage
E.D	Energy Demand for Specific Place
E.P	Energy Production from Wind Farm
HSNSD	The Number of Hours System Cannot Satisfy Demand
L_{TES}	Length of the Packed Bed Thermal Energy Storage Tank
L.O.S	Lack of Storage
m	Mass of the Air
max.cap	Maximum Pressure Level of Air Storage Cavern
min.cap	Minimum Pressure Level of Air Storage Cavern
P_a	Air Pressure After Thermal Energy Storage Tank
P_c	Air Storage Cavern Pressure
$P_{c,max}$	Maximum Pressure of the Air Storage Cavern
$P_{c,min}$	Minimum Pressure of the Air Storage Cavern
R	Ideal Gas Constant
R_{TES}	Radius of the Packed Bed Thermal Energy Storage Tank
R_s	Sizing Ratio
T	Temperature of the Air
TC	Thermocouple

TES	Thermal Energy Storage
TMY2	Typical Meteorological Year Data Set
V_{cavern}	Volume of the Air Storage Cavern
V_{TES}	Volume of the Thermal Energy Storage Tank

CHAPTER 1

INTRODUCTION

1.1 Background

Global energy demand increases as the population and production rate increase, industrialization spreads, standard of living gets higher and people gain easier access to the energy sources. In this manner, in 2035 global energy demand is expected to increase one-third relative to its current state [1]. It is a well known fact that current global energy demand is met by fossil fuels all around the world. Although fossil fuel will be superseded by renewable energy and natural gas, fossil fuels still dominate energy resource market [1]. According to BP Energy Outlook 2030, coal is expected to be the main energy resource (39%) over the next decade [2]. As shown in Figure 1.1, fossil fuels including coal will be predicted to be used commonly to generate energy well into the future and this usage will bring several problems along.

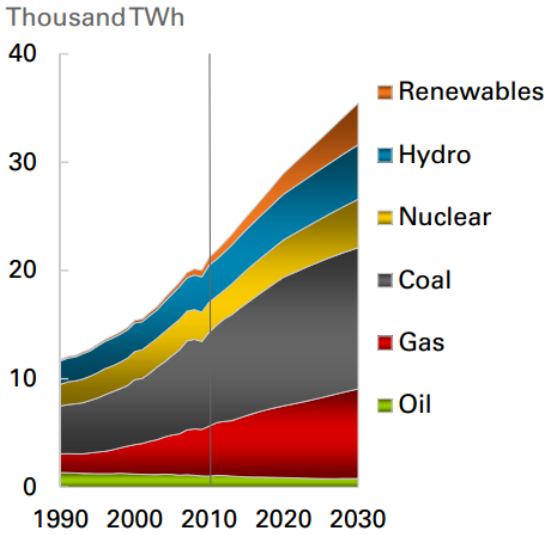

Figure 1.1 World power generation source [2]

One of the obvious problems of widespread usage of coal is that coal releases combustion products to the atmosphere and these cause global warming. According to Special Report on Emissions Scenarios (SRES) project, green house gases are predict to increase by a range of 25 to 90% between 2000 and 2030 [3]. In addition to this, it is predicted that the long term average global temperature will have an increase rate of 3.6 °C with reference to recent studies on the world climate map [1]. It becomes more and more difficult to prevent this increase of the average temperature around the world and energy not being used efficiently because of governmental policies and precautions not being taken to prevent carbon emission by countries. If the precautions to decrease the temperature rise to 2 ^{o}C are not taken immediately, sanctions may be required to limit the energy generation of the power plants that cause CO_2 emission [1]. The EU has set mandatory emission reduction targets for CO_2 sources such as cars, power plants. Additionally, Turkey has started to implement several projects to prevent or reduce CO_2 emissions. One of these projects is about a new technology whereby CO_2 emitted by coal power plants is captured and stored in underground geological environments which was conducted by TÜBİTAK in 2009 [4] . The aim of this project was to determine whether there are suitable foundations underground to store CO_2 in Turkey, to analyze their structure and quantify their potentials. Although such projects can potentially decrease the amount of CO_2 emissions in the world, the economic aspects of these projects, the potential for unintended CO_2 emission and it's a threat to the environment are barriers to this technology. Therefore, it becomes a need for the primary energy source used in the generating stations to be carbon free. This leads to the concept of widespread usage of resources such as wind, water and sun to generate energy. Though renewable energy sources did not make any significant contributions to the power generation in the world prior to 2010, over the next two decades, it is predicted to become an important power source [2].

In Figure 1.2, it can be seen that coal and natural gas contribute 65% of total electricity production in 2010. However this rate is predicted to significantly

decrease to 25% in the next two decades as a result of increases in renewable energy production all around the world [2].

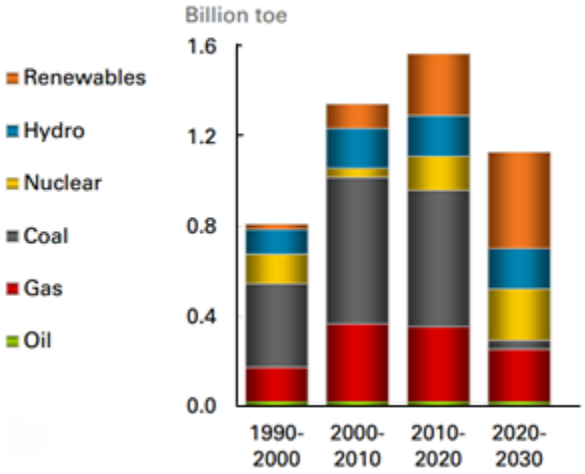

Figure 1.2 Growth of fuel inputs to power [2]

If the usage of renewable energy for energy production is evaluated with regard to Turkey, the results are not different from other developing countries. As can be seen from Figure 1.3, except hydro, renewable resources have been almost untouched recently in Turkey [5].

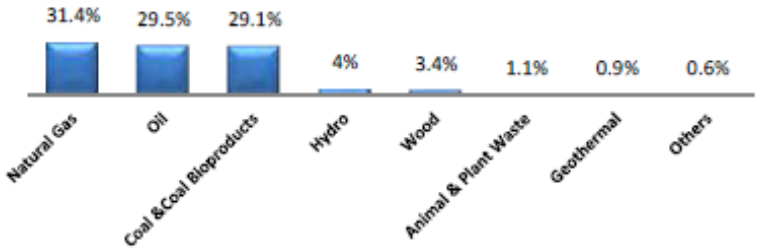

Figure 1.3 Primary energy consumption in Turkey 2009 [5]

However, Turkey has a great renewable energy potential compared to other developing countries. The estimation of The Republic of Turkey Ministry of Energy

and Natural Resources about the solar energy is that Turkey has an average annual total sunshine duration approximately 2640 hours and average total radiation per m^2 as 1311 kWh/year. Hence, solar energy potential is calculated as $3.8x10^8$ kWh/year. Additionally, the estimations about wind energy is that Turkey has a minimum wind energy potential of $5x10^3$ MW in regions with annual wind speed of 8.5 m/s and higher, and $4.8x10^4$ MW with wind speed higher than 7.0 m/s.

As shown in Figure 1.4, since countries throughout the world especially in European Union (EU) expect renewable energy sources to make significant contributions to their energy production plans for the next two decades, serious drawbacks coming from renewable energy sources immediately come to the forefront. Two of the main drawbacks of wind and solar energy, the two most common and widespread clean energy sources, are their inherent intermittency and unreliability. As a result of the related fluctuations, renewable energy power outputs may not match the power requirements of a specific region. They may exhibit large fluctuations in power output in diurnal, monthly or even annual cycles. Similarly, the demand can vary diurnally or annually [6]. This leads to an increase in power network stability problems because of supply demand energy imbalances [7]. This characteristic of a renewable energy puts a barrier to large scale penetration of renewable energy sources. Thus, this problem must be solved by the specific countries that are planning to get significant amounts of energy from renewable energy sources.

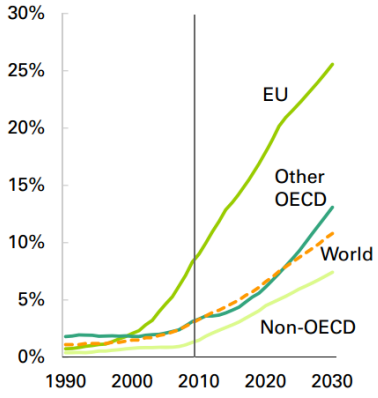

Figure 1.4 Share of power generation from renewable energy [2]

In order to stabilize the supply and demand fluctuations between renewable energy output and the grid, there should be a buffer power, that is, a technology that stores energy when excess is produced and then released when production levels do not meet the requirements [6]. The easiest and most acceptable way of making renewable energy reliable is through energy storage for later usage however currently large scale energy storage is often not feasible in terms of economy and settlement. Generally energy storage requires bulky and costly equipment.

1.2 Energy Storage

As the usage of renewable energy sources is getting more important and widespread day by day all around the world, providing high quality power from renewable energy sources to the grid is gaining importance in parallel [8]. To provide high quality energy to the grid, there should be an energy storage technology between the renewable energy source and the grid to compensate for the intermittent nature of renewable energy and demand. Generally energy storage concepts are divided into two subgroups which are large scale and small scale energy storage systems. Although the installation of a large scale energy storage system is difficult when compared to a small scale energy storage system, large scale energy storage systems have some significant advantages over small scale energy storage systems. They are capable of storing very large amounts of energy and, they have a long service life. Also they have low cost of maintenance, operation and the cheapest capital cost per kWh [9]. Three types of important large scale energy storage systems are pumped hydro, thermal, and compressed air energy storage. A brief overview of each of these energy storage technologies is presented in Sections 1.2.1-3.

1.2.1 Pumped Hydro Energy Storage

The pumped hydro energy storage system is one of the most common large scale energy storage systems and consists of two large water reservoirs located at two different elevations. It uses directly the power of water. The energy storage principle of pumped hydro systems is simple and well-known. When the demand is low, low

price electricity coming from the grid is used for pumping the water from the lower reservoir to upper reservoir. When demand is high, the water flows from the upper reservoir to the lower reservoir and runs the turbines to generate electricity [7].

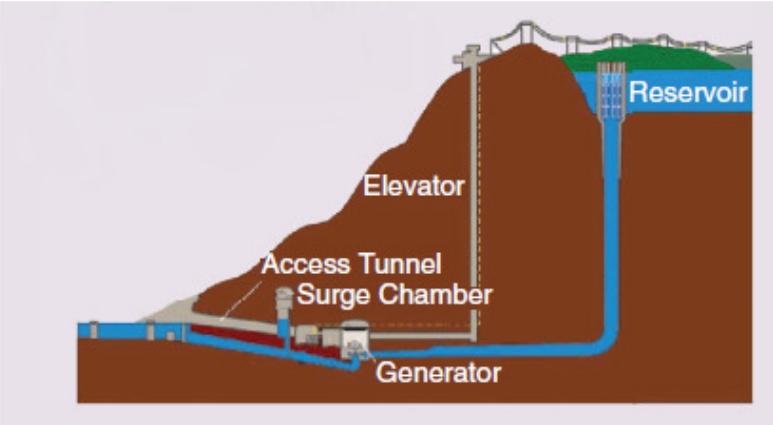

Figure 1.5 Pumped hydro energy storage system [9]

The pumped hydro energy storage system is the most efficient energy storage system among the large scale energy storage systems. The conversion efficiency is between approximately 65-80%. It can store large amounts of energy (over 2000 MWh) for a long period. In addition to that the operating cost per unit of energy is the cheapest among all large scale energy storage systems and it has relatively little harmful effect to the environment [6]. On the other hand, this system has its drawbacks too. The main drawback of the pumped hydro energy storage system is its dependency on geological formations. There should be two reservoirs at different elevations and its construction is difficult.

1.2.2 Thermal Energy Storage (TES)

Thermal energy storage is a storage system utilizing changes in internal energy of a material in the form of sensible heat, latent heat, and thermal chemical or combination of these [10]. Generally thermal energy storage systems exist as large scale energy storage systems, however there are a few types that exist as small scale energy storage systems. There are three methods used and still being investigated in

order to store thermal energy: 1) sensible heat storage (SHS); 2) latent heat storage (LHS); and, 3) thermal chemical thermal energy storage. An overview of thermal energy storage types is shown in Figure 1.6 [10].

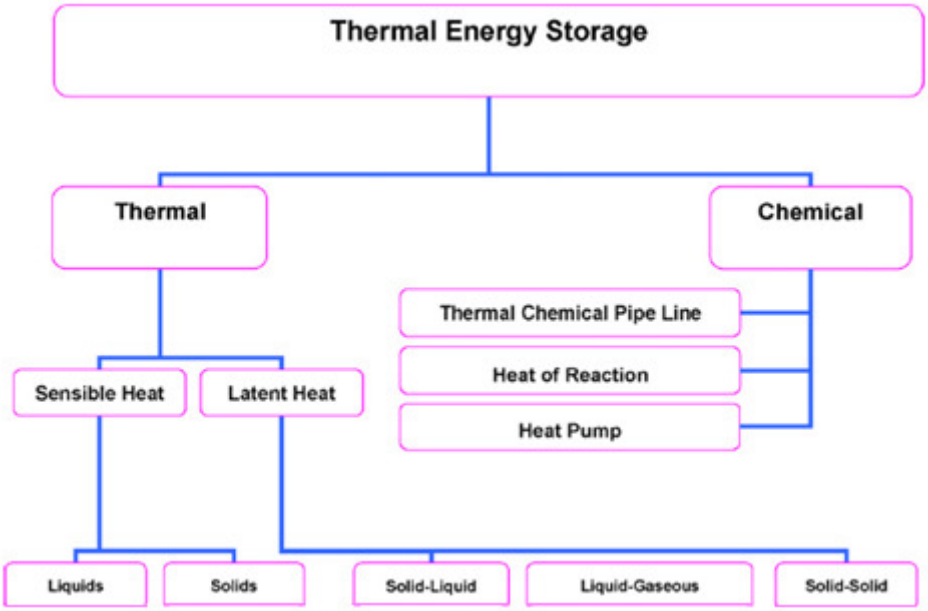

Figure 1.6 Thermal energy storage types [10]

In sensible heat thermal energy storage system, thermal energy produced in the steps of production electricity from renewable energy is stored by raising the temperature of a solid or liquid. The total amount of energy stored in the storage material is directly proportional with the amount of thermal storage material, the heat capacitance of the thermal storage material and temperature difference between medium and thermal energy storage material. This method has started to be used in concentrating solar power plants.

In latent heat thermal energy storage systems, the phase change takes place. The thermal energy storage material stores heat when change from solid to liquid or liquid to gas. To release the energy, they have the reverse phase change [11]. Due to their high heat energy storage for a small temperature change, this method is the most preferred among the thermal energy storage techniques.

Thermo chemical energy storage depends on the energy absorbed and released in breaking or reforming molecular bonds of the storage material in a completely reversible chemical reaction [10]. In this process the total amount of energy stored directly depends on the amount of energy storage material, endothermic heat of reaction and the extent of conversion [10]. This method is still under development. It is not used in any applications yet.

1.2.3 Compressed Air Energy Storage (CAES)

Compressed air energy storage (CAES) is one of the most important energy storage techniques and stores renewable energy by compressing air using power taken from a wind or solar energy integrated system. As shown in Figure 1.7, the system consists of a motor, compressor trains, combustion chamber, turbine trains, high pressure storage tanks and a generator.

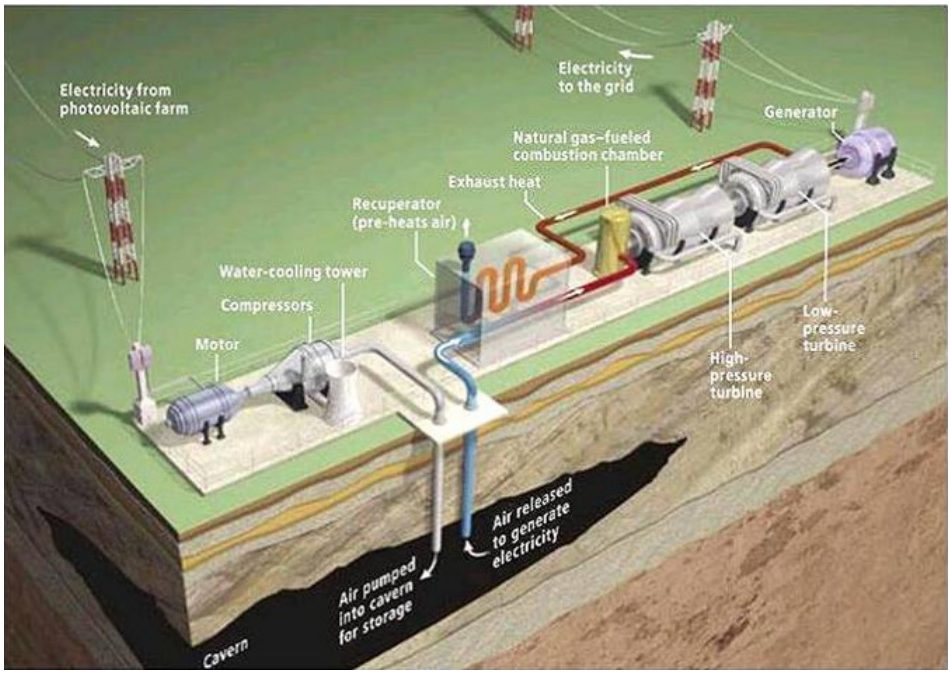

Figure 1.7 Compressed air energy storage system [12]

In order to increase its efficiency, some additional components such as a recuperator can be added to the system. The storage principle of CAES is basic. When low price electricity is available in the grid and grid demand is low, air is pressurized in the compressors using electricity from the grid and pumped into large storage tanks such as a cavern, aquifer or pressure vessel. When grid demand is high or at a peak, stored pressurized air leaves the storage tank, is heated in a combustion chamber, expanded in the expanders and drives a generator to produce electricity. Application of this storage technique is explored to store renewable energy especially for wind and solar energy. The idea is simple and applicable. When the renewable energy is available, electricity is produced from the energy and this electricity is used in compressors to compress the air for later energy production.

One of the major advantages of CAES is that it is a large scale energy storage method like pumped hydro energy storage, which is in operation with 50-300MW capacities [13]. Also CAES is a less geologically dependent energy storage system when compared to pumped hydro. The system only needs a large air storage volume such as a salt cavern or aquifers. As a result of this, installation costs tend to be lower. On the other hand, CAES has several drawbacks. The fossil fuel usage to heat up the air before entering the turbine is the main shortcoming of the system. Obviously, this causes environmental problems. In addition, the total system efficiency is not as high as for other large scale energy storage systems. The system efficiency is about 48%. The last but not least drawback is its geological structure reliance [6]. The size of the air storage volume directly affects the amount of storable energy. There are three general types of CAES.

- Conventional Compressed Air Energy Storage System (CAES);
- Advanced Isothermal Compressed Air Energy Storage System (I-CAES);
- Advanced Adiabatic Compressed Air Energy Storage System (AA-CAES);

In conventional CAES, stored air is heated in the combustion chamber before entering the turbine. During the combustion process, natural gas or a fossil fuel is used. Isothermal CAES is an alternative CAES system which eliminates the need for fuel and high temperature thermal energy storage. Isothermal CAES can minimize the compression work and maximize the expansion work done through isothermal compression/expansion by means of effective heat transfer with the vessel's surroundings, which involves slow gas pressure changes by liquid piston shown in Figure 1.8 [14]. In AA-CAES system, thermal energy storage (TES) system replaces the combustion chamber as shown in Figure 1.9. The waste heat releasing from the compression trains is stored in TES and used to heat the air before entering the turbine.

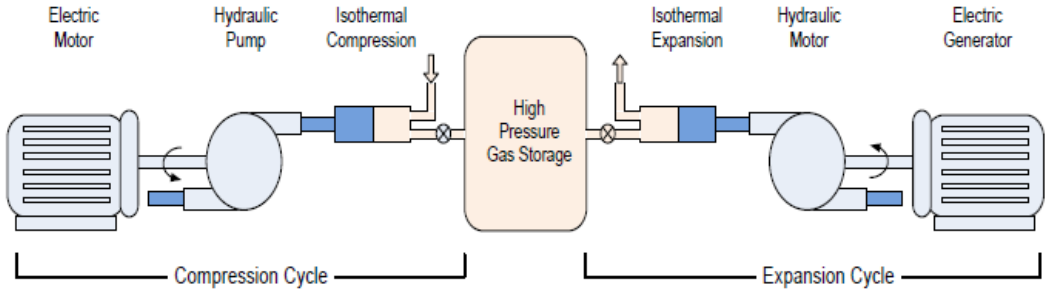

Figure 1.8 Isothermal CAES system [14]

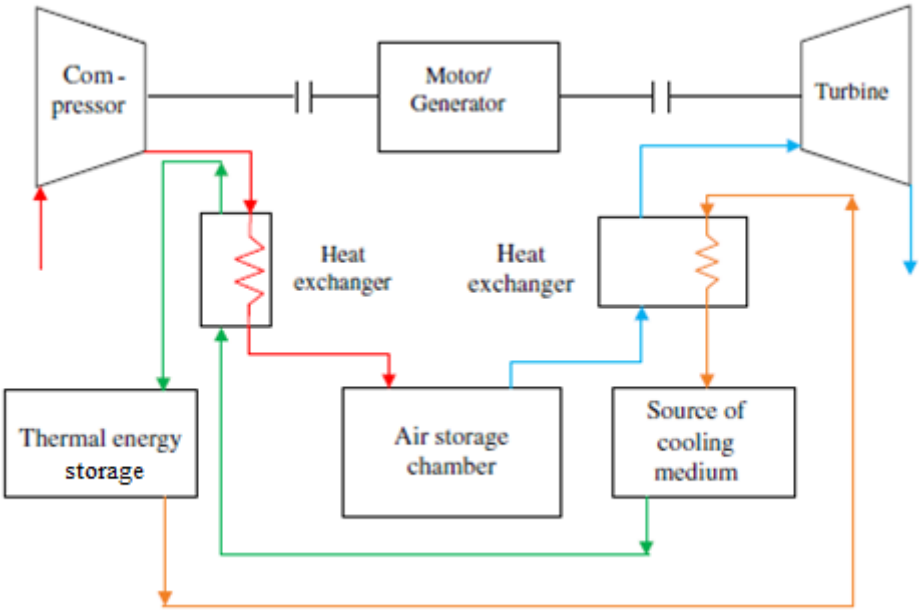

Figure 1.9 Scheme of AA-CAES system [15]

1.3 Survey of Studies Regarding AA-CAES

As a result of carbonless energy storage power plant concepts becoming more important recently, several studies have been conducted on carbon free energy storage power plants in general and specifically on AA-CAES. Zunft et al. evaluated the feasibility and performance of a AA-CAES system, and highlighted the key technological problems for this system. In their study, Zunft et al. stated that the TES system is the most critical element impacting the system efficiency, however there is almost no example of a TES system with comparable operating conditions. Additionally, Zunft et al. present several TES techniques that may be implemented to the AA-CAES system [16]. In another study, the feasibility of AA-CAES system in terms of economic criteria was investigated by Bullough et al. In their study, Bullough et al. gave brief information about the economic and technical aspects of AA-CAES system. Also, some applicable technical solution to TES of the system are presented by Bullough et al. [17]. A study conducted by Zhang Yuan et al. investigated the thermodynamic model of a CAES system with TES to analyze the effect of TES on system efficiency. In this study the effects of temperature and

pressure on the utilization of heat in a TES coupled with heat exchangers is evaluated [15].

In a study conducted by Beeman, an advanced adiabatic compressed air energy storage system is evaluated considering the psychometric properties of air and the effects of humidity changes. In the study of Beeman, condensation due to humidity change is checked in each stage of an AA-CAES and application of this study to Michigan-Utah mine is evaluated [18]. In the thesis of Steta, an advanced adiabatic compressed air energy storage system is modeled for achieving optimal operation strategy for energy markets by using predictive control method. In the thesis of Steta, mathematical model for each AA-CAES components such as compressor and turbine trains are introduced. Additionally, a solid concrete system with two embedded heat exchanger coils is presented for TES in this study [9]. In another study, Kim et al. presented the energy and exergy flow of AA-CAES in a single stage configuration for the production of 1 kWh energy [19]. In the study of Milazzo and Grazzini, the thermodynamic analysis of system parameters and their influence are investigated [20]. Although the study of Riaz is not directly interested in AA-CAES, the content of the thesis is within the scope of the present study. In the research of Riaz, the behavior of wind integrated CAES system is investigated on a monthly and daily basis. The power mismatch between supply and demand is explored and a CAES is shown to be a possible a solution to compensate for the energy gap in the study of Riaz [21].

1.4 Motivation of the Study

Intermittent renewable energy sources such as wind presently only supply a fraction of our primary energy needs due in part to their inherent intermittency. In order to allow large amounts of renewable energy as a primary energy source to the grid, there should be some improvements in the methodology used to design and assess energy storage systems. Additionally, improvements in this design and assessment

methodology enable renewable energy to become more widespread in terms of the usage and lowers capital cost.

CAES is one of the important large scale energy storage systems. It has several benefits when compared to other types of large scale energy storage systems. The dependency of geological structure is at the moderate level in CAES. Ease in installation and a capacity to store large amounts of energy are the two of the most important reasons why this method is selected as an energy storage system. Additionally, as a large scale energy storage technology, CAES can be an enabling technology to allow significant penetration of intermittent renewable energy sources such as wind and solar into the grid. On the other hand, CAES has also some drawbacks. Conventional CAES's use hydrocarbon fuels such as natural gas in the combustion process, and therefore contribute to climate change and if fossil fuels are used resource depletion. Also, the efficiency for conventional CAES's is not as high as other large scale energy storage techniques. Advanced adiabatic compressed air energy storage systems (AA-CAES) have the potential to both eliminate the use of hydrocarbon fuels and have higher efficiencies. AA-CAES eliminates the combustion chamber of the compressed air energy storage system and instead uses thermal energy storage to preheat the air entering turbine. This method stores the heat energy released during the compression process and then uses this heat before the turbine stage. As a result, a carbon-free compressed air energy storage system is created. The ever increasing demand for energy technologies that are clean, carbon free and reliable has created a need to study advanced adiabatic compressed air (AA-CAES) systems. Researches about TES of the AA-CAES are still investigated especially German Aerospace Center (DLR) whose target is to build first AA-CAES with RWE Power AG in Germany in 2016 [22] [23].

Although thermal energy storage brings several important advantages for AA-CAES, there are not any well defined, proven and ready to use any type of thermal energy storage systems for AA-CAES that was found in the open literature. This causes a problem when sizing and assessing the AA-CAES systems in reality. In addition to

that, there aren't any studies of AA-CAES systems coupled with wind energy found in open literature. Although wind integrated CAES system is not a new concept for the open literature, the integration of wind energy and AA-CAES system will be a new type of energy storage system for the next generation.

1.5 Objective of the Study

The main objective of the present work is to fill a gap in the literature by providing a methodology for sizing and assessing wind integrated AA-CAES for use in large scale energy storage applications. Sub-objectives considered fulfilling or supporting the main objective are listed as follows:

- Presenting an implementation of a packed bed thermal energy storage model to an AA-CAES system.
- Verification of the packed bed thermal energy storage model by using existing example in the open literature.
- Propose a methodology for sizing and assessing for wind integrated AA-CAES in order to utilize wind energy effectively.
- Integration of wind energy production and grid demand as an input to AA-CAES system to study system behavior.
- Parametric analyses of quantifying how changing air storage cavern and thermal energy storage size impacts the number of hours per year an AA-CAES system meets or does not meet the electricity demand.
- Parametric studies exploring how changing the properties of the key system parameters affects AA-CAES system behavior.

1.6 The Organization of the Study

In this study, a methodology for sizing and assessing wind integrated advanced adiabatic compressed air energy storage system is developed. This work consists of 5 different chapters.

In Chapter 2, the theory of this work will be explained. The compression part of the AA-CAES model is introduced and governing equations are given. The packed bed thermal energy storage is introduced and governing equations are presented for simplified model. The simplified packed bed TES method is verified. The model for air storage part is given. The chapter concludes by presenting the model of the expansion stage of AA-CAES.

In Chapter 3, the main aspects of the sizing and assessing methodology are given. Energy source and energy demand integration to the mathematical model of the system are presented. In addition, system performance metrics and evaluation of these metrics are given.

In Chapter 4, application of the methodology for sizing and assessing a wind integrated AA-CAES system to Datça Peninsula in Turkey is presented. By using hourly weather data of Datça, the output of DARES wind farm is predicted. Comparison of power supply and scaled grid demand for Datça is given. The sizing and assessing of thermal energy storage tank and air storage cavern for AA-CAES system are also represented. At the end of this chapter, how changes in the properties of system components affect the performance of AA-CAES system is presented.

Finally, a brief summary of the thesis is given, conclusions are drawn, and possible future works of the study are represented in Chapter 5 Summary and Conclusion.

CHAPTER 2

THEORY FOR AA-CAES MODEL

2.1 Introduction

In this study, AA-CAES system with packed bed TES model is developed. The model consists of a single compressor, single turbine, a TES tank and an air storage cavern as shown in Figure 2.1. In this chapter each system component is introduced and the assumptions and governing equations corresponding to each component are stated in the subsections of this chapter.

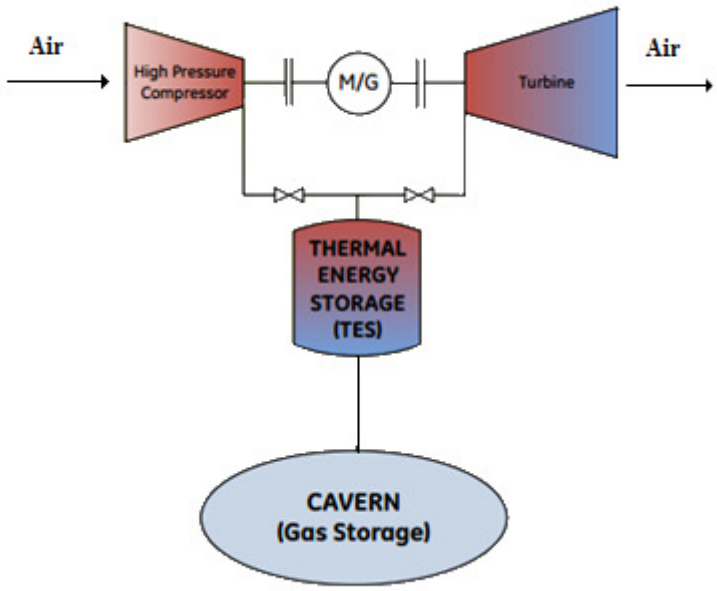

Figure 2.1 AA-CAES system schematic diagram [24] (M/G = Motor/Generator)

As shown in Figure 2.1, during charging hot air coming from the high pressure compressor goes to the thermal energy storage tank in order to dissipate its energy. If the temperature of the air is still high after the TES stage, there should be an after cooler to further cool the air to store more air in the air storage cavern reservoir. During discharging, the cold air coming from the air storage cavern reservoir goes to thermal energy storage tank to be preheated before entering the turbine. In this model, ambient air is used as the working fluid to transfer heat with TES tank

2.2 Compression Stage

In existing conventional CAES plants industrial compressors are used due to their modularity and flexible structure [16]. However, such industrial compressor trains are generally intercooled, and they are not suitable for high temperature operations. In addition to that they operate generally at lower pressures [16]. In order to create AA-CAES plant, a new high pressure and temperature design is required, based on high temperature turbines.

In this study, a new generation compressor which has a high pressure and temperature design is assumed. For the sake of the simplicity, the compression stage is formed by a single compressor that can resist high temperatures up to 600^{o}C [24] and high pressure fluctuations. In the compression stage atmospheric air is taken as an input fluid. As stated previously, the compression ratio of the compressor can take very large values in this model. Additionally, the initial start-up time for the compressor is assumed to be zero. The power consumption of the compressor is calculated as the difference between isentropic outlet and inlet enthalpy of the fluid multiplied by the fluid mass flow rate as given in equation (2.2.1).

$$W_c = \frac{1}{\eta_c}\ \dot{m}\ (h_o - h_i) \tag{2.2.1}$$

In equation (2.2.1), η_c term is the isentropic efficiency of the compressor. It is assumed that this isentropic efficiency does not change during the compression

process. If equation (2.2.1) is extended assuming ideal gas behavior, the power consumption of the compressor is found as:

$$W = \frac{1}{\eta_c} \dot{m}\ C_{p,ave}\ (T_o - T_i) \tag{2.2.2}$$

In equation (2.2.2), $C_{p,ave}$ is the average value of Cp for T_o and T_i which are the isentropic outlet and inlet temperatures of air respectively. The relation between inlet and isentropic outlet temperatures of air can be found by combining ideal gas law and polytropic and adiabatic compression equations. A polytropic and adiabatic compression assumption is made in this model so there is a relation between pressure and volume of the fluid which is:

$$P\ V^n = \text{Constant} \tag{2.2.3}$$

Here n is the polytropic and adiabatic index of the compression so it follows that

$$P_i\ V_i^n = P_o\ V_o^n \tag{2.2.4}$$

If equation (2.2.4) is arranged,

$$\frac{P_o}{P_i} = \left(\frac{V_i}{V_o}\right)^n = \beta \tag{2.2.5}$$

Equation (2.2.5) is obtained. In this equation β is the compression ratio term of the compressors.

In parallel, the ideal gas law can be applied to the air

$$P\,V = m\,R\,T \tag{2.2.6}$$

where R is the ideal gas constant (286.7 J/kg.K), P is the pressure of the gas, V is the volume occupied by the gas, m is the mass of the gas and T is its temperature [9].

Equation (2.2.6) can be formed as

$$V = \frac{m\,R\,T}{P} \tag{2.2.7}$$

By combining equation (2.2.5) and equation (2.2.7), equation (2.2.8) is obtained.

$$\left(\frac{V_i}{V_o}\right)^n = \left(\frac{T_i}{T_o}\right)^n \left(\frac{P_o}{P_i}\right)^n \Rightarrow \left(\frac{V_i}{V_o}\right)^n = \left(\frac{T_i}{T_o}\right)^n \beta^n \tag{2.2.8}$$

By using the term $\left(\frac{V_i}{V_o}\right)^n = \beta$ from equation (2.2.5) and putting into the equation (2.2.8), inlet and isentropic outlet temperature relation is obtained as shown in the equation (2.2.9).

$$T_o = T_i\,\beta^{\frac{n-1}{n}} \tag{2.2.9}$$

As a result of this, power consumption of each compressor can be calculated by arranging equation (2.2.2).

$$P_c = \frac{1}{\eta_c}\,\dot{m}\,C_{p,ave} T_i \left(\beta^{\frac{n-1}{n}} - 1\right) \tag{2.2.10}$$

In AA-CAES, the power input to the compressor is known and equal to excess electricity while the mass flow rate is unknown. The mass flow rate through the compressor can be obtained by rearranging equation (2.2.10).

$$\dot{m} = \frac{P_c\ \eta_c}{C_{p,ave}\ T_i \left(\beta^{\frac{n-1}{n}} - 1\right)} \tag{2.2.11}$$

2.3 Thermal Energy Storage Stage

In this section, thermal energy storage part of the AA-CAES system is explained. In the AA-CAES system modeled herein, a packed bed TES is used to store the heat released during the compression stage and to give back this energy at the expansion

stage. The transient heat transfer analysis between the pressurized air and the packed bed TES material is modeled in MATLAB.

2.3.1 Model of Simplified Packed Bed Thermal Energy Storage System

In this section, simplified packed bed TES model, which is used in AA-CAES model, is introduced.

In the packed bed TES, the rate of heat transfer from fluid to solid in packed bed is a function of the physical properties of the fluid and solid, the local temperature of the fluid and surface of the solid, the mass flow rate of the fluid and characteristics of the packed bed. The characteristics of the packed bed depend on the shape and orientation of the packing material and porosity [25].

It is pointed out that the use of packed beds as thermal energy storage devices has certain advantages since the response of such a unit is relatively fast due to a large surface to volume ratio. On the other hand, the pressure drop across the packed bed is the main disadvantage of the system [25]. In this study, a simplified model of a packed bed TES with pebbles is used for the analytical solution of the thermal energy storage stage. The simplified model is developed for the transient response of the packed bed by Schumann neglecting intraparticle conduction and fluid dispersion. In Schumann solution the basic differential equations are presented for the case of a constant inlet fluid temperature [25]. The following assumptions [25], [26] are made to simplify the solution.

- Constant thermal and physical properties are used.
- There is a uniform convective heat transfer coefficient.
- There is no transverse heat transfer in the bed and the container walls are perfectly insulated.
- The bed material has zero thermal conductivity in the direction of flow.
- The bed material has infinite thermal conductivity in the transverse direction.
- Radiation effects are neglected.

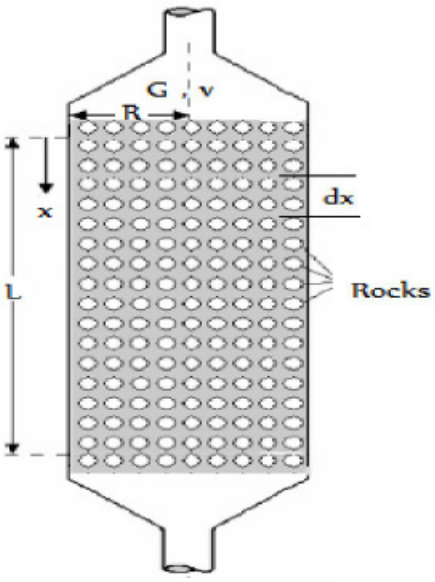

Figure 2.2 Packed bed thermal energy storage system [27]

Referring to Figure 2.2, during the heat charging period, hot air enters the packed bed tank at the top ($x = 0$) and leaves the tank at the bottom ($x = L$). Conversely, during the heat discharging period, cold air enters the packed bed tank at the bottom and leaves the tank at the top. During the discharging period the bottom of the tank is taken as $x = 0$ and top of the tank is $x = L$. This convention for location x must be taken into consideration when calculating dimensionless parameters as given below.

In order to make the transient heat transfer analysis of the system, the two dimensionless parameters dimensionless length (ξ) and dimensionless time (η) are used. These dimensionless parameters help to find the fluid and solid temperatures in the packed bed TES at any instant and any location. In equations (2.3.1) and (2.3.2) the calculation of dimensionless length and time are given respectively.

$$\xi = \frac{h_v \, S_{fr} \, x}{\dot{m} \, c_f} \tag{2.3.1}$$

$$\eta = \frac{h_v \, \tau}{(1-\varepsilon) \, \rho_m \, c_m} \tag{2.3.2}$$

In equation (2.3.1) and (2.3.2) definition of the parameters are given as:

h_v : Volumetric heat transfer coefficient

S_{fr} : Frontal cross-section area of packed bed

ε : Void fraction of packed bed

τ : Time duration of heat transfer in packed bed

x : Location of the desired temperature in terms of length

$\dot{m}$: Mass flow rate of the fluid

ε : Porosity of the packed bed TES Tank

c : Specific heat at constant pressure

ρ : Density

Here the subscripts are:

m : Storage material

f : Fluid

The relationship between surface heat transfer coefficient (h) and volumetric heat transfer coefficient (h_v) is given in [25].

$$h_v \, S_{fr} = \frac{h \, A}{L} \tag{2.3.3}$$

$$h = \frac{k((7-10\varepsilon+5\varepsilon^2)\,(1+0.7\mathrm{Re}^{0.2}\,\mathrm{Pr}^{1/3})+(1.33-2.4\varepsilon+1.2\varepsilon^2)\mathrm{Re}^{0.7}\,\mathrm{Pr}^{1/3})}{d_r} \tag{2.3.4}$$

The surface heat transfer coefficient (h) between a porous media and heat transfer fluid is calculated in equation (2.3.4), which is valid to $\mathrm{Re} = 10^5$ [28].

where

$$\mathrm{Re} = \frac{\dot{m}}{\pi R^2} \frac{d_r}{\mu_f} \tag{2.3.5}$$

and

$$\mathrm{Pr} = \frac{v}{\alpha} \tag{2.3.6}$$

In equation (2.3.6), v is the kinematic viscosity of the fluid and α is thermal diffusivity of the solid. By using dimensionless length and time parameters, the dimensionless temperatures for the fluid (T_f) and solid (T_m) defined as:

$$T_f(\eta, \xi) \equiv \frac{t_f - t_o}{t_{fi} - t_o} \qquad T_m(\eta, \xi) \equiv \frac{t_m - t_o}{t_{fi} - t_o} \tag{2.3.7}$$

where t_o is the initial bed temperature, t_{fi} is the fluid inlet temperature. t_f and t_m are the temperature of heat transfer fluid and solid at any instant and location respectively. The calculation of $T_f(\eta, \xi)$ is done according to Klinkenberg [25] as shown in equations (2.3.8), (2.3.9) and (2.3.10)

$$\eta < 2.0 \qquad \xi < 2.0$$

$$T_f(\eta, \xi) = 1.0 - e^{-\eta - \xi} \sum_{N=1}^{N=\infty} \left(\frac{\xi^N}{N!} \sum_{k=0}^{k=N-1} \frac{\eta^k}{k!} \right) \tag{2.3.8}$$

$$2.0 \le \eta < 4.0 \qquad 2.0 \le \xi < 4.0$$

$$T_f(\eta, \xi) = 1.0 - \frac{1}{2}\left[1 + erf(\sqrt{\xi} - \sqrt{\eta}\,\right] - \frac{\xi^{1/4}}{\eta^{1/4} + \xi^{1/4}} e^{-\eta - \xi} I_o(2\sqrt{\eta\xi}) \tag{2.3.9}$$

$$\eta \geq 4.0 \quad \xi \geq 4.0$$

$$T_f(\eta,\xi) = 1.0 - \frac{1}{2}\left[1 + erf\left(\sqrt{\xi} - \sqrt{\eta} - \frac{1}{8\sqrt{\xi}} - \frac{1}{8\sqrt{\eta}}\right)\right] \tag{2.3.10}$$

Since the equations used in the description of the mathematical model of the packed bed are symmetric, the value of T_m can be obtained by using equation (2.3.11) from [25].

$$T_m(\eta,\xi) = 1 - T_f(\xi,\eta) \tag{2.3.11}$$

In equations (2.3.8), (2.3.9) and (2.3.10), T_f values are estimated according to uniform bed temperature for a given time period. In many instances, the temperature at any location of the packed bed TES tank may not reach an equilibrium state within the given period, thus the bed is not at a uniform temperature. The technique given in equation (2.3.12) is for the prediction of the transient response of fluid outlet temperature (t_{fo}) for varying bed temperature. It will be based on the principle of superposition. The inlet temperature of the air is assumed to remain constant during the process. The packed bed will be subdivided into sections from $x = 0$ to $x = L$ and each of these sections will be approximated as being at uniform temperature.

The general expression for the outlet fluid temperature is:

$$t_{fo} = t_o + (t_{fi} - t_o)T_f(\eta,\lambda) + \sum_{j=1}^{J}(t_{o,j} - t_{o,j-1})(1 - T_f(\eta,\xi(x=L) - \xi_j)) \tag{2.3.12}$$

In equation (2.3.12), the parameter t belongs to temperature of any section. The definition of subscripts used above is given as:

o : Outlet

j : The number of section

i : Initial condition

2.3.2 Verification of Simplified Packed Bed Thermal Energy Storage System

In Section 2.3, a simplified packed bed TES model for AA-CAES system is introduced. For the simplified packed bed TES model, several assumptions are made to simplify the solution. These assumptions are given in Section 2.3. To verify the simplified model packed bed TES system, the results of the model are compared with an experimental study conducted by Karaki et al. [29] about a packed bed TES system.

2.3.2.1 Experimental Set-up

Karaki et al. present an experimental study and analysis of the heat transfer during charging and discharging process in a cylindrical shape packed-bed TES system [29]. The setup of test system used for the experiment is shown in Figure 2.3.

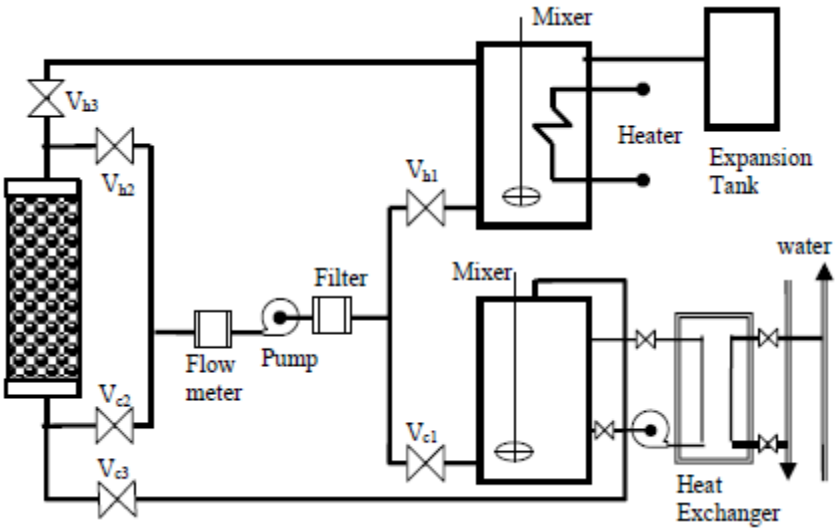

Figure 2.3 Schematic of experimental setup [29]

The system consists of a packed bed TES tank with filler material connected to two thermal reservoirs, one with high temperature and one with low temperature with a heat transfer fluid (HTF). During the heat charging process, valves V_{h3}, V_{c1}, and V_{c2}

are closed and the hot HTF is pumped so it flows through the packed bed TES tank, transfers thermal energy to the solid material, and flows out at a low temperature. After heat is released from HTF, it flows to the cold reservoir tank. During a heat discharge process, valves V_{h1}, V_{c3}, and V_{h2} are closed and the cold HTF is pumped through the tank to extract heat from the packed bed and flows to the hot reservoir. The whole system is insulated by using multiple 6.35 mm fiberglass insulation layers, and 31.75 mm fiberglass for pipe insulation. The hot HTF reservoir has an 11.0 kW heater and mixer to ensure a uniform temperature (T_H) in the HTF tank. The cold HTF reservoir is connected to a copper brazed plate heat exchanger, with 1.04 m^2 surface area, to bring down the HTF temperature to T_L. A mixer is also used to ensure proper mixing of the HTF [29].

2.3.2.2 Packed Bed TES Tank, Storage Filler Material and HTF Properties

In this experimental setup, the chosen storage filler materials are composed of river and sea pebbles and the chosen HTF is Xceltherm 600 synthetic oil by Radco Industries [30]. In Table 1 and Table 2, the packed bed storage filler material properties and heat transfer fluid properties are tabulated respectively.

Table 1 Packed Bed Storage Filler Properties [29]

Rock Nominal Diameter	0.01 m
Density of Rock	2632.8 kg/m^3
Rock Heat Capacity	790 J/kg K
Conductivity of Rock	2.5 W/m K

Table 2 Heat Transfer Fluid (Xceltherm 600) Properties @300 K [30]

HTF Heat Capacity	2100 J/kg K
Density of HTF	800 kg/m^3
Conductivity of HTF	0.13W/m K
Dynamic viscosity of HTF	0.035 Pa.s

In Table 3, diameter, length and porosity of the tank are presented.

Table 3 Packed Bed Tank Properties [29]

Tank Length Measured	0.65 m
Tank Inner Diameter	0.241 m
Porosity	0.324

2.3.2.3 Test Procedures

The tank is enclosed 14 thermocouples and each of them is buried into the rocks located at the center of the tank in 5cm interval from the top to the bottom. They measure local average temperatures of rocks and HTF fluid, because all thermocouples are in contact with rocks and HTF at the same time [29].

For the heat charging process, both heater and mixer are turned on in the hot reservoir. At first the desired temperature of HTF is obtained, then the heater is switched off and valves are manually opened or closed according to needs of the test. After that, the pump starts to pump the HTF to the tank. Finally, the HTF is accumulated in the cold reservoir.

The heat discharging process follows the heat charging process. The accumulated HTF in the cold reservoir is cooled down to the desired temperature with a help of heat transfer between the HTF and water in the heat exchanger shown in Figure 2.3. After the required temperature is obtained valves are opened or closed according to the needs for discharging test. The pump is activated in order to pump cold HTF from tank through the packed bed where heat transfer cools the packed bed and heats the HTF, and the hot HTF flows to the hot reservoir [29].

For each process, conditions are tabulated in Table 4 Test Conditions for Heat Charging and Discharging Period

Table 4 Test Conditions for Heat Charging and Discharging Period [29]

CONDITIONS	Charging	Discharging
HTF Flow Rate (dm^3/min)	1.0	1.96
Test Period (min)	70.08	39.74
Initial Temperature(^oC)	21.9	129
Hot Temperature (^oC)	79.82	129
Cold Temperature (^oC)	21.9	56

2.3.2.4 Experimental Results

Two experiments were conducted for the packed bed TES system. The first experiment is of heat charging process and second one is of the heat discharging process. In the first and second experiments, results taken from thermocouples are gathered in real time and presented in Figure 2.4 and Figure 2.5 [29].

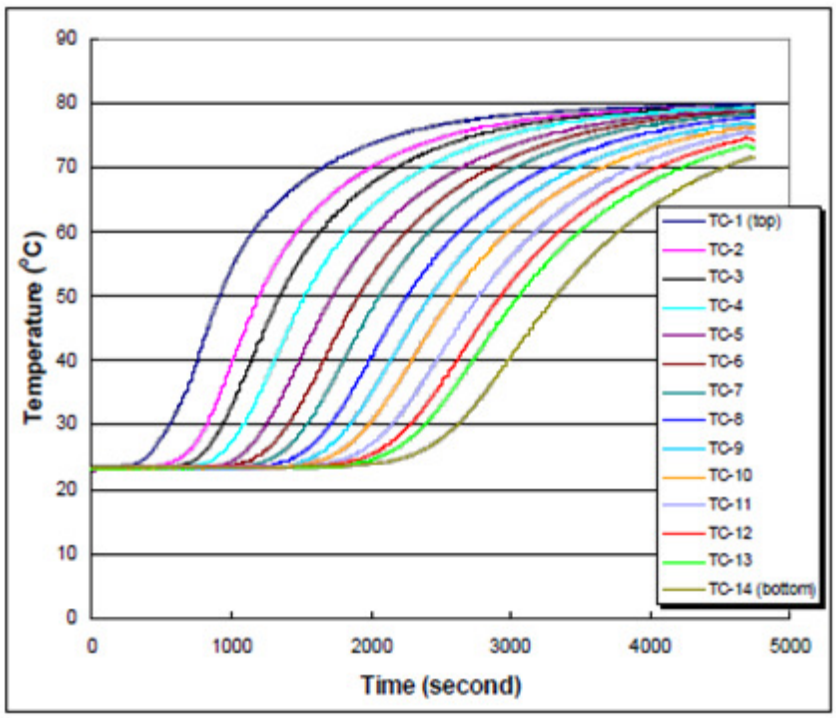

Figure 2.4 The experimental results for heat charging period [29]

From Figure 2.4, the thermocouple located at the top of the packed bed tank is labeled as TC-1 and the thermocouple located at the bottom of the packed bed is labeled as TC-14. Other thermocouples are located between TC-1 and TC-14 and labeled accordingly. The initial temperature of the packed bed storage tank is about 21.9^{o}C. Hot HTF first enters to the tank from the top and leaves the tank from the bottom for approximately 4200 seconds. As can be seen from Figure 2.4, the top of the packed bed TES system reaches the temperature ~80^{o}C first, which is the inlet temperature of hot HTF, and the bottom of the tank only reaches a temperature of~73^{o}C, which is minimum temperature of the final readings. Other thermocouples readings are between ~80 ^{o}C and ~73 ^{o}C and decrease from top to the bottom.

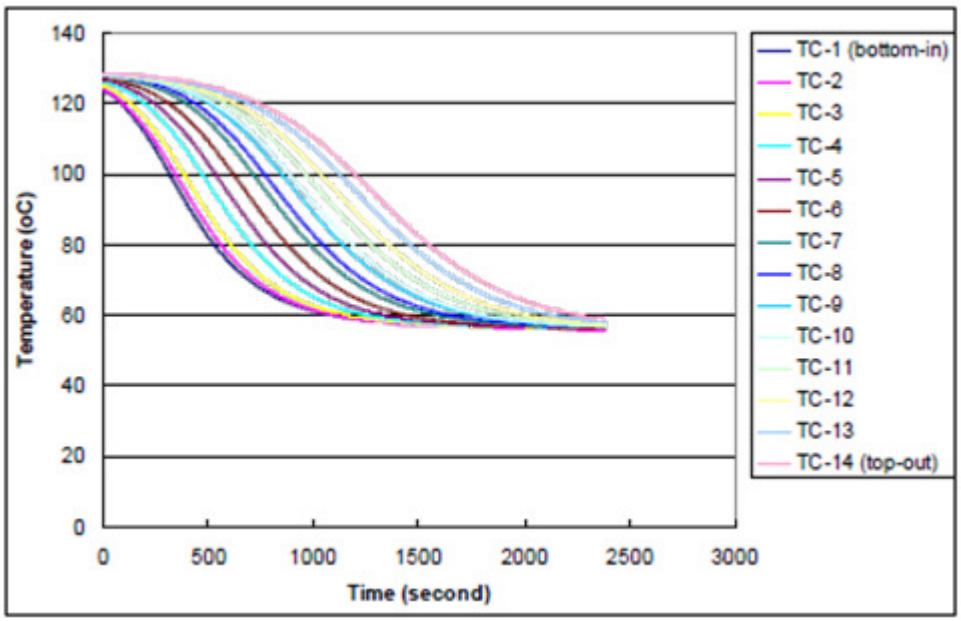

Figure 2.5 The experimental results for heat discharging period [29]

For the heat discharge process, cold HTF fluid (56^{o}C) enters from the bottom of the tank and leaves from the top. The initial temperature of packed bed storage tank is about 129^{o}C. The heat discharging period is approximately 2400 seconds and thermocouple locations are labeled in opposite order of the heat charging process (in this experiment TC-1 is located at the bottom and TC-14 is located at the top of the tank). As can be seen from Figure 2.5, the bottom of the tank, which is the inlet of

the cold fluid, reaches the temperature ~56°C first and the top of the tank, which is the outlet of the cold fluid, reaches the temperature ~59°C during the heat discharging period. Other thermocouple readings are between ~56°C and ~59°C and increase bottom to the top.

2.3.2.5 Packed Bed Thermal Energy Storage Simplified Model Results

In this part, results from the simplified model of a packed bed TES model for heat charging and heat discharging are presented. For the model, the storage filler materials, heat transfer fluid, packed bed thermal energy storage tank physical properties and experiment duration are taken as the same as in the experiment study by Karaki et al. Moreover, locations of thermocouples in the model for the heat charging and discharging process are also the same as the experimental setup.

Model results are presented in Figure 2.6 and Figure 2.7 for the heat charging and discharging respectively.

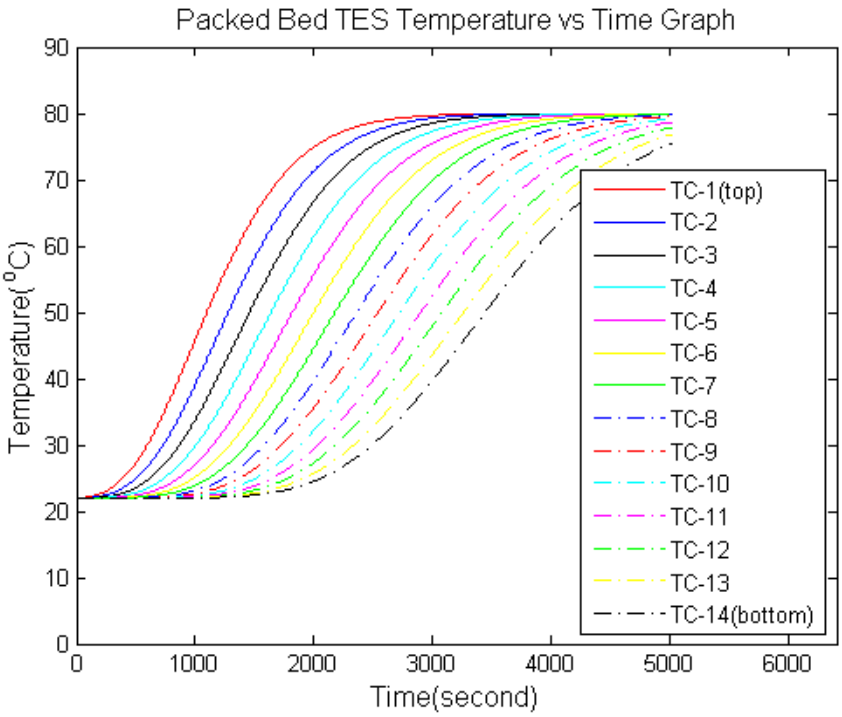

Figure 2.6 Simplified model results for heat charging

As it can be seen from Figure 2.6, thermocouple TC-1 located at the top of the tank reached ~80^{o}C first and thermocouple TC-14 located at the bottom of the tank reached ~72^{o}C which is the minimum of final readings. The other thermocouples and their final readings are changing between 80^{o}C and 72^{o}C from top to the bottom of the tank shown in Figure 2.6

In the heat discharge model, thermocouple TC-1 located at the bottom of the tank reached nearly 56^{o}C first and thermocouple TC-14 located at the top of the tank reached approximately 62^{o}C which is the maximum of the final readings. The other thermocouples and their final readings increased from 56^{o}C to 62^{o}C from bottom to the top of the tank shown in Figure 2.7 Simplified model results for heat discharging

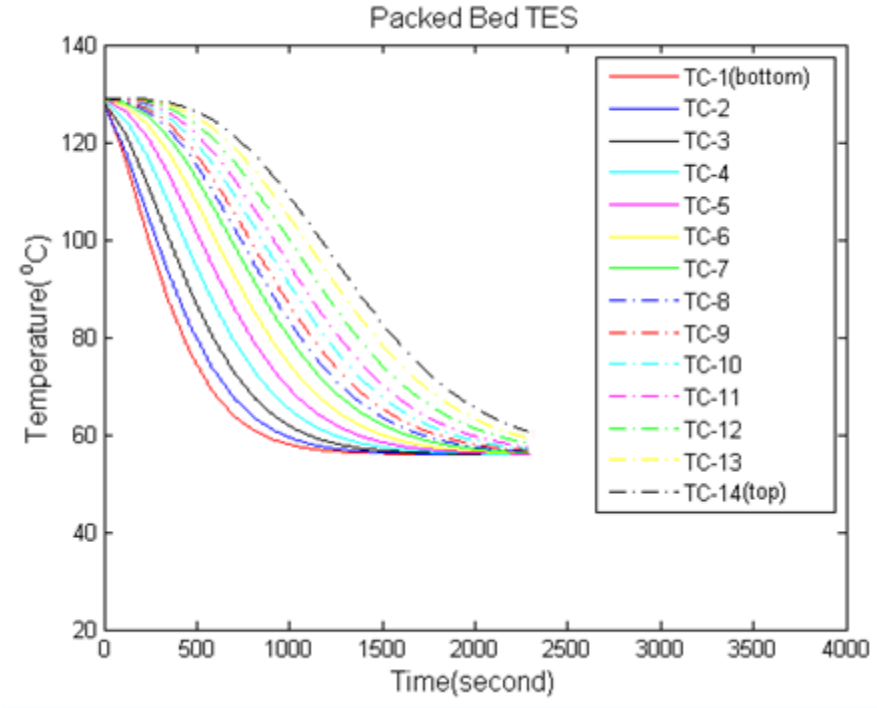

Figure 2.7 Simplified model results for heat discharging

2.3.2.6 Comparison of Simplified Model Results and Experimental Results

In this part, simplified model packed bed TES system results presented in Section 2.3.2.5 and experimental results presented in Section 2.3.2.4 are compared and differences are discussed.

The model and experimental results are plotted in the same graph shown in Figure 2.8 and Figure 2.9 in order to compare the behavior of the temperature curves during the heat charging and discharging periods. In these figures, the "TC-#" notation indicates data taken from the model and "TC-# (Ex)" shortcuts belong to data taken from the experiments. Although fourteen thermocouple data points are available for both the model and experiment for both processes, only six of them are presented in order to increase the visibility of the comparison. As it can be seen from Figure 2.8 and Figure 2.9, thermocouples numbered 1, 4, 7, 10, 12 and 14 are used for comparison in both the model and experiment.

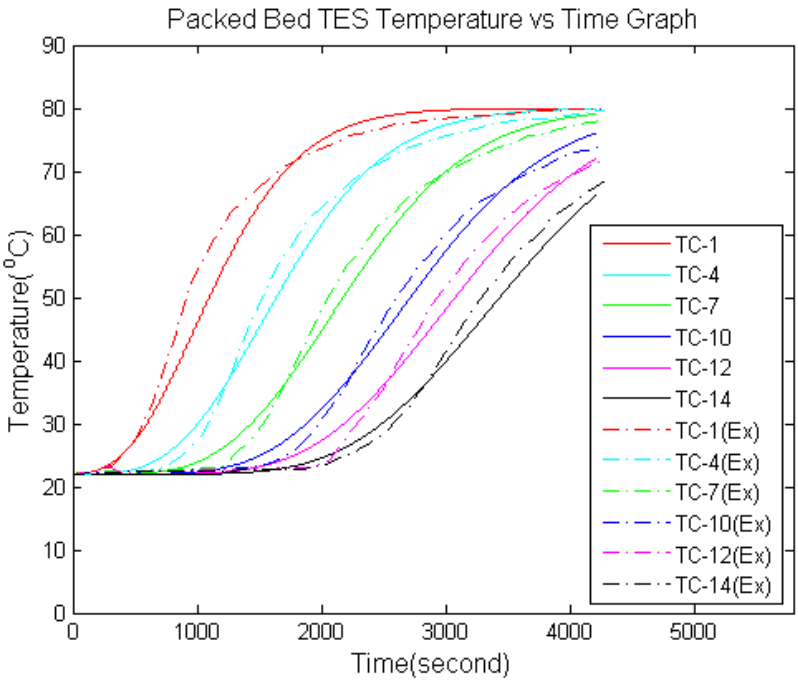

Figure 2.8 Comparison of experimental results and model results for heat charging process

In Figure 2.8, model and experimental results are presented for the heat charging process. There are slight differences between the model and experiment results. At the end of the process, both model and experimental thermocouple readings reach nearly the same temperature values. There are several possible reasons why there are slight differences in the temperature curves for the model and experimental results.

- It is assumed in the simplified model that there is no transverse heat transfer in the bed and the container walls are perfectly insulated. On the other hand transverse heat transfer in the bed is present in the experiment and some heat losses from the walls are inevitable even though the experimental tank is well insulated.

- In simplified model, radiation effects are neglected. Although it is small heat loss when compared to conduction and convection losses, in the experiment it is a valid radiative heat loss.

- For the simplified model, constant thermal and physical properties are used however in reality these will vary with temperature.

- For the simplified model, the bed material has zero thermal conductivity in the direction of flow however in experiment this is not valid.

- For the model, there is a uniform convective heat transfer coefficient. In reality convective heat transfer coefficient will not be perfectly uniform due to changes in mass flow rate of HTF in different cross sections and irregularly shaped material.

- The simplified model neglects intraparticle conduction and fluid dispersion however in reality these will be present.

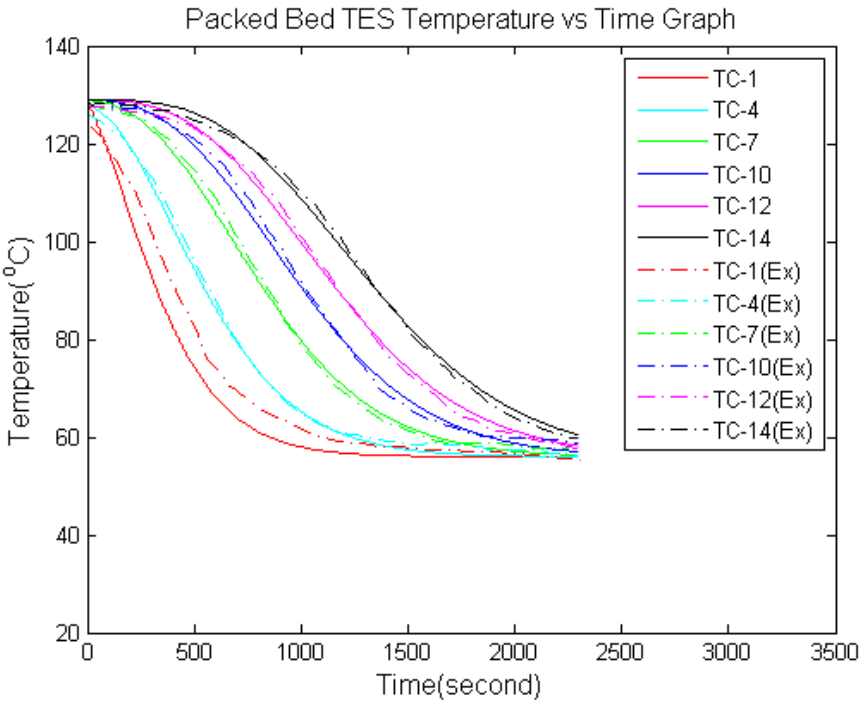

Figure 2.9 Comparison of experimental results and model results heat discharging process

As can be seen from Figure 2.9, the temperature profile is nearly the same for the model and experimental results for the heat discharging process. At the end of the process, both model and experimental results reach nearly the same temperature value and the reasons of slight temperature differences between the model and experimental results for heat discharging process can be explained by the reasons for the heat charging process.

2.3.3 Pressure Drop In the Packed Bed Thermal Energy Storage System

The potential for significant pressure drops is one of the main drawbacks of a packed bed TES system. Before pressurized hot air enters the air storage cavern, it passes through the packed bed TES in order to leave its heat energy. After this process, the pressure of the moving air should be higher than the pressure of the stored air in the storage tank in order to store the moving air.

Many researchers are interested in calculation of pressure drop across the packed bed system. According to Diedericks, it is impossible to calculate the pressure drop in the packed bed TES at a microscopic scale. It is necessary to average over the microscopic scale to predict a macroscopic scale pressure loss such as by using a volume averaging method [28]. Kaviany uses three different methods of analysis for packed bed models. The first one is a capillary model, which applies Navier-Stokes equations to flow in small diameter conduits; the second one is a hydraulic radius model, which uses an equivalent diameter of the particles and models them as spheres; and the final one is a drag model, in which the Navier-Stokes equations are solved for flow over a collection of particles [28]. The main and classical equation for prediction of pressure loss belongs to Ergun [31]. The equation called Ergun is based on a hydraulic radius model.

$$-\frac{\Delta p}{L} = 150\frac{(1-\varepsilon)^2}{\varepsilon^3}\frac{\mu_f v_s}{D^2} + 1.75\frac{(1-\varepsilon)}{\varepsilon^3}\frac{\rho_f v_s}{D} \tag{2.4.1}$$

where L is length of packed bed, ε is porosity of the system and v_s is the superficial speed through the porous medium ρ_f and μ_f are density and absolute viscosity of the fluid respectively. In the AA-CAES model, the Ergun equation is used for pressure drop prediction.

2.4 Air Storage Stage

In this stage, compressed air is assumed to be stored in a constant volume porous medium. The compressibility factor of the air is checked in order to apply the ideal gas law. By taking the critical temperature and pressure values of air [32], compressibility factor can be calculated based on the reduced temperature and pressure given in equation (2.5.1)

$$T_r = \frac{T}{T_c} \qquad and \qquad P_r = \frac{P}{P_c} \tag{2.5.1}$$

In this stage the temperature and pressure of the air are approximately 75 bar and 300K respectively. For air the critical temperature is 132.5 K and critical point for air pressure is 37.7 bar. Using equation (2.5.1), the compressibility factor is calculated as approximately 0.99 [33]. Therefore, the ideal gas assumption can be accepted for all stages.

$$P\,V = m\,R\,T \tag{2.5.2}$$

If equation (2.5.2) is rearranged and the derivative is taken with respect to time for both sides, equation (2.5.3) is obtained.

$$\frac{dP}{dt} = \frac{1}{V}\frac{dm}{dt}RT \tag{2.5.3}$$

$$\frac{dP}{dt} = \frac{1}{V}\dot{m}\,R\,T \tag{2.5.4}$$

Therefore, the pressure of the air storage cavern at any time t can be calculated as

$$P = \int_0^t \frac{1}{V}\dot{m}\,R\,T\,dt \tag{2.5.5}$$

During the compression stage air is compressed into the air storage cavern and pressure of the cavern increases. In the same manner, during the expansion stage air is extracted from the storage tank and pressure of the tank decreases. The storage temperature is assumed to be constant due to the porous medium of the cavern since the mass of porous medium reduces the temperature variations in the air storage cavern. The volume of the cavern is constant, and therefore the pressure is only a function of mass of air.

2.5 Expansion Stage

In this stage, different from the commercial products, a new type of air turbine is assumed to be used in order to utilize the energy of the pressurized air. The new type

air turbine does not have any combustion chamber and compressor stage and it is assumed to be operated very large pressure ratio application.

In this study, the expansion process is assumed to be a polytropic and adiabatic. Hence, the governing equations for turbine stage are similar to compression stage.

The total enthalpy difference across the inlet and outlet of the turbine determines the power production of the turbine according to the isentropic efficiency (η_t). As air passes through the turbine stage, the pressure of the air is decreases. From Section 2.2, equation (2.2.5) is changed as:

$$\frac{P_o}{P_i} = \left(\frac{V_i}{V_o}\right)^n = \beta_t^{-1} \tag{2.6.1}$$

β_t is the pressure ratio of the turbine and P_o is the isentropic outlet state. As a result of this equation (2.2.9) is revised in the same manner.

$$T_o = T_i \, \beta_t^{\frac{1-n}{n}} \tag{2.6.2}$$

Power production in the expansion stage is:

$$P_t = \eta_t \, \dot{m} \; C_{p,ave}(T_o - T_i) \tag{2.6.3}$$

If equation (2.6.2) is substituted into equation (2.6.3), the power production in the turbine is calculated as:

$$P_t = \eta_t \; \dot{m} \; C_{p,ave} T_i (1 - \beta_t^{\frac{n-1}{n}}) \tag{2.6.4}$$

In the compression stage, the mass flow rate of air depends on the excess electricity produced from wind turbines. In the expansion stages, the mass flow rate of the air is one of the system performance parameters and the effects of change in the mass flow rate of air is investigated and presented in Chapter 4.

2.6 Conclusion

In this chapter, the AA-CAES model developed for this study is presented. The stages of the models are introduced. The governing equations and necessary assumptions for each stage are defined. The model for the packed bed TES is verified using experimental data available in the literature.

CHAPTER 3

METHODOLOGY FOR SIZING AND ASSESSING OF WIND INTEGRATED AA-CAES

3.1 Introduction

In Chapter 2 a model for a basic AA-CAES system is presented. In this chapter, this AA-CAES model is extended to model a wind integrated AA-CAES system. Metrics are defined to assess the system's performance and a methodology is proposed to size and assess an AA-CAES. The model is programmed using MATLAB and parametric studies are conducted to assess the impact of key design and operational parameters on the system performance. While similar but not identical work to Chapter 2 was found in the literature, to the best of the author's knowledge work similar to Chapter 3 does not exist in the literature.

For this work on a wind integrated AA-CAES, a place where a wind integrated AA-CAES is to be built is selected. The site is explored for a suitable air storage cavern in terms of topology and volume. For this place, a detailed meteorological data set for a year is obtained such as a typical meteorological year data set (TMY2) using the software program Meteonorm v.7.0. Hourly grid energy demand data is obtained from the National Electricity Transmission Company. By using wind speed of TMY2 hourly meteorological data, hourly electricity production from wind farm located in selected site is calculated and compared with hourly grid energy demand data at the same time for a selected place where the wind farm is built for every hour of the year. For this methodology, the meteorological and demand data should be taken

ideally for the same year but if TMY2 data or similar data sets are used this is not possible.

In this model the difference between wind power production and the by the grid is calculated at hourly time steps. This difference is the input for the AA-CAES to determine its operating condition. If the production of electricity from the wind is higher than the demand by the grid, the AA-CAES system is charged. On the other hand, discharge takes place in order to compensate difference between electricity production and demand. According to the type of the process and its duration, sizing of AA-CAES system for a selected site is investigated. Additionally, several parametric studies are performed for assessing of the system's performance by changing the size and operating limits of the system components.

There are some restrictions that place limits on the system's performance for assessing the AA-CAES system. Volume, pressure limits of the cavern, and pressure loss in the thermal energy storage system are examples that will be explained in this chapter in the following sections.

3.2 Site Selection

Site selection is one of the critical issues for all types of CAES systems. The primary requirement of a CAES plant is to find a suitable cavern to hold air at high pressure without any deformation or losses. The pressure range that the system operates can vary with the physical properties of the selected cavern. For example, the cavern pressure requirement is between approximately 46 and 72 bars in existing CAES plants [34].

Before the selection of the air storage cavern, the topology of the cavern should be inspected carefully. The cavern should be able to resist large variations in pressure levels during charging and discharging.

In the United States, the Utah and Colorado Mines were examined in order to construct a CAES plant [18], [35]. Several possible place in Germany where a CAES

plant can be constructed were identified. In Turkey, although CAES system is a new concept for the energy sector, there are some potential places where a CAES system can be constructed. As can be seen from Figure 3.1 south-west, south-east and the south of Turkey are wealthy in terms of caverns.

Figure 3.1 Density of cavern distribution in Turkey [36]

The size of the cavern is another important parameter that should be taken into consideration. The size of the cavern directly affects how much energy can be stored in the cavern. An increase in the storage volume increases in the capacity to store energy; likewise a decrease in the storage volume decreases in the capacity to store energy. Moreover, it would be beneficial for the site to be located near a significant wind generation source. This will allow for optimum utilization of transmission lines, and reducing transmission costs and losses will have a significant positive impact on the economics of CAES projects.

Generally there are three cavern options that can be used in AA-CAES system: 1.salt dome; 2.aquifers; and 3.hard rock mine.

Salt domes are the best option available for a CAES reservoir. They can be solution-mined relatively inexpensively, and this creates a very well-sealed cavern [35]. Also

salt domes are used for the caverns in both existing CAES plants. Aquifers are the second best option available, and they exist underground nearly everywhere. The third option for a CAES reservoir is a hard rock mine. Hard rock mined caverns are developed by boring and digging out the rocks by using blasting procedures. Rock mined caverns are known to be one of the best options for storage in terms of having the ability to store pressurized air for long durations [21] .

3.3 Wind Speed Information and Wind Turbine Power Calculation

3.3.1 Wind Speed Information

Wind speed is one of the most crucial inputs for wind integrated an AA-CAES system because it directly affects the system behavior. For this study a relation has been established between wind energy and AA-CAES system. If the power output of the wind farm is greater than energy demand for a selected place, charging takes place and the excess energy is stored. Otherwise, discharging takes place and stored energy is used to compensate for the gap between energy demand and production. In this system hourly wind speed data is taken from TMY2 formatted meteorological data. The elevation of the wind speed data for TMY2 data is not the same as the elevation of wind turbine hub. There is a correlation between wind speed and elevation from ground level:

$$u_z = u_m \left(\frac{z}{z_m} \right)^{\alpha} \tag{3.1.1}$$

All terms in equation (3.1.1), are given below with their explanations:

u_z :corrected wind speed at desired elevation

u_m : measured wind speed at specific elevation

z : desired height above ground level in meters

z_m : measured height above ground level in meters

α : correction factor

In the wind integrated AA-CAES model, the elevation of the TMY2 formatted wind data is assumed as 10 m, the desired height of wind data is taken as 50 m based on the turbine information, and the correction factor is taken as 0.147 for all calculations.

3.3.2 Wind Turbine Power Calculation

Wind turbine power production is calculated by using corrected the wind speed data in the function describing the wind turbine power curve. There are several key terms used to characterize this wind turbine power curve function. At very low wind speeds, there is not sufficient force applied by the wind on the turbine blades to make them rotate. However, as the wind speed increases, the wind turbine begins to rotate and generates electrical power. The speed at which the turbine first starts to rotate is called the cut-in speed. As the wind speed rises above the cut-in speed, the level of electrical output power rises rapidly. At the rated output speed, the power output reaches the maximum that the electrical generator can produce and the power output remains constant with further increases in wind speed. However as the wind speed increases more, the forces on the turbine structure continue to rise and, at some point, there is a risk of damage to the rotor. As a result, a breaking system is employed to bring the rotor to a standstill. The wind speed at which the rotor is brought to a standstill by the break is termed cut-out speed.

As can be seen from Figure 3.2, for Enercon E-82 Wind Turbine, the cut in speed is 3 m/s, rated wind speed is between 13 m/s and cutout speed is 25 m/s. Maximum power output is approximately 2050 kW.

In order to calculate the total wind farm power output, the types of wind turbines, number of wind turbines and location of each wind turbine according to one another are other necessary and important parameters. In this methodology only the number

of wind turbines and types of wind turbines are taken into consideration; i.e., the influence of one wind turbine on another is neglected.

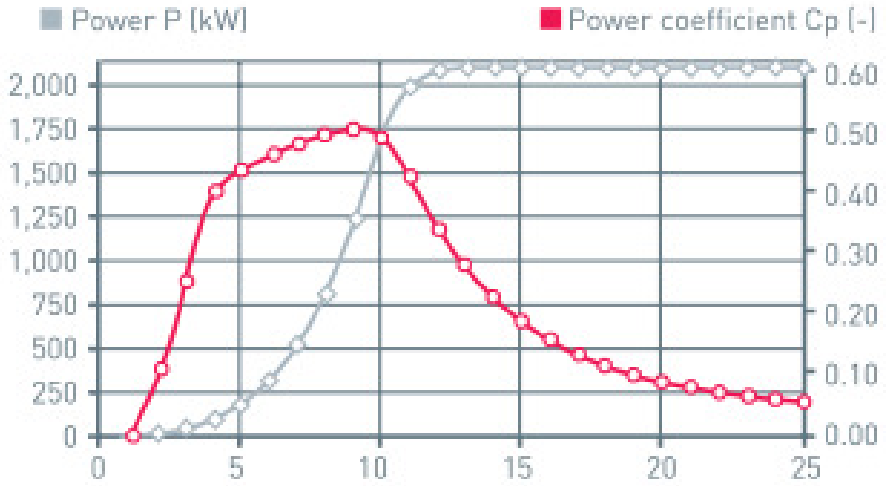

Figure 3.2 Enercon E-82 wind turbine power curve [37]

3.4 The Comparison of Energy Production and Energy Demand of a Selected Site

In a conventional CAES system, when compression and expansion stages occur depend on the price of the electricity. When the price of the electricity is low, inexpensive electricity is used in compressors to compress the air into the caverns. When the price of the electricity is high, expansion starts to produce high profit electricity for the grid. In the methodology presented herein, the working principle of a wind integrated AA-CAES is different from a conventional CAES system. When the wind energy produced ($E.P$) for a specific period and the energy demand ($E.D$) of the selected site is less than the energy production of wind turbines ($E.P - E.D > 0$), compressors use excess energy to compress the air into the cavern. When the energy demand of a selected place is higher than energy production ($E.P - E.D < 0$), expansion starts to compensate for the energy gap between demand and production. If the demand and energy production are at the same amount ($E.P - E.D = 0$), the idle stage takes place and neither compression nor expansion

observed. A schematic of the working principle of wind integrated AA-CAES model is given in Figure 3.3 without considering operating limits of the AA-CAES system.

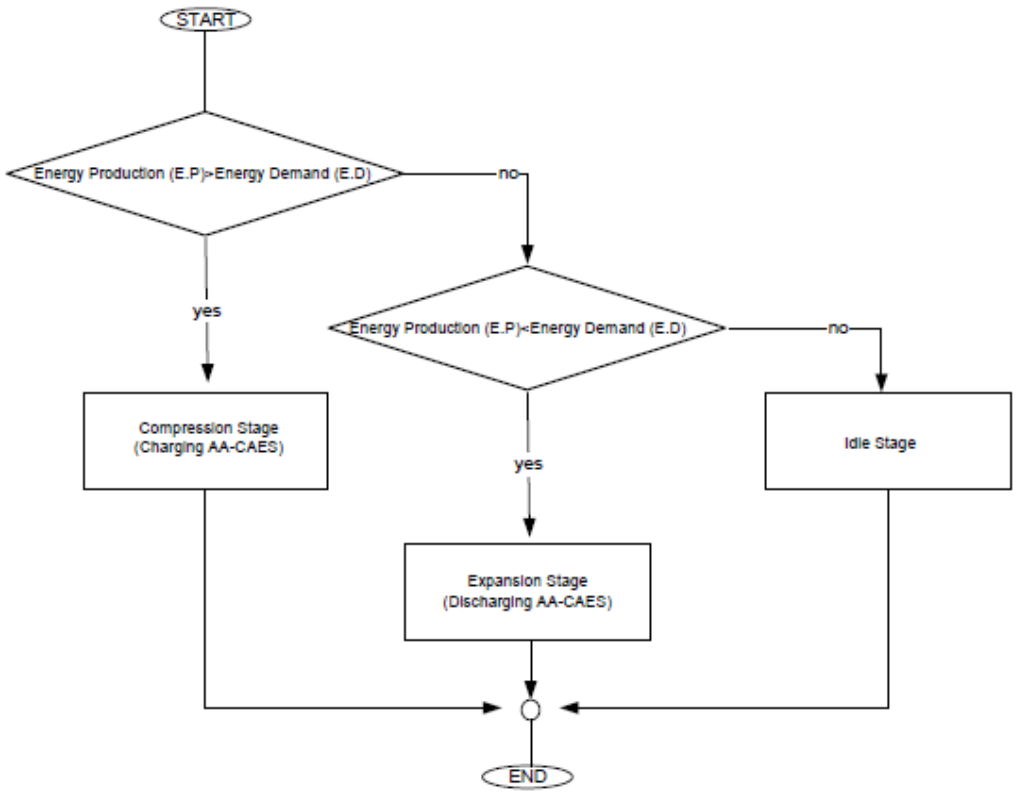

Figure 3.3 Wind integrated AA-CAES working principle

In this methodology, energy production and energy demand data are compared in hourly resolution based on the hourly wind turbine power calculation and energy demand inputs. For clarity, a "Cascade Compression Period" is defined when $E.P - E.D > 0$ for several consecutive hours and "Cascade Expansion Period" is defined when $E.P - E.D < 0$ for several consecutive hours.

3.5 Determination of Size of Packed Bed Thermal Energy Storage Tank

Packed bed TES size is an important parameter that directly affects the temperature, pressure of the air and turbine power output. Increase in the size of the packed bed

TES tank should be parallel to the increase in the energy storage capacity of the AA-CAES system. In this study, a cylindrical shape packed bed TES tank is used. The size of the packed bed TES can be increased by increasing the length or radius of the tank. This increment however may result in an unavoidable performance loss of the system.

There are many options for selecting the size of the TES. For example in this methodology, the TES tank size is calculated according to the site specific maximum cascade compression period for the AA-CAES model.

In the model, maximum cascade compression period for a year is found from the comparison of energy production and energy demand inputs explained in Section 3.4. The total excess energy ($E.P - E.D > 0$) released during that period is calculated. By using the excess energy in the compressor, constant mass flow rate of the air for the maximum cascade compression period is calculated using equation (2.2.11). After calculation of mass flow rate for a given period, heat charging temperature analysis of the packed bed TES model is used for designing a specific packed bed TES tank to store all the heat energy released during maximum cascade compression period by changing the length and radius of the tank. In this study the length of the tank is estimated and radius is obtained according to the specified length. For the specific length, the radius is changed until the temperature of the hot pressurized air at the entrance and exit become equal at the end of the cascade compression period. In Figure 3.4-3.8, temperature distribution of the packed bed TES tank is shown for the same length (10 m) and different radius for 10 hours maximum cascade compression period. It is estimated that constant mass flow rate of the air in the compressor is calculated as 25 kg/s according to the excess wind energy for 10 hours.

In these figures, the “TC-#” notation is used to denote data taken from the thermocouples and each number shows the specific position in the tank in terms of distance from the inlet. TC-1 belongs to the inlet temperature of the tank and TC-14 belongs to the outlet temperature of the tank. Other thermocouples are equally spaced

along the length at the center of TES tank. These figures are used to show how to select the radius of TES tank for a specific length (10 m).

In Figure 3.4, tank is reaches a steady state temperature after only approximately an hour and a half for a radius equal to 1 m. Although hot air is still passing through the tank, the TES tank is full after only an hour and a half. After an hour and a half, the bed reached an equilibrium point and the outlet temperature of the air is the same as the inlet temperature. Hence the TES is undersized and all the thermal energy of the flowing hot air after an hour and a half until the end of the cascading compression period is lost.

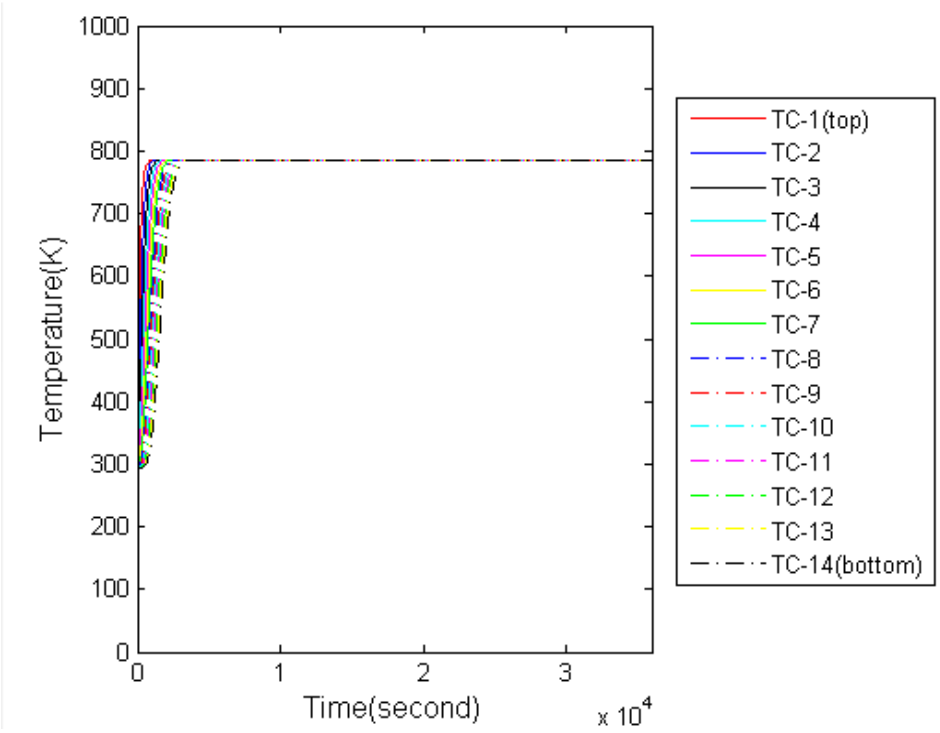

Figure 3.4 Temperature distribution for R=1m

In Figure 3.5, if the radius of the packed bed TES tank is increased to 2 m, and the TES tank reaches its equilibrium temperature at the end of approximately 3 hours. After 3 hours, the outlet temperature of the air is the same as the inlet temperature

and all the thermal energy of the flowing hot air is lost until the end of process. The radius of the air packed bed TES tank can be increased more.

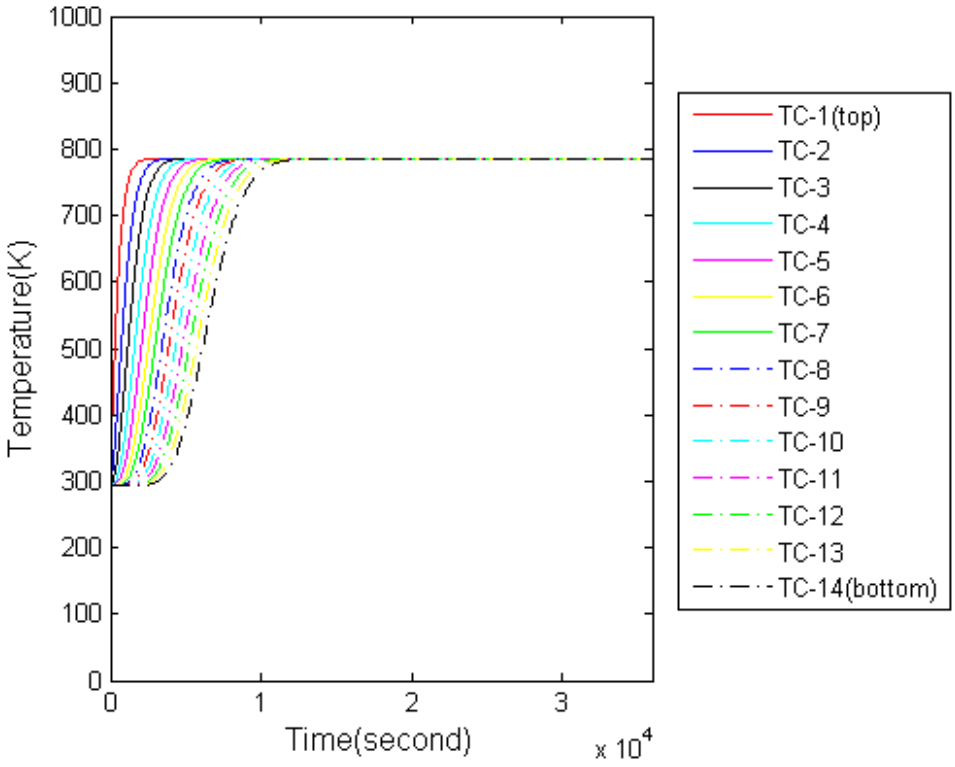

Figure 3.5 Temperature distribution for R=2m

If the radius of the packed bed TES tank is increased to 3 m, the bed has uniform equilibrium temperature at the end of 7 hours approximately and there is still some thermal energy lost until the end of the process. The evolution of the temperature distribution within the packed bed TES is presented in Figure 3.6. In Figure 3.7, for a radius of 4 m, the packed bed TES tank reaches its equilibrium temperature at the end of 10 hours. After the 10 hour period, if the air flow continued, the thermal energy of the air would be lost. Consequently for a 10 hour flow period, a 4 m radius is suitable for storing energy of the hot air flow for 10 m length.

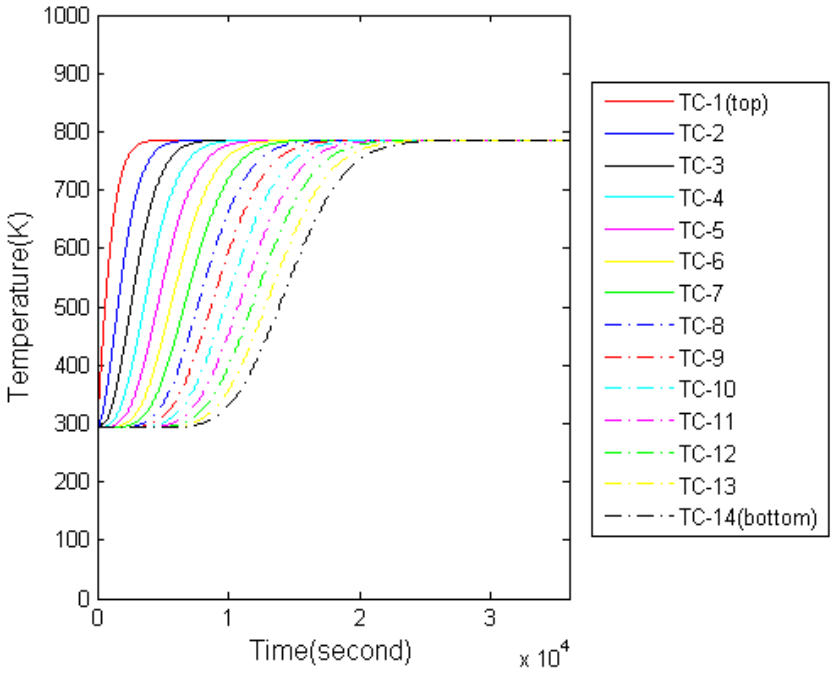

Figure 3.6 Temperature distribution for R=3m

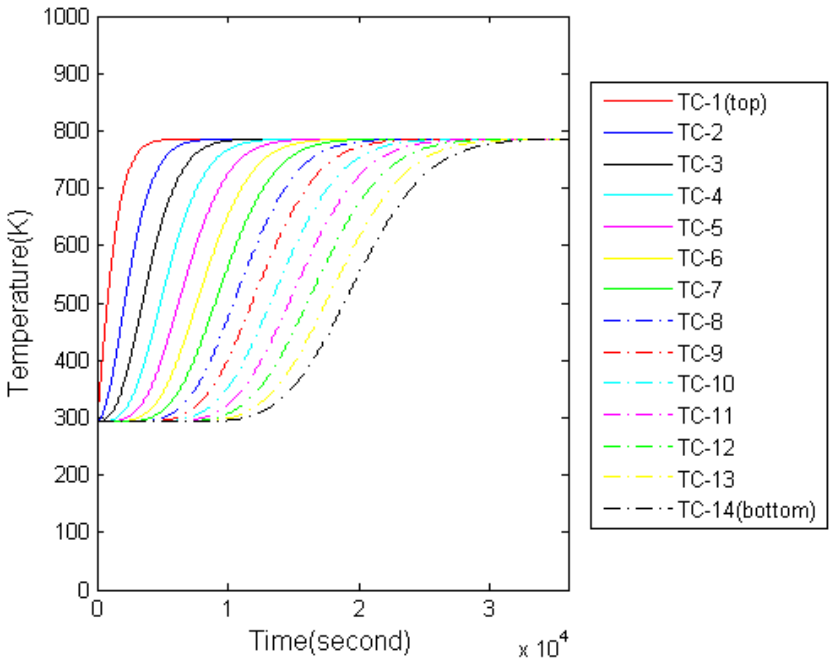

Figure 3.7 Temperature distribution for R=4m

As shown in Figure 3.8, if the radius is increased to 5 m, the TES tank cannot reach its equilibrium temperature, the outlet region of the tank becomes colder than inlet temperature, and the tank is oversized.

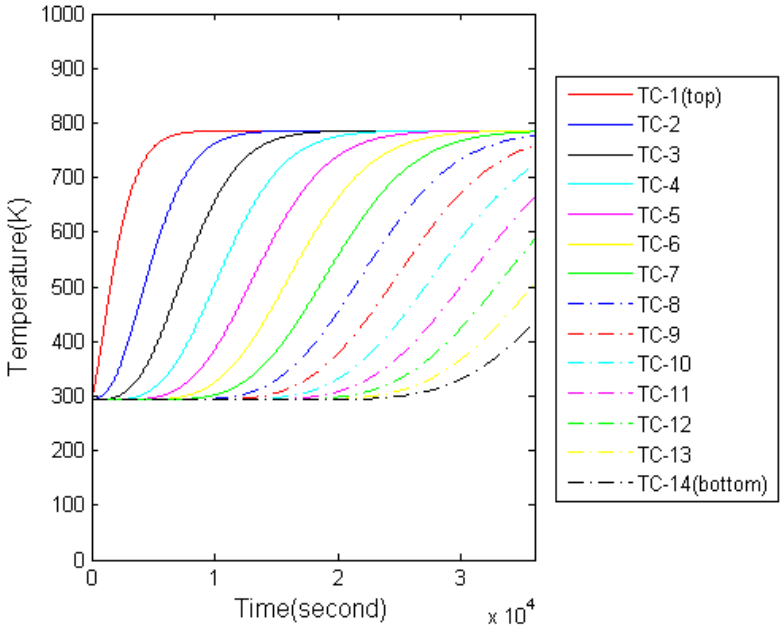

Figure 3.8 Temperature distribution for R=5m

The same process can be applied to the same system by fixing the radius of the packed bed TES tank and changing the length under the same maximum cascade compression. In Section 4.4.1, the application of storing the same amount of thermal energy in different length and radius pairs of TES tank is presented. The flow chart of this methodology is given in the Appendix A.

As was stated, an increase in the length or radius of the tank leads to a larger thermal storage capacity for the TES however this increment may create a problem in terms of pressure drops for the system. Although an increase in the radius of the packed bed TES system decreases the pressure drop for the same length, the convective heat transfer coefficient between fluid and solid decreases due to a fixed mass flow rate and increase in the cross sectional area of the fluid flow as shown in Figure 3.4 to Figure 3.8. This leads to a decrease in the heat transfer rate which may be important

in terms of system performance. Consequently, parametric studies for both length and radius are presented in Chapter 4 for Datça Peninsula maximum cascade compression period to determine the size of TES.

3.6 Determination of the Minimum Volume of the Air Storage Cavern

The determination of the size of the packed bed TES tank is given in Section 3.5. For that TES size, a specific amount of air is determined in order to consume all the stored thermal energy to use in the turbine stage during the maximum cascade expansion stage. By using the heat discharging model, specific mass flow rates of the air is determined to decrease the uniform temperature of the packed bed TES from high temperature to ambient temperature within the maximum cascade expansion period. During the calculations, the temperature of the stored air is assumed to be at ambient temperature (293 K) and constant during maximum cascade expansion period.

In Section 3.5, for 10 hours maximum cascade compression period, the ideal size of the TES is estimated as L=10 m and R=4 m without considering pressure drops. By using the same size TES tank and same period, a specific air mass flow rate is determined to consume all the thermal energy stored in the maximum cascade compression period. In the following example, the maximum cascade expansion period is taken as 10 hours which is the same as maximum compression cascade period. By changing the mass flow rate of air at ambient temperature, the temperature distribution of the packed bed TES is obtained and presented in Figure 3.9, Figure 3.10 and Figure 3.11. If the mass flow rate of air at ambient temperature is increased, the packed bed TES tank reaches its equilibrium temperature more quickly.

In Figure 3.9, the 10 hour duration is not sufficient to completely discharge the TES for 10 kg/s mass flow rate. There is still heat energy left in the TES tank. Hence, the mass flow rate of air should be increased more to use all the thermal energy in the given period.

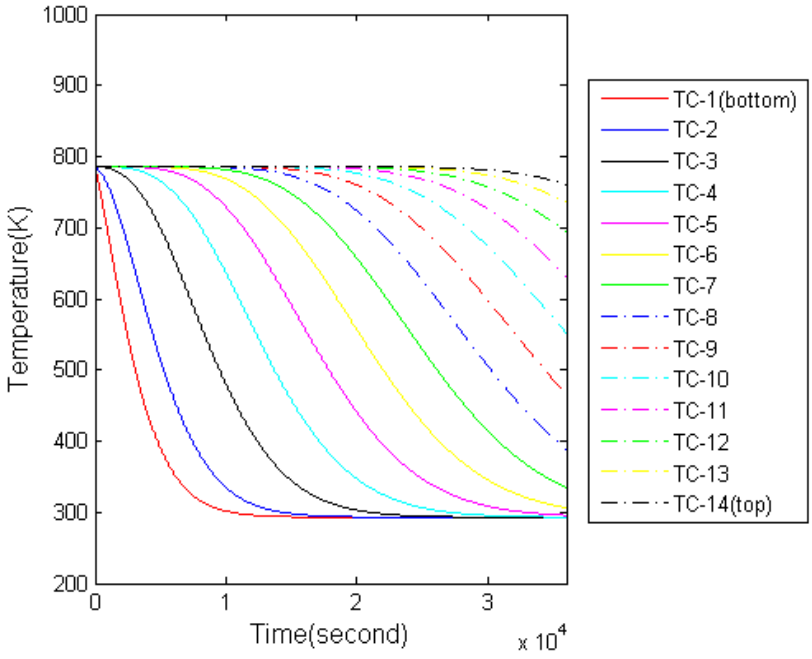

Figure 3.9 Temperature distribution of the packed bed for 10 kg/s air mass flow rate

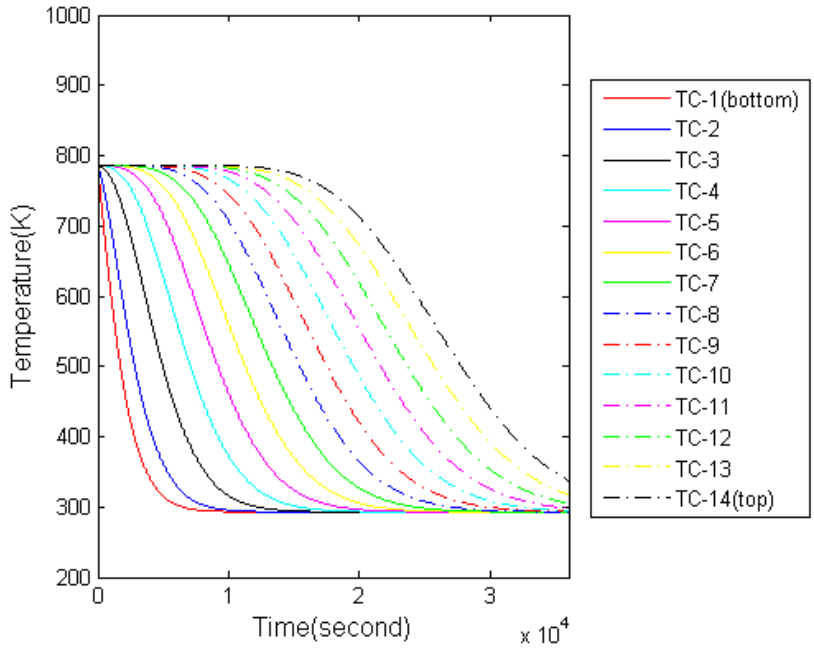

Figure 3.10 Temperature distribution of the packed bed for 20 kg/s air mass flow rate

As can be seen from Figure 3.10, 20 kg/s mass flow rate is also not sufficient to

extract all the thermal energy from the TES tank. Hence the mass flow rate of the air should be increased. In Figure 3.11, the effect of 25 kg/s air mass flow rate on bed temperature distribution is presented. As it can be seen from Figure 3.11, the bed reaches the equilibrium temperature and no thermal energy remains in the tank.

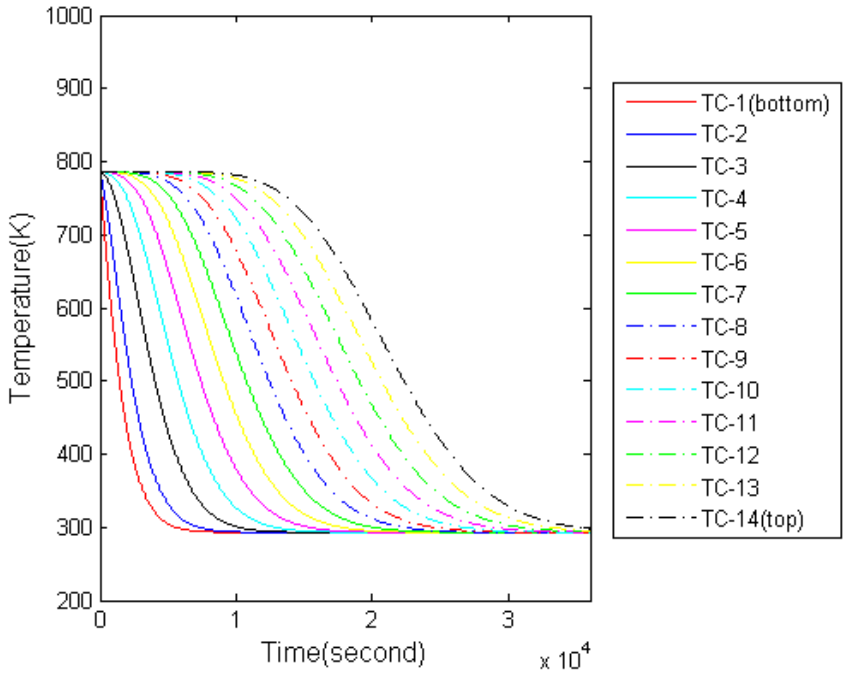

Figure 3.11 Temperature distribution of the packed bed for 25 kg/s air mass flow rate

In order to utilize all the stored heat energy in a packed bed TES tank in a given maximum cascade expansion period, approximately $9x10^5$ kg air entering the TES at ambient temperature should pass through the tank. Hence, the volume of the air storage cavern should be large enough to accommodate that change in air within the cavern tank without exceeding the maximum and minimum pressure limits. In order to determine the minimum volume of the air storage cavern, $9x10^5$ kg of air should be used starting from the maximum pressure of the cavern to the minimum pressure limit of cavern. By using the pressure limits of the cavern and total mass of the air, the minimum volume of the tank is calculated by equation (2.5.5). If the maximum and minimum pressure of the tank is assumed 70 and 45 bar respectively, a minimum volume of $3.027x10^4$ m^3 is sufficient to store $9x10^5$ kg within the maximum and

minimum pressure limits. As a result, a relation is expected between the size of the energy storage tank and a minimum size of the cavern for the same maximum and minimum cavern pressure limits, initial temperature of the TES tank before the cascade expansion period and cascade compression and expansion period. For the 10 hours cascade compression and expansion period, 70 and 45 bar maximum and minimum cavern pressure limit and 786 K inlet temperature of TES tank, the sizing ratio (R_s) of volume of TES and cavern is approximately calculated as 0.0166 using equation (3.6.1).

$$R_s = \frac{V_{TES}}{Min.V_{cavern}} \tag{3.6.1}$$

where V_{TES} is:

$$V_{TES} = \pi R_{TES}{}^2 L_{TES} \tag{3.6.2}$$

and $Min.V_{cavern}$ is:

$$Min.V_{cavern} = \frac{P_{\max} - P_{\min}}{mRT} \tag{3.6.3}$$

The flow chart of the methodology is given in the Appendix B. The volume of the cavern generally depends on geological formation of the earth. Hence the volume of the cavern can be undersized or oversized according to minimum volume of the cavern.

3.7 Pressure Limits and Size of Air Storage Cavern

In an AA-CAES system air storage is the most critical process that directly affects the energy production. However the volume of the air storage cavern depends on geological formation. Moreover, for a cavern, there should be maximum and minimum operational pressure limits in order to maintain the AA-CAES system to

allow pressure load to cycle without any deformation. For the charging stage, AA-CAES system is not allowed to compress the air more when the air storage cavern pressure (P_c) is at the maximum ($P_{c,max}$). This state is defined as "Maximum Capacity is Reached (max.cap)" in the system. The energy released from wind turbines during that period cannot be stored. Moreover, during the compression stage pressurized air passes through the packed bed TES and loses some amount of its pressure. If the pressure of the air (P_a) at the outlet of the packed bed TES is lower than cavern pressure (P_c) at that instant, air cannot be pumped into the air storage cavern. This is defined as a "Lack of Storage (L.O.S)" in the AA-CAES system.

For the discharging period, AA-CAES system is not allowed to expand more stored air when the stored air pressure is at the minimum level ($P_{c,min}$). This state is defined as "Minimum Capacity is Reached (min.cap)" in the system. Both pressure limits and the size of the air storage cavern determine how much pressurized air can be stored or expanded during the stages of charging and discharging. Thereby, the cavern volume and pressure limits determine the number of hours that the system does not satisfy the selected site demand. The assessment of the flow chart of the AA-CAES system is given in the Appendix C. The example of the effects of pressure limits on different volumes for the AA-CAES system will be given in Chapter 4.

3.8 System Performance Metric

As was stated in previous sections, for some of the hours in a year the AA-CAES system tries to compensate for the energy gap between production and demand and for some of the hours in a year the AA-CAES system tries to store the excess energy of energy production.

If the condition $E.P - E.D < 0$ occurs, the AA-CAES system may not satisfy the energy demand of selected site due to limitations of the system such as pressure limit and TES capacity. In order to see the effects of system parameters and limits, a system performance metric "*the number of Hours that the System canNot Satisfy the*

Demand (HSNSD)" is used to compare the effects of changes in all system parameters on the system performance.

3.9 The Assessment of System Design Parameters

In this thesis, the effects of system design parameters on the system performance are investigated. In Table 5, selected system design parameters are tabulated. In order to see the impacts of each parameter on the system, HSNSD performance metric is used. During the exploration of one term's effect on the system other parameters remain constant. The impacts of changes in the values of selected parameters on system performance will be presented in a case study in Chapter 4 in detail.

Table 5 System Design Parameters

1	Size of the thermal energy storage tank
2	Size of the air storage cavern
3	Minimum turbine operation temperature limit
4	Air mass flow rate that goes to turbine
5	Initial fullness of the air storage cavern

3.9.1 Effects of the Size of the Thermal Energy Storage Tank

In Section 3.5, determination of the size of the TES tank is explained. In this section it is investigated what would happen in the annual system performance if the length or the radius of the TES tank were increased or decreased relative to its initial size. When one design parameter is changed, all other parameters are kept constant.

3.9.2 Effects of the Volume of the Air Storage Cavern

The size of the air storage cavern is important for energy storage concept. The determination of the minimum volume of the air storage cavern is explained in

Section 3.6. In this section, it is investigated what would happen in the annual system performance if the volume of the air storage cavern is decreased or increased relative to this the minimum volume.

3.9.3 Effects of the Air Turbine Operation Temperature on System Performance

The air temperature that goes to the turbine is an important parameter for power production calculation. In addition to that, it directly influences turbine performance. During the turbine stage, the hot air coming from TES tank starts to expand to extract the power. During the expansion, air is getting colder and there should be a temperature limit for a turbine minimum operation temperature in order to prevent the turbine blades from becoming too brittle. In this assessment, the effect of minimum turbine operation temperature on annual system performance is investigated. An example of this parameter study is given in Chapter 4.

3.9.4 Effects of the Air Mass Flow Rate that Goes To Turbine on System Performance

Mass flow rate of air is a critical factor for an increase or decrease in power production of the turbine. In this parametric study, the mass flow rate of air to the turbine is an input to the model and it influences both the air temperature that goes to the turbine and the rate of air consumption from the air storage cavern. During the discharging, cold air is extracted from the cavern in a certain amount and that amount of air makes heat transfer with the TES tank. As a result of this process, air gets warm and is ready to produce power at the turbine stage. At this point increasing the mass flow rate unnecessarily may consume the thermal energy in TES tank more rapidly. For the expansion stage, the turbine may not work due to cold air that could not warm up as a result of rapid consumption of the stored thermal energy. How the system performance is affected by the change in the mass flow rate input will be discussed in Chapter 4 more detailed.

3.9.5 Effects of the Initial Fullness Ratio of Air Storage Cavern on System Performance

In the previous sections, the importance of the size of the air storage cavern is discussed. In addition to the air tank storage size, the initial fullness ratio of the air storage cavern is another parameter that affects the system performance directly. During the charging, the system starts to feed pressurized air to the air storage cavern. Conversely, in the discharging stage, the system starts to consume pressurized air. If the air storage cavern is initially at its minimum limit (empty) and the first process is discharging, there will be no expansion due to the air storage pressure being at its minimum limit (min.cap). In contrast, if the air storage cavern is initially between its minimum and maximum pressure limits, it may initially be able to supply air if the first process is discharging. The duration how long air storage cavern supplies air to the turbine is changed based on a initial fullness ratio of the tank will be discussed in detail in Chapter 4.

3.10 Conclusion

In this chapter, a methodology for sizing and assessment of wind integrated AA-CAES system is introduced. First, a specific location where AA-CAES plant is built is determined and wind farms power production and energy demand profile belonging to the selected site are gathered. An hourly comparison between energy production and energy demand data is made and according to sign of a difference between demand and production, energy storage or energy consumption profiles are obtained. By using these profiles, maximum cascade compression and expansion durations are determined. The sizing of packed bed thermal energy storage tank and minimum volume of the air storage cavern are calculated according to the maximum cascade compression and expansion periods respectively. System limitations such as maximum and minimum pressure limits of the cavern, and pressure loss in packed bed TES are presented under different conditions of the system. Finally, several parametric studies about system design parameters with sizing are introduced.

CHAPTER 4

CASE STUDY: APPLICATION OF METHODOLOGY TO DATÇA PENINSULA

In this chapter, the application of the methodology given Chapter 3 to Datça Peninsula is presented.

4.1 Site Selection for AA-CAES Model

In the previous chapter, site selection is stated to be an important parameter for AA-CAES model. For this study, the Datça Peninsula is chosen as the location where the AA-CAES plant is built. The main reason for selecting the Datça Peninsula is the DARES Wind Farm which is located in Datça and supplies 81GWh electricity in a year [38]. In addition, Datça is wealthy in terms of underground cave and aquifers however; there are not any proven cavern that is suitable for AA-CAES air storage.

Figure 4.1 DARES Datça wind farm [38]

4.2 Power Calculation of Wind Farm

4.2.1 Wind Speed Information of Datça

Wind speed information is taken from the TMY2 data of Datça Peninsula. For one year, hourly wind speed data are presented in Figure 4.2 for Datça.

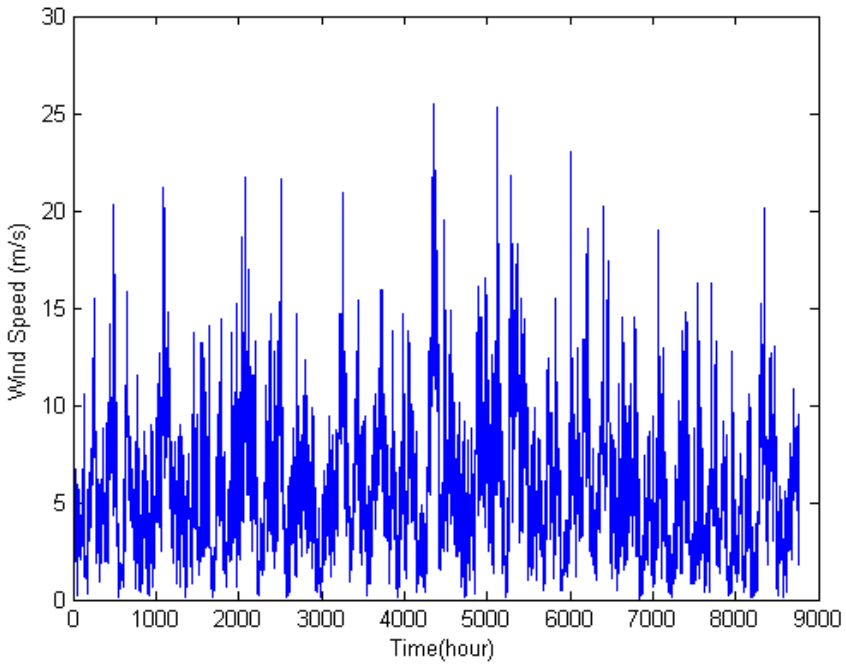

Figure 4.2 Hourly wind speed for Datça for a year

The mean value of wind speed is 5.68 m/s and it is assumed that the elevation of wind speed data is located at 10 m above ground level. Wind turbines hub height data are taken from Table 6. As a result of this, wind speed at the hub height is calculated by the correlation given in equation (3.1.1). The mean value of corrected wind speed for the year is 7.14 m/s. In Figure 4.3, an example of comparison of wind speed data and corrected wind speed data is given for January. It can be seen that hourly comparison of corrected wind speed is approximately 24% higher than the wind speed for Datça for January. This ratio is same for corrected wind speeds and wind speeds for all data for Datça.

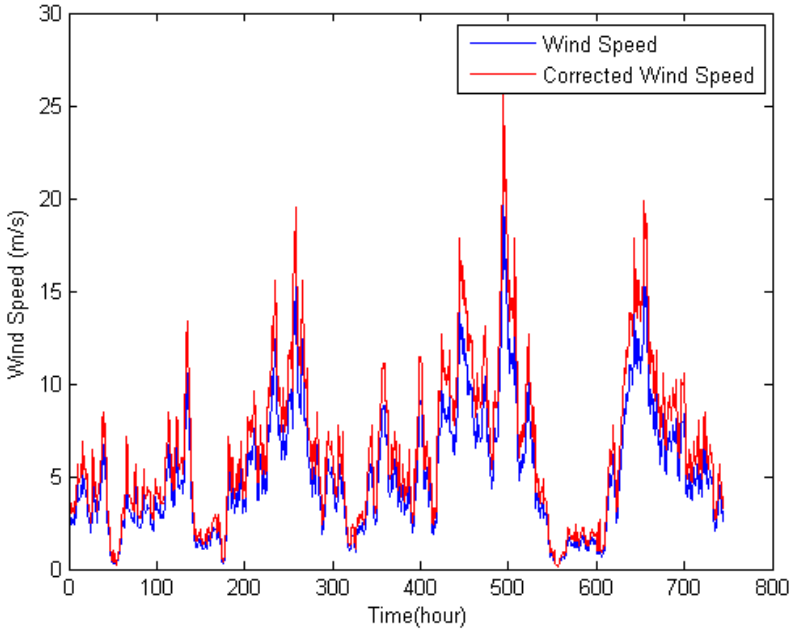

Figure 4.3 The hourly wind speed and corrected wind speed for January for Datça.

4.2.2 Power Production of DARES Wind Farm

In the DARES wind farm, there are 28 Enercon 800kW (E-48) and 8 Enercon 900kW (E-44) wind turbines available to produce electricity. In Table 6, the technical specifications of the E-48 and E-44 are given. In addition, both Figure 4.4 and Figure 4.5 show the calculated power versus wind speed curves for E-48 and E-44 respectively.

Table 6 Technical Specifications of E-48 and E-44 [37]

Tech. Spec.	Enercon E-48	Enercon E-44
Rated Wind Speed	14 m/s	16 m/s
Rated Power	800 kW	900 kW
Rotor Diameter	48 m	44 m
Hub Height	50 m	50 m
No. of Blades	3	3
Cut-in Cut out Speed	3-28 m/s	3-28 m/s

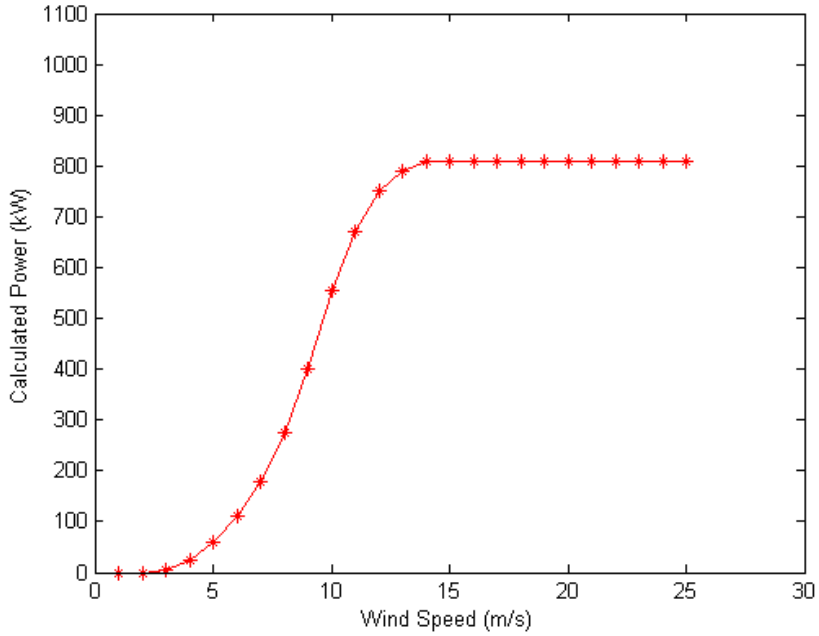

Figure 4.4 Enercon E-48 power vs. wind speed curve (f_{E-48}) [37]

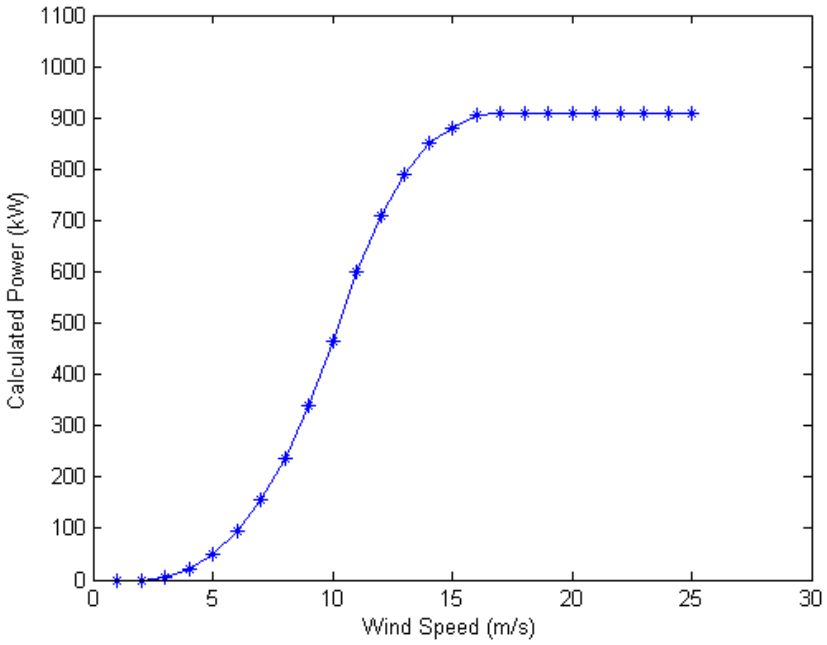

Figure 4.5 Enercon E-44 power vs. wind speed curve (f_{E-44}) [37]

Hourly total power production of DARES wind farm is estimated by using equation (4.2.1).

$$Total\ Wind\ Power = n\_48\, f_{E-48}\left[V_{corr.}\right] + n\_44\, f_{E-44}\left[V_{corr.}\right] \qquad (4.2.1)$$

The right-side of the equation can be changed according to the number and types of wind turbines for different sites. In Figure 4.6, an example of hourly power production of the DARES Wind Farm for January using equation (4.2.1) is presented.

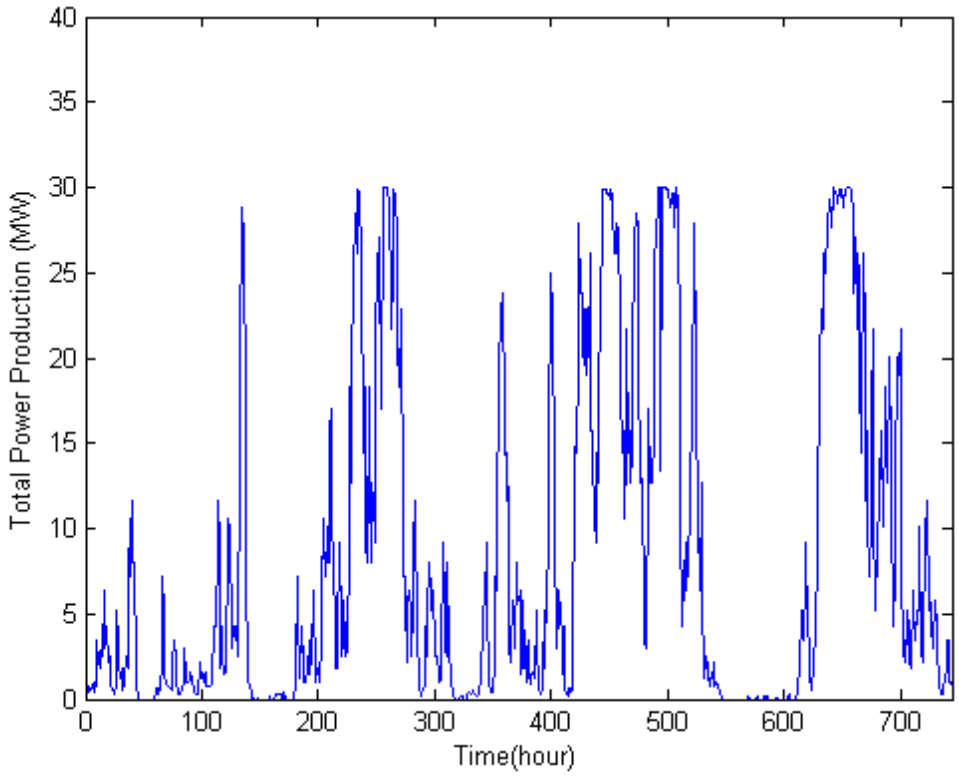

Figure 4.6 Hourly total power production for DARES Datça wind farm for January

4.3 Comparison of Energy Production of DARES Wind Farm and Datça Peninsula Energy Demand Data

In this energy storage methodology, the major goal is to store excess wind energy for later usage. If the demand is higher than the wind turbine power production the

stored energy is used to compensate the energy deficiency. In order to determine whether to charge or discharge the AA-CAES for the Datça Peninsula, the DARES wind farm power production and Datça Peninsula demand data are compared in the AA-CAES model. The energy production data is obtained from TMY2 data given in Section 4.2.2 and energy consumption data is obtained from Dr. Merih Aydinalp who obtained energy consumption data from Turkish Electricity Transmission Company (TEİAŞ) and made post processing for year 2009 for Aegean region. Datça energy consumption data is scaled according to population ratio of the Datça Peninsula to the Aegean region. As stated that wind and demand data are not gathered for the same year due to using TMY2 data set. Ideally, it is better to get energy production and demand data for the same year. In Figure 4.7, hourly power consumption for Datça Peninsula for January is represented. The hourly difference of power production and power consumption data of Datça is given in Figure 4.8. This energy difference is one of the main inputs to AA-CAES model.

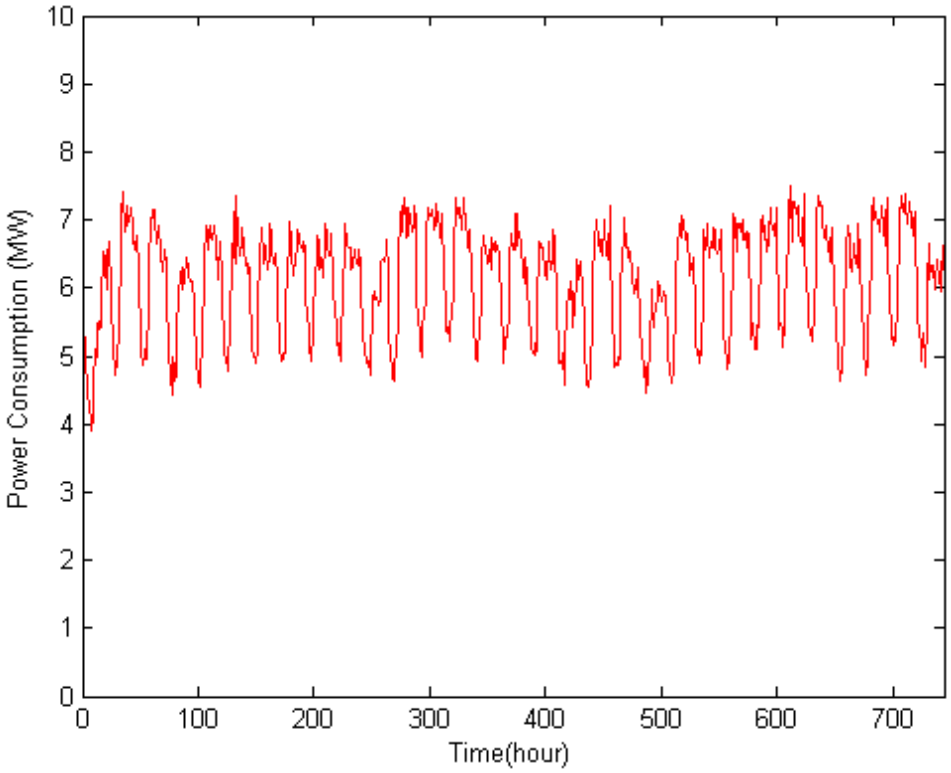

Figure 4.7 Hourly power consumption data for Datça Peninsula for January

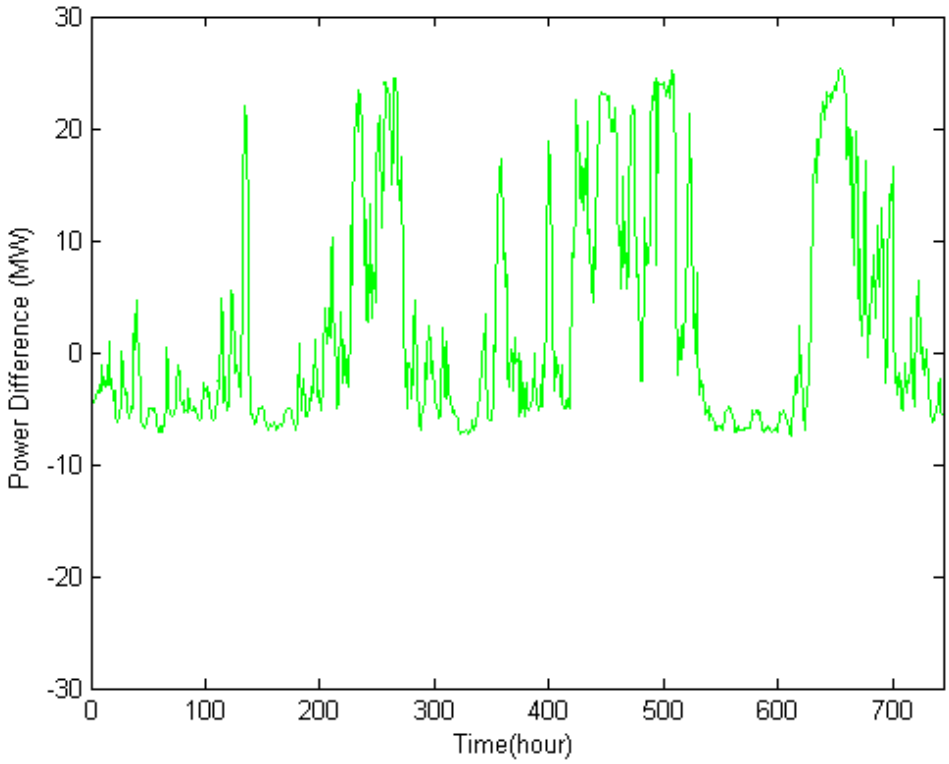

Figure 4.8 Hourly power difference for Datça Peninsula for January

As can be seen from Figure 4.8, for any hour period energy difference values can be grater or less than zero. For the negative values of the energy difference, if the AA-CAES is not empty, the system starts to operate the turbine to generate the power to compensate the demand. Conversely, for the positive values of the energy difference, if the AA-CAES is not full the system starts to operate the compressor to store excess energy. As a result of this comparison, 4710 hours of a year system tries to compensate for the negative energy difference by discharging while on the other hand for 4050 hours of a year system tries to store excess positive energy difference by charging. Hence AA-CAES system tries to compensate for the negative energy difference for 4710 hours by using the excess energy 4050 hours. According to the present model for Datça, there is 32.6 GWh of excess energy that can be obtained from the wind turbines to store for later usage.

4.4 Determination of the Size of the Packed Bed TES and Air Storage Cavern

4.4.1 Determination of the Size Estimation of the Packed Bed TES

In this model, for Datça the maximum cascade compression period is 83 hours between the hours of 14th September 12:00 and 17th September 22:00. During that period, the DARES wind farm produce approximately 1.488 GWh of excess electricity. This energy can be used in the compressor to pressurize the air and charge the system for that period. The average mass flow rate of the air in the compressor is approximately calculated as 23.5 kg/s for this period by using equation (2.2.11). The properties of air, pebbles and thermal energy storage tank used in the heat charging model are given in Table 7. By assuming a length of the TES tank, the radius of TES tank is iterated in the heat charging model until a viable radius for that length is obtained for heat storage without considering the pressure drop across the packed bed TES tank as discussed in Section 3.5.

Table 7 Properties of Air, Pebbles and TES Tank at 800 K

Specific heat capacity of the air	1098 J/kg.K
Specific heat capacity of the pebbles	860 J/kg.K
Void ratio of the tank	0.4
Average pebble diameter	0.05 m
Dynamic viscosity of air	0.00008216 Pa.s
Thermal conductivity of pebble	2.8 W/m.K
Thermal conductivity of the air	0.065 W/m.K
Density of the air	0.4412 kg/m^3
Density of the pebbles	2460 kg/m^3

In this case studies, lengths considered for the energy storage tank are 10, 20, 30, 40, 50, 60 and 70 meters. For an each length considered, a viable radius is calculated for

the heat charging model and the results are presented in Table 8 for DARES Datça AA-CAES system.

Table 8 Length and Radius Pairs

Length (m)	Radius (m)	Total Mass (kg)
10	10.2	$2.79x10^6$
20	7.5	$3.02x10^6$
30	6.2	$3.09x10^6$
40	5.4	$3.13x10^6$
50	5.0	$3.35x10^6$
60	4.6	$3.41x10^6$
70	4.3	$3.47x10^6$

In Table 8, the length and its corresponding radius in order to store all heat energy released during the compression are given. For a constant mass flow rate 23.5 kg/s, the on pressure drops across the packed for each of these length-radius pairs calculated by equation (2.4.1) are given Figure 4.9.

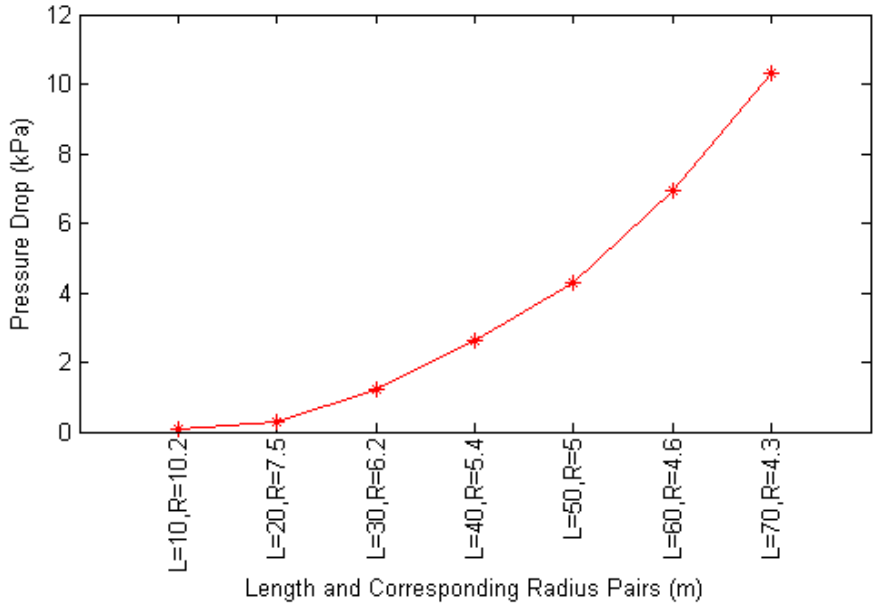

Figure 4.9 Pressure drop of air across the packed bed TES tank for different length and radius pairs

Both the length and the radius affect the pressure drop of air in the TES tank. As can be seen from equation (2.4.1), an increase in the radius of the TES tank decreases the pressure drop due to decrease in superficial fluid velocity. On the other hand, an increase in the length of the TES tank increases the pressure drop due to the friction. As shown in Figure 4.9, as the pressure drop is increased although the radius of TES is decreased. This is because of the percentage of increment of the length is greater than square of percentage of decrement of the radius.

From Figure 4.10, the volume of the TES tank for different length and radius pairs scales almost linearly from 3.2 x10^3 to 4.1 x10^3 m^3 as the length increases from 10 to 70 m.

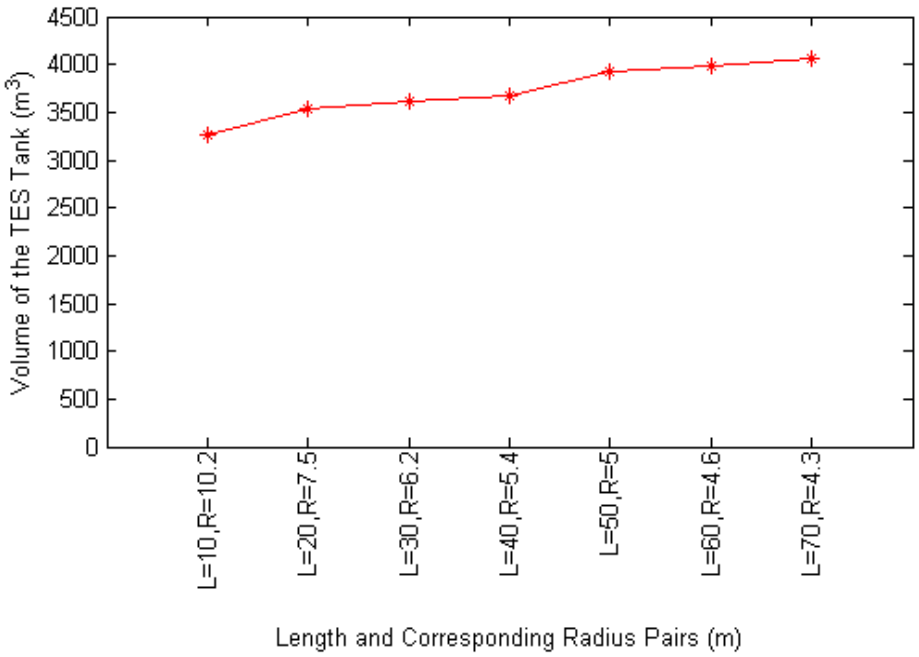

Figure 4.10 Volume of the TES tank for given length and radius pairs

In heat transfer phenomenon, an increase in the radius of the TES tank decreases the convective heat transfer coefficient shown in Figure 4.11 for the same mass flow rate of 23.5 kg/s for different lengths. For the convective heat transfer coefficient, the length has no direct effect on convective heat transfer coefficient. Hence a decrease

in the radius of the packed bed increases the convective heat transfer coefficient due to increase in the Reynolds number. This is important for the heat transfer rate because it is necessary to make rapid heat transfer for AA-CAES system in the limited charging and discharging process.

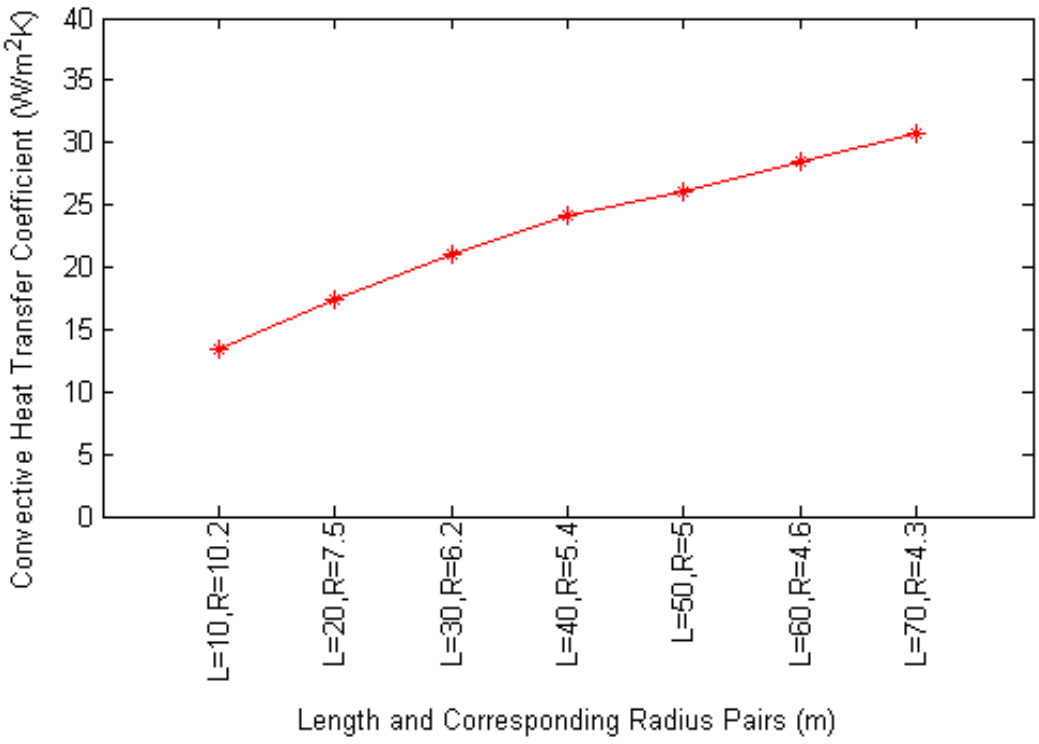

Figure 4.11 Convective heat transfer coefficient for different length and radius pairs

In order to select appropriate length and radius pairs for the packed bed TES tank in terms of system performance considering both heat transfer rates and pressure drop, these pairs are put in the AA-CAES model and HSNSD value is calculated for each pair under the same conditions (10 kg/s turbine mass flow rate, Initially full cavern and size of the air storage cavern is 10^6 m^3). For an AA-CAES system located in Datça, HSNSD values are presented in Figure 4.12.

In Figure 4.12, HSNSD values are minimum for L=40 m and R=5.4 m TES tank. AA-CAES system which has the minimum HSNSD value will give better energetic

performance for a specified condition. The effect of change in the length or radius on the "HSNSD" will be given in Section 4.6.1 in detail .

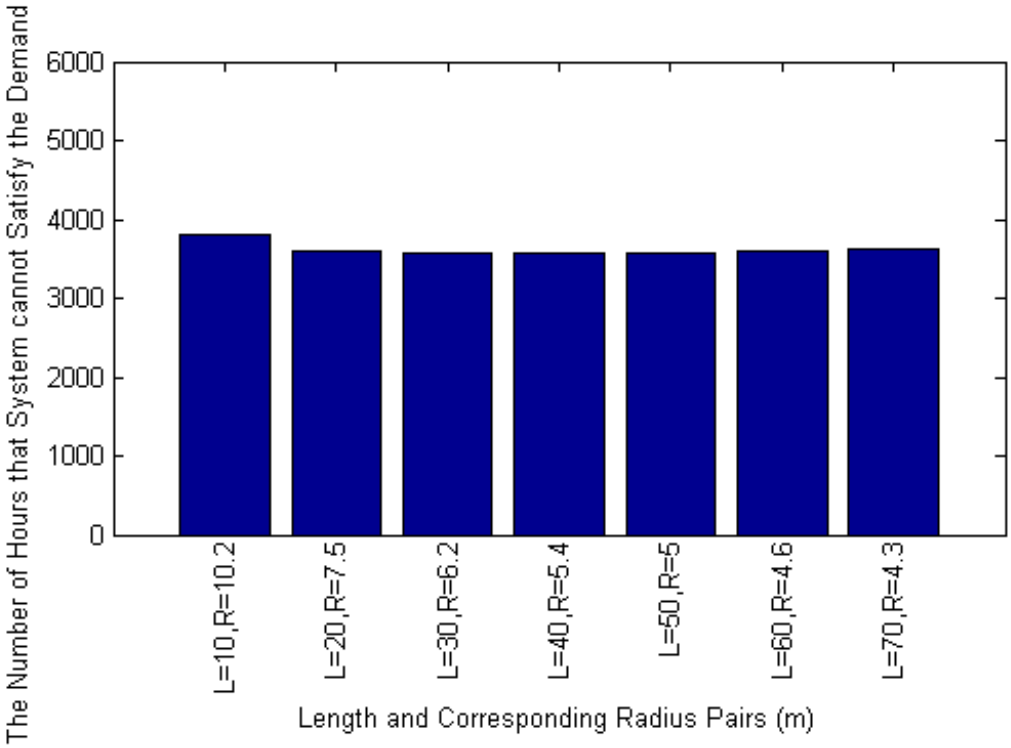

Figure 4.12 HSNSD for calculation length and radius pairs of TES tank

As stated that HSNSD value depends on both energy production and energy demand of the AA-CAES system. The capability of power production is different from HSNSD performance metric because it only presents how much power is produced in a given period (year). The capability of power production results for each pairs is given in Figure 4.13 for a year. From Figure 4.12, it can be said that R=5.4 m. and L=40 m TES tank provides the highest energy to the air for the same mass flow rate and duration among the given pairs for a year. Hence, the power production capacity is supported to HSNSD value which is presented in Figure 4.12.

From Figure 4.12 and Figure 4.13 except L=10m, R=10.2m, any of the last 6 cases yields similar performance and the final size may be selected based on other considerations such as costs or size limitations in terms of length and radius. In the

next section minimum volume of the cavern is calculated according to L=40m and R=5.4m TES tank which is the best option among others without considering cost and size limitations.

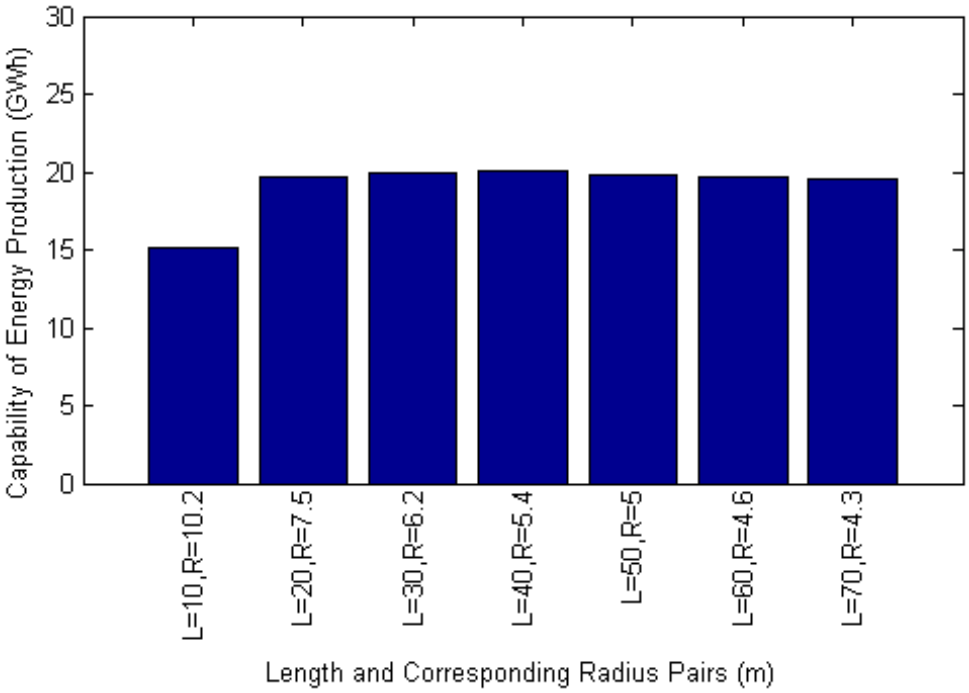

Figure 4.13 The capability of power production of AA-CAES system according to given length and radius pairs in a year

4.4.2 Determination of Minimum Volume Estimation of the Air Storage Cavern for Datça

In the previous section, the size of the packed bed TES system is calculated according to total excess energy of the maximum cascade compression hours of year 2009. The minimum volume of the cavern should be large enough to store air that can use the total capacity of the TES tank during the maximum cascade expansion period. For Datça, maximum cascade expansion period is found 134 hours between hours 21st June 21: 00 and 27th June 9:00. For 40 m length and 5.4 m radius TES tank, air mass flow rate is approximately calculated as 13 kg/s in the heat discharging model to consume all stored thermal energy in the maximum cascade compression

period. The total amount of air should be stored is calculated approximately 6.271×10^6 kg. In order to find the minimum cavern capacity for the sizing and assessment methodology, that amount of mass should be stored between the maximum and minimum pressure limits of the cavern. In addition, the temperature of the air in cavern is assumed to be constant (293 K) during the maximum cascade expansion period. From Table 9, maximum and minimum cavern pressures are taken from the Huntorf CAES plant operational pressure which are 70 and 45 bar respectively [34]. By using equation (2.5.5) the minimum volume of the air storage cavern should be approximately 2.1×10^5 m^3. The sizing ratio (R_s) of TES tank and minimum volume of the cavern is found as 0.005 for 83 hours compression cascade period and 134 hours expansion cascade period.

4.5 The Assessment of Pressure Limits and Size of the Air Storage Cavern

In the Datça Peninsula, Tekesuyu aquifer is one of largest aquifers discovered in Turkey. Although it is not proven that Tekesuyu can be used as an air storage cavern for CAES, it is taken as an air storage cavern by making assumptions for the size and pressure limits of the cavern to make some parametric studies for the year 2009.

In this section, the number of hours for which the air storage cavern is at its maximum air capacity (max.cap), the number of hours the compressor cannot pump air into the cavern due to the pressure limit (L.O.S), and the number of hours the air storage cavern cannot send any air to turbine (min.cap) are studied for Datça by changing the volume of the air storage cavern and mass flow rate of the air that goes to the turbine. For this study, the parameters given in Table 9 are taken into consideration to determine max.cap, min.cap and L.O.S. Mass flow rates of turbine and air storage cavern size, both of which are not presented in Table 9, can be selected different values in order to increase the impact of the assessment.

Table 9 Constant System Parameters

Maximum air storage cavern pressure	70 bar
Minimum air storage cavern pressure	45 bar
Compression/Expansion Ratio	72/42
Initial fullness of air storage cavern	Full Capacity (70 bar)
The number of hours system should produce energy	4710
The number of hours system should store excess energy	4050
The size of packed bed TES	L=40 m R=5.4 m
The temperature of air in air storage cavern	293 K

4.5.1 The Assessment of Minimum Capacity of Air Storage Cavern (min.cap)

Under the given conditions in Table 9, how the change in volume of air storage cavern affects the min.cap value at the given minimum and maximum pressure limits for constant 5kg/s turbine mass flow rate is investigated. As can be seen from Figure 4.14, if the capacity of the air storage cavern volume is increased, the operation of the AA-CAES turbine is not affected significantly from the minimum pressure limit of the cavern (min.cap). From Table 9, the number of total hours that AA-CAES system should produce energy is 4710. If the volume of Tekesuyu aquifer is assumed 10^3 m^3, for 4440 hours of a year AA-CAES system cannot produce energy due to lower pressure limit of the cavern (min.cap) without considering whether system can

satisfy the demand or not. Hence, AA-CAES have a chance to operate its turbine approximately 270 hours which is equal to 5.8% of the number of total hours that the system should produce energy due to the minimum pressure limit of the cavern.

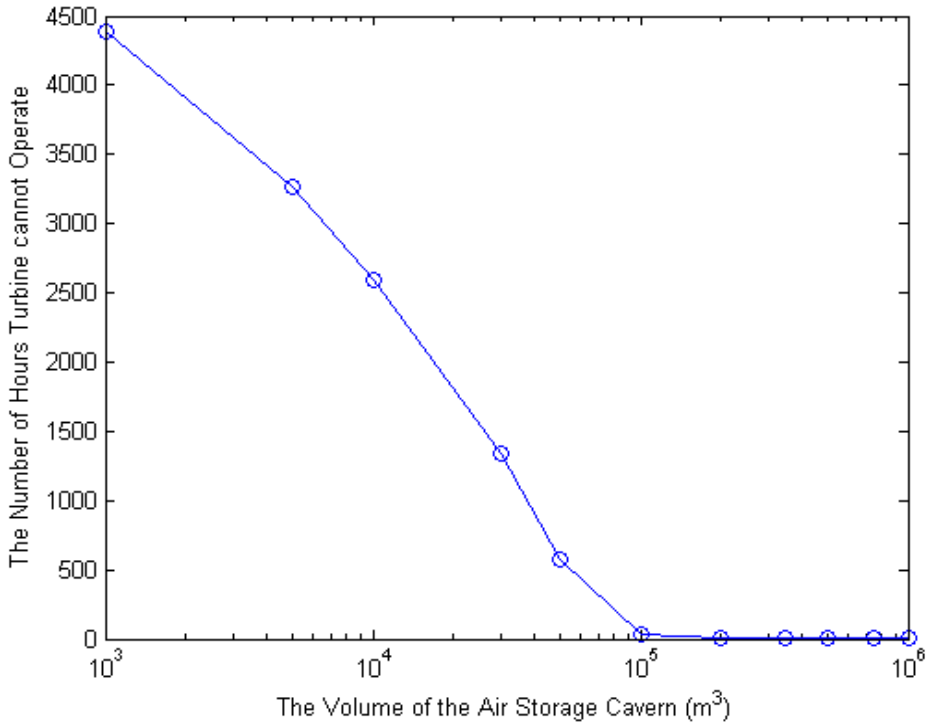

Figure 4.14 The number of hours AA-CAES turbine cannot operate for 5 kg/s

If the volume of the Tekesuyu aquifer is taken as $2x10^5$ m^3, AA-CAES system can operate its turbine 100% of the required time without being influenced by the minimum pressure limit of the cavern (min.cap) for the given constant mass flow rate of 5kg/s. For the different mass flow rate values and initial fullness of the air storage cavern, the curve given in Figure 4.14 can obviously change. For an AA-CAES system, the operation of turbine is not the same as the compensation of energy demand. In order to meet the demand, not only a high mass flow rate is sufficient but also temperature of the air is important. In order to explain how min.cap is calculated, Figure 4.15-16 are presented.

Figure 4.15 and Figure 4.16 are examples of pressure variations in the cavern for 8760 hour period. During the period the air storage cavern can be charged or discharged according to the comparison of energy production and demand data. The mass flow rate of the charging period directly depends on wind turbine power production; however for discharge period turbine air mass flow rate is taken 5kg/s as a constant. In these figures, the black line shows the minimum pressure limit of the cavern. From the figures $5x10^4$ m^3 air storage cavern reaches minimum pressure limits 576 hours of the total 8760 hours in a year and 10^5 m^3 air storage cavern reaches minimum pressure limits 34 hours of 8760 hours for 5 kg/s turbine air mass flow rate. Hence min.cap values in Figure 4.14 are obtained as the same procedure given Figure 4.15and Figure 4.16 for different volume of the air storage cavern for 5kg/s.

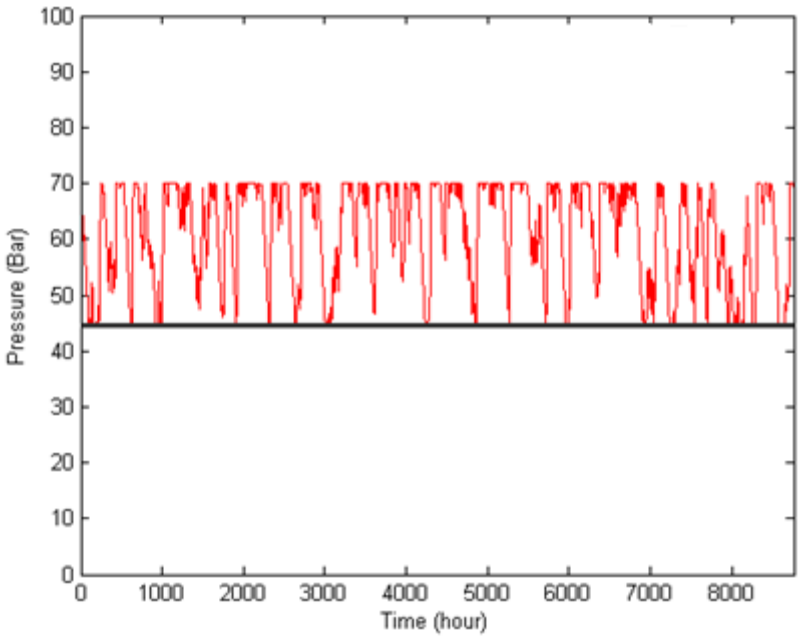

Figure 4.15 Pressure variation of the air storage cavern ($5x10^4$ m^3) for 5 kg/s

In Figure 4.17, how the min.cap value of the system is affected by changes in the mass flow rate of air that goes to turbine is presented. The minimum and maximum pressure limits of the cavern are fixed and taken as the same as Table 9.

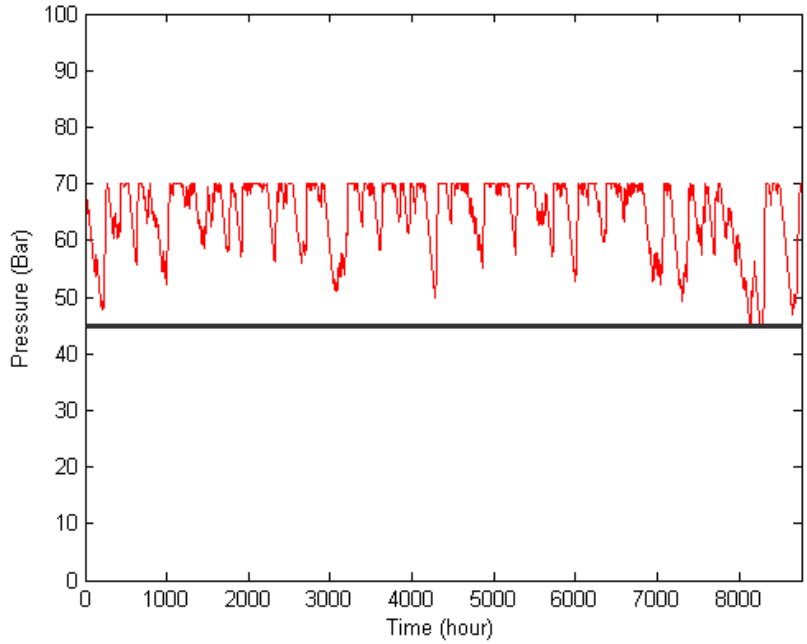

Figure 4.16 Pressure variation of the air storage cavern (10^5 m^3) for 5 kg/s

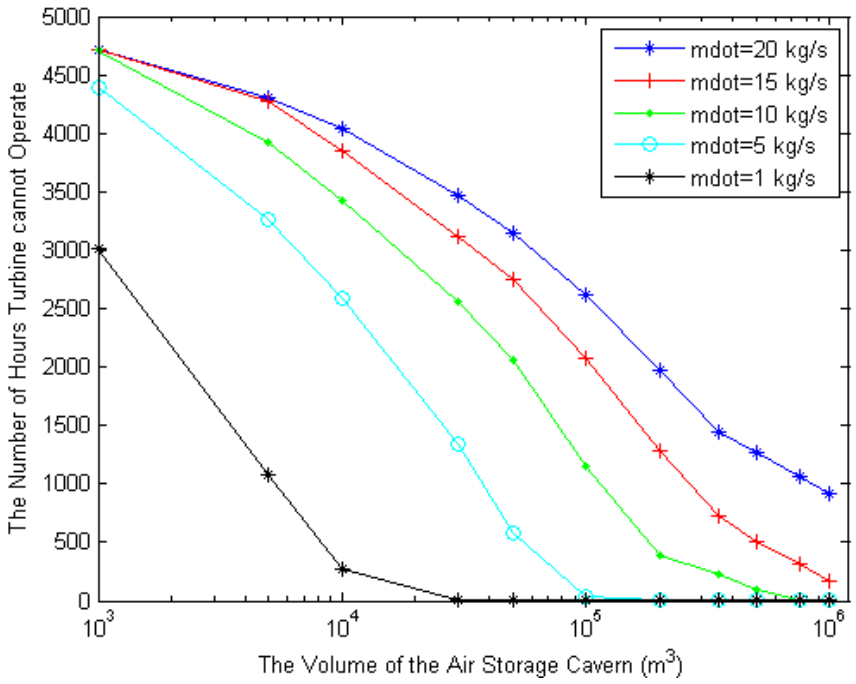

Figure 4.17 The number of hours AA-CAES turbine cannot operate due to minimum capacity of the cavern in different mass flow rate

From Figure 4.17, if the mass flow rate of air in turbine is increased, the usable air in the cavern is quickly depleted and the number of hours AA-CAES turbine cannot operate (min.cap) is increased due to the minimum cavern pressure limit. Although a decrease in the mass flow rate of air in the turbine decreases the min.cap value, low mass flow rates of the air in the turbine may not be able to satisfy the energy demand due to low mass flow rate of the air in turbine stage; this issue is explored in Section 4.6.2. As shown in Figure 4.17, if the turbine mass flow rate is equal to 1 kg/s, the cavern pressure does not reach the minimum (min.cap) for cavern volumes greater than $3x10^4$ m^3. Likewise, if the turbine mass flow rate is 10 kg/s, the cavern size should be greater than $5x10^5$ m^3 to avoid reaching the minimum cavern pressure.

4.5.2 The Assessment of Maximum Capacity of Air Storage Cavern (max.cap)

In Datça, for 4050 hours, compressor must be operated for year 2009 to store excess energy; however, during some parts of the year, the compressor should not be operated because the air pressure in the cavern is at its maximum level. As a result of this, some amounts of energy produced in wind turbines are not stored and lost. In this section, the relation between the number of hours that compressor should not be operated (max.cap) and the change in volume of the cavern is investigated for different turbine mass flow rates. If initially the air storage cavern is full at the beginning of the year 2009, how max.cap value varies with changes in cavern volume for fixed turbine mass flow rate 20 kg/s is presented in Figure 4.18.

As can be seen from Figure 4.18, an increase in the volume of the cavern decreases the number of hours that the cavern pressure reaches its maximum limits (max.cap) for the maximum pressure limit of the tank given in Table 9. This means that the lower volume of the air storage cavern has high pressure fluctuations for the same mass changes when compared to larger volume of the cavern. From Figure 4.18, for 20 kg/s turbine air mass flow rate, 10^3 m^3 cavern reaches 3522 times to its maximum capacity; on the other hand, 10^6 m^3 cavern never reaches its maximum capacity and compressor always operates.

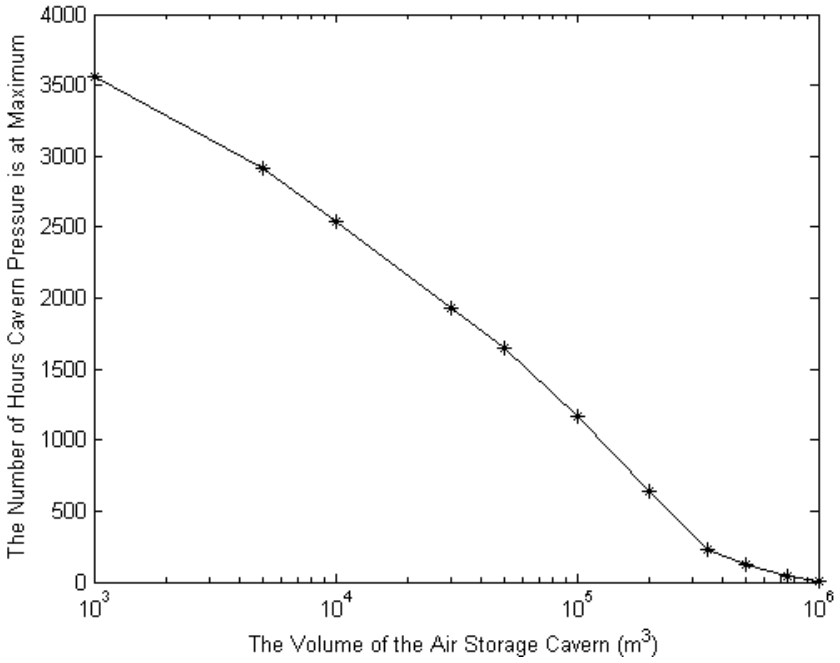

Figure 4.18 The number of hours cavern pressure is at max. for 20 kg/s

In Figure 4.19, the relation between max.cap, mass flow rate of air for turbine and air storage cavern size is given for an initially full air storage cavern.

As can be seen from Figure 4.19, an increase in the mass flow rate of the turbine leads to a decrease in the max.cap value because the stored air is consumed quickly due to higher turbine mass flows rate; hence, the pressure of the is less likely to reach its maximum level. Moreover, after a specific volume for lower turbine mass flow rates, the curves start to become steady although the volume is increased. The two main reasons for this are the initially full tank and the value of the mass flow rate of the turbine. If the total compressed air is higher than the total expanded air in the throughout the year, there should always be a period that the air storage cavern reaches its maximum capacity for lower turbine mass flow rate. In addition, for a specific turbine mass flow rate, increases in the volume of the cavern decreases the pressure fluctuations in the cavern. Examples of this are given in Figure 4.20 and Figure 4.21 for 10^5 m^3 and $3x10^5$ m^3 tank volumes respectively.

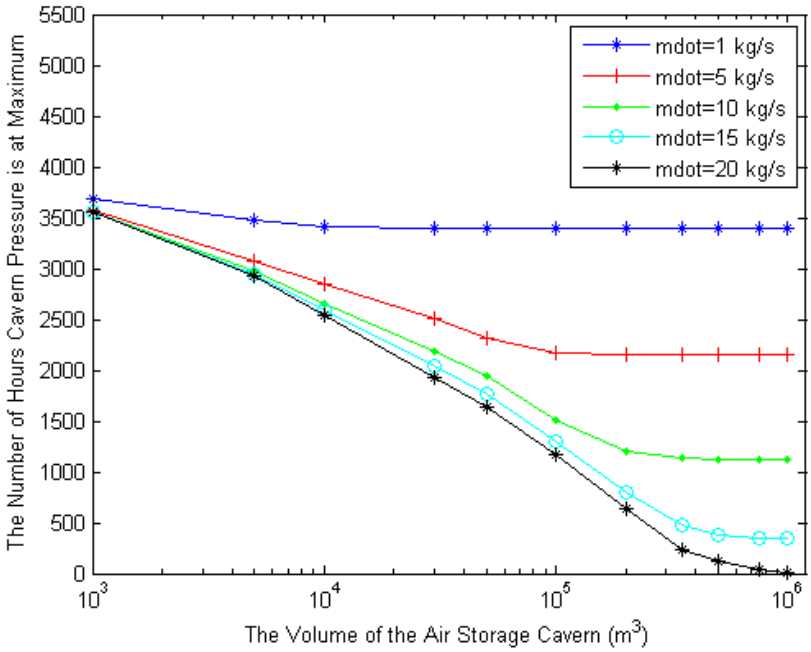

Figure 4.19 Max.cap vs. the volume of air storage cavern

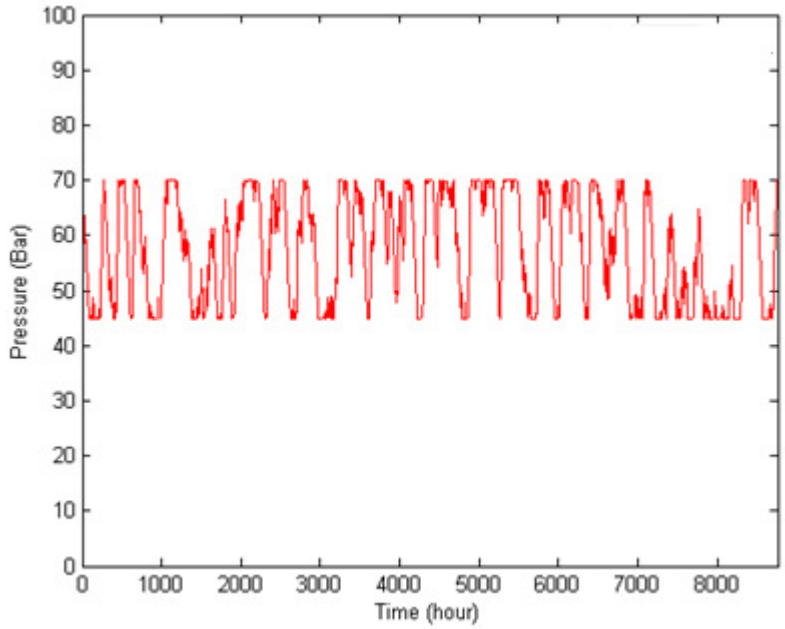

Figure 4.20 Pressure change of the air storage cavern for a year for 10^5 m^3 volume

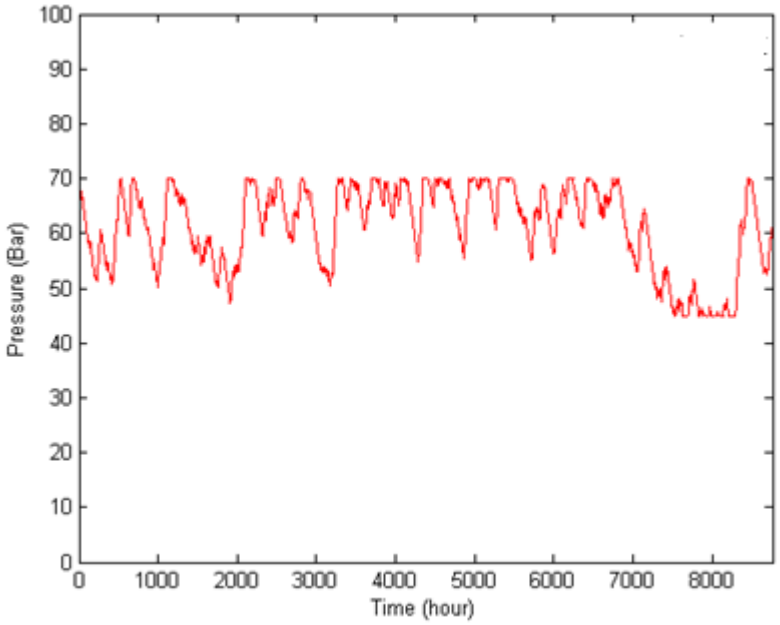

Figure 4.21 Pressure change of the air storage cavern for $3x10^5$ m^3 volume for a year

Consequently, in order to decrease the max.cap value of the system, the air mass flow rate of the turbine and air storage cavern should be increased as much as possible to use the packed bed thermal energy storage tank energy efficiently.

4.5.3 The Assessment of Lack of Storage (L.O.S)

It was stated that during the compression and expansion stages the air experiences a pressure drop when it passes through the TES tank. Due to this pressure drop, the air may not be pumped to the air storage cavern because of the high pressure in the air storage cavern (L.O.S). In Table 9, it is seen that the air is compressed up to 72 bar and the maximum cavern storage pressure is 70 bar. For the charging period, 2 bars, which is the difference between the pressure after the compressor and maximum cavern pressure limit, tries to not to influence from pressure drop across the packed bed. Hence the AA-CAES system must have compressor which has very large compression ratio to overcome the maximum pressure limit of the cavern and pressure drop. The relation between L.O.S value and size of the TES tank such as length and radius is presented in this section.

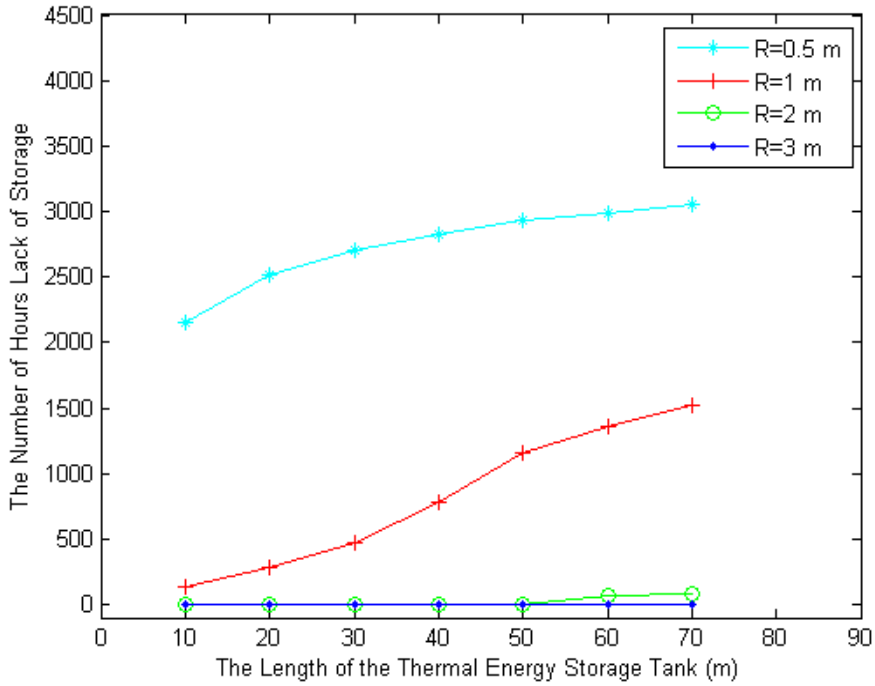

Figure 4.22 Effects of size of TES on air storage

In Figure 4.22, for a $4x10^5$ m^3 cavern volume and 20 kg/s turbine mass flow rate, an increase in the length of the packed bed TES increases the L.O.S values and increases in the radius of the TES tank decreases the L.O.S. values. To get zero L.O.S, radius of packed bed TES tank size should be greater than 3m for Datça Peninsula for each length from 10 to 70 m. If the average mass flow rate of the compressor is increased for Datça, a 3 m radius may not be sufficient to obtain zero L.O.S. value due to the increase in the compressor mass flow rate for each length from 10 to 70 m.

In Figure 4.23, the relation between L.O.S and volume of the air storage cavern is presented for the same size of the TES (Length=40 m, R=1 m), assuming an initially full tank and 20 kg/s turbine mass flow rate.

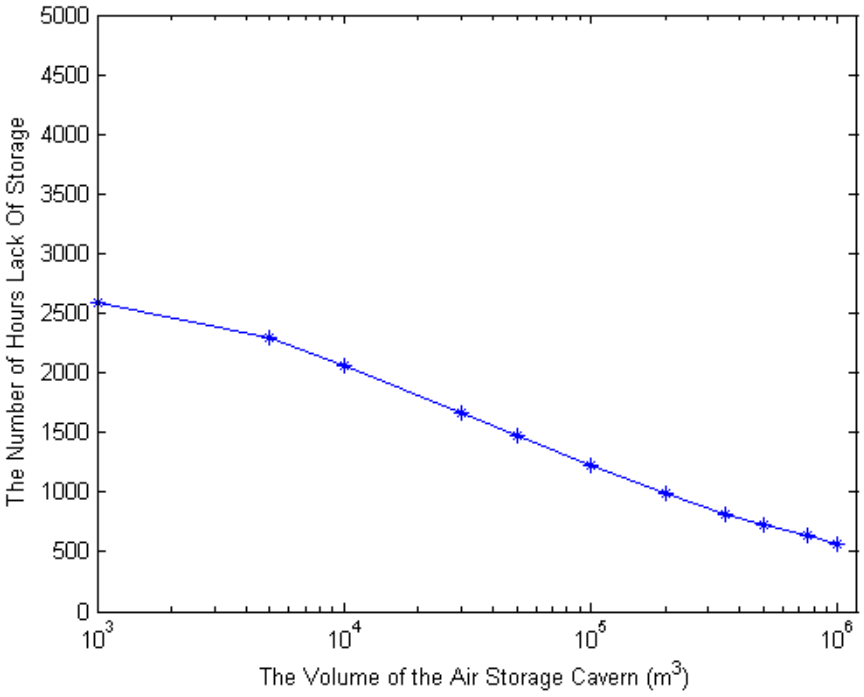

Figure 4.23 The number of hours that system cannot compress the air into the cavern vs. volume of the cavern

As can be seen from Figure 4.23, an increase in the volume of the air storage cavern decreases the number of hours that the pressure of the air leaving the TES is lower than the cavern pressure (L.O.S). As shown in Figure 4.20 and Figure 4.21, an increase in the volume of the cavern makes the pressure of the air in the cavern less sensitive to mass changes. Hence the pressure inside the cavern experiences smaller fluctuations for large volumes and larger fluctuations for small volumes.

4.6 The Assessment of System Design Parameters

In this section, the effects of variations in the system design parameters on the AA-CAES performance are investigated. In order to evaluate the effect of changing system parameters, "*the number of Hours that the System canNot Satisfy the Demand (HSNSD)"* performance metric is used.

4.6.1 Size of the Packed Bed Thermal Energy Storage System Effect

Size is an important parameter for a packed bed TES system for storing thermal energy. Hence, how variations in the length and radius of the TES tank impacts system performance is investigated in this section.

4.6.1.1 Changes in the Length of Packed Bed

In this section, the effect of changes in the TES tank length on system performance is calculated by using performance metric HSNSD. During the calculations, the radius of the tank is taken as 5.4 m, and it is held constant for each length. Initially the air storage cavern is assumed full and the volume is taken as 10^6 m^3, which is sufficient for preventing min.cap and L.O.S. The mass flow rate of turbine is 10 kg/s for this parametric study.

As it can be seen from Figure 4.24, if the length of thermal energy storage tank is 40 m, the system can satisfy total energy demand of 1144 of 4710 hours for Datça. This length gives the maximum performance of the TES tank to the system as it is supported in the selection of length and radius pairs for Datça in Section 4.4.1

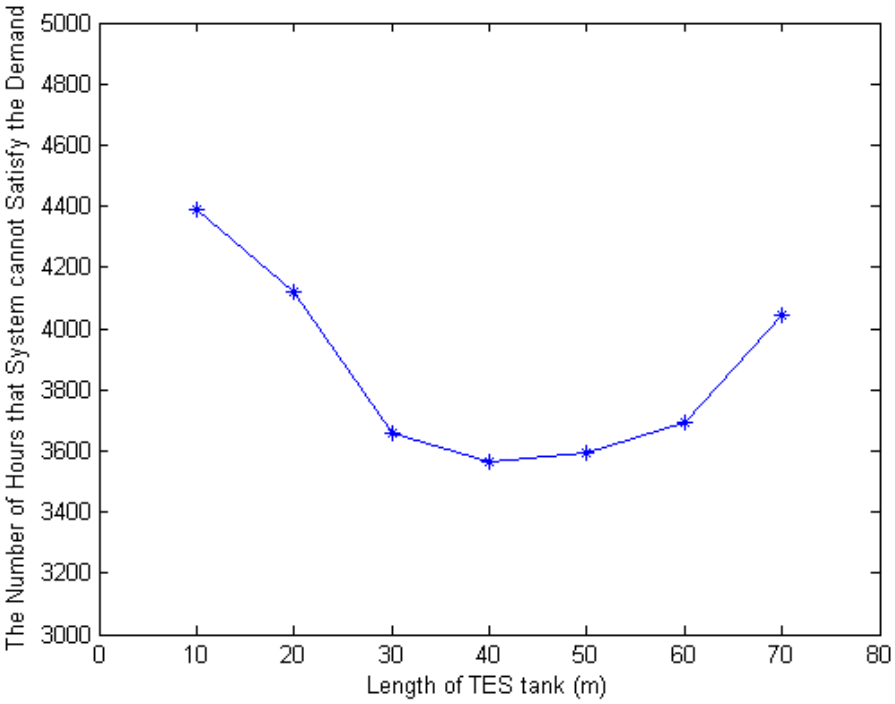

Figure 4.24 Hourly system not satisfy the demand vs. length of TES tank

4.6.1.2 Changes in the Radius of Packed Bed

In this section, the effect of increases in the thermal energy storage tank radius on system performance is calculated by using performance metric HSNSD. During the calculations, the length of the tank is taken as a constant 40m, and initially the air storage cavern is full and the storage volume is taken as 10^6 m^3. The mass flow rate of turbine is assumed as 10 kg/s.

As can be seen from Figure 4.25, if the radius of TES tank is 5.4 m, the system can satisfy total energy demand of 1144 hours for Datça. This radius gives the maximum performance of TES tank to the system as it was explained and supported in Section 4.4.1.

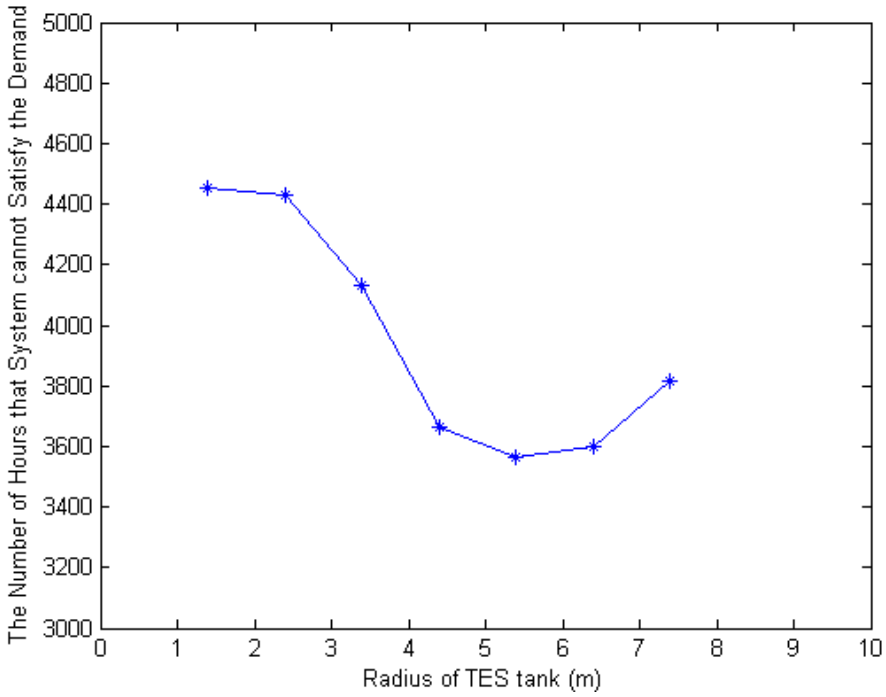

Figure 4.25 Hourly system not satisfy the demand vs. radius of TES tank

4.6.2 Changes in the Air Mass Flow Rate of the Turbine

In this section, the effect of changes in the air mass flow rate of the turbine on system performance is calculated by using performance metric HSNSD. During the calculations, the length and radius of the tank are taken as 40m, 5.4m respectively and remained constant across all mass flow rates. Initially air storage cavern is assumed full and the volume is taken as 10^6 m^3.

As it can be seen from Figure 4.26, increases in the turbine's mass flow rate of the air decreases the HSNSD value of the AA-CAES system until the mass flow rate is 13 kg/s. After the mass flow rate reaches to 13 kg/s, the volume of the cavern starts to reach the minimum capacity (min.cap) for certain periods within year 2009 and the turbine cannot operate due to the minimum cavern pressure limit. In addition, increasing the mass flow rate also decreases the average temperature of the air that goes to the turbine as shown in Figure 4.27 . Hence 13 kg/s is the best choice for Datça as the turbine's operating mass flow rate for the given size of the air storage

cavern and packed bed TES tank. Datça Peninsula energy demand can be completely satisfied 1545 of 4710 hours for which demand exceeds supply.

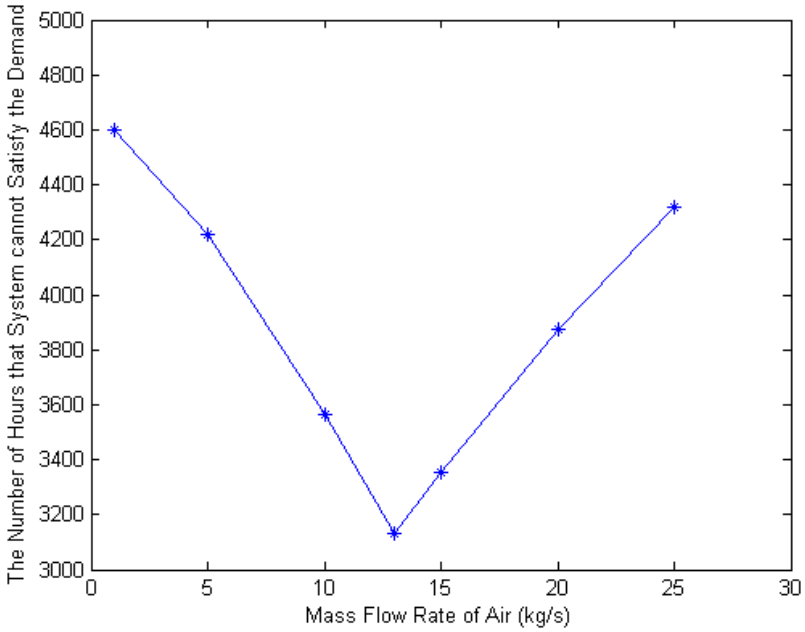

Figure 4.26 Hourly system not satisfy the demand vs. turbine air mass flow rate

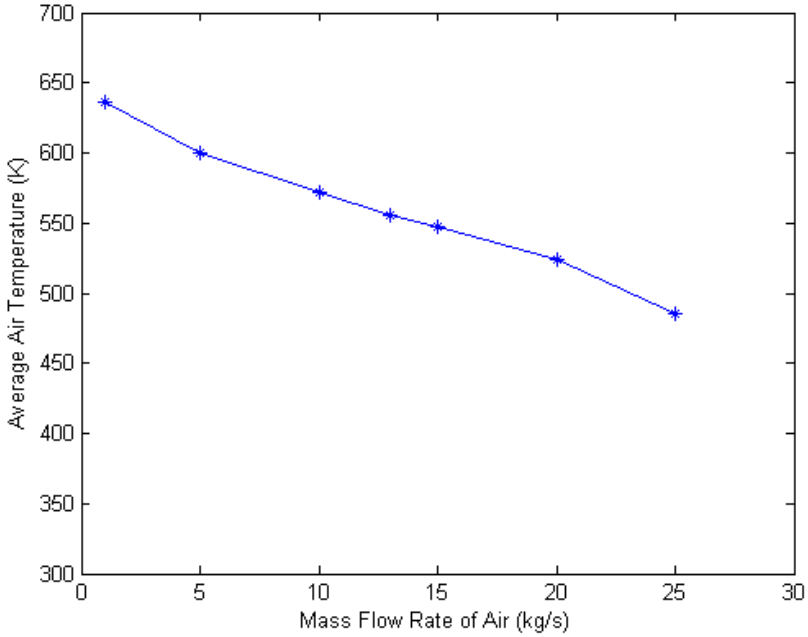

Figure 4.27 Average air temperatures vs. mass flow rate of air

4.6.3 Change in the Volume of Air Storage Cavern

In this section, the effect of changes in the air storage cavern volume on system performance is calculated by using the performance metric HSNSD. During the calculations, the length and radius of the tank are taken as 40 m and 5.4 m respectively and the mass flow rate of the air is assumed 13 kg/s constant for each volume. Each air storage volume is initially at full capacity.

In Section 4.4.2, the estimation of minimum air storage cavern volume is explained. In this section, smaller volumes of air storage cavern are also investigated in the parametric studies.

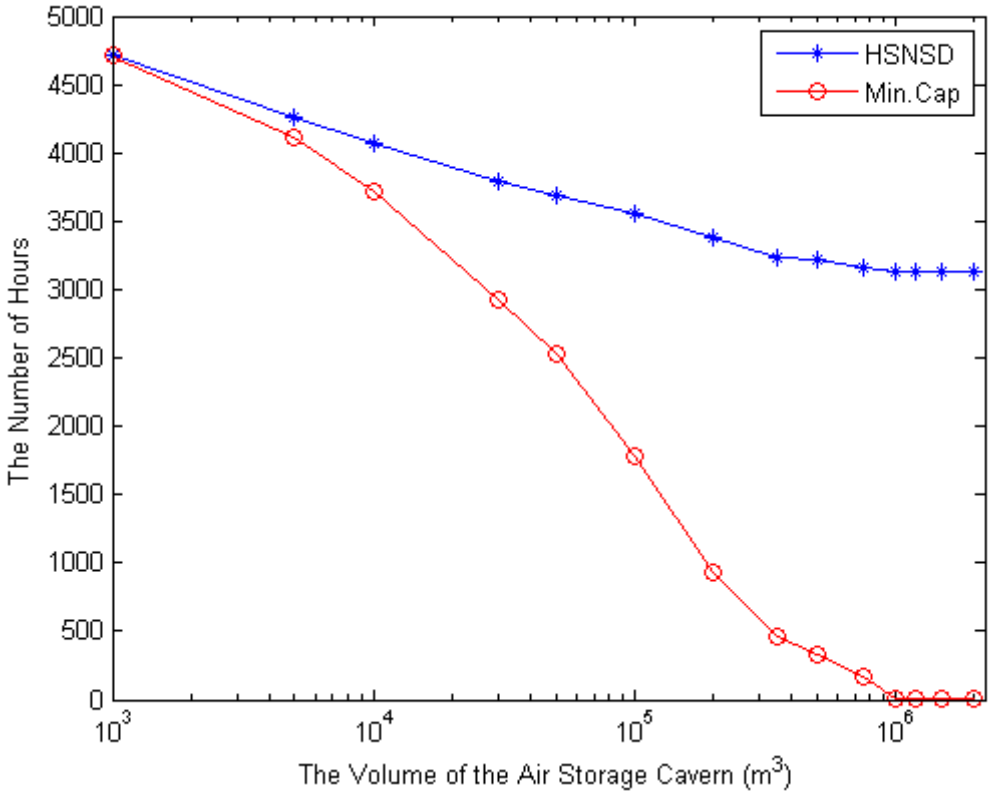

Figure 4.28 Hourly system not satisfy demand and min.cap vs. air storage cavern volume

As it can be seen from Figure 4.28, both HSNSD and min.cap values decrease with increasing air storage cavern volume until the volume of the cavern reaches 10^6 m^3. From this point, increases in the volume of the storage tank do not make change HSNSD value. The reason of this can be explained in the following way. The HSNSD value depends on both min.cap and size of the TES tank. After 10^6 m^3 volume, min.cap is started to be constant and take zero value and TES tank size has been already fixed at the beginning of this study. Hence, HSNSD value becomes constant after min.cap value is started to be constant. There is no need to increase the volume of the air storage cavern more than 10^6 m^3 for 13 kg/s mass flow rate and 40 m 5.4 m TES tank for Datça Peninsula AA-CAES system.

4.6.4 Changes in Minimum Turbine Operating Temperature

The inlet temperature of the air has a significant effect on the turbine efficiency and power production. In this study, the efficiency of the turbine is assumed independent of the air temperature and taken as a constant 0.8. The length and radius of the TES tank are taken as 40 m and 5.4 m respectively and mass flow rate of the air for turbine is assumed 13 kg/s. The volume of the air storage cavern is assumed 10^6 m^3 and initially full.

Generally there is an operating temperature range available for a turbine. If temperature of the air is increased or decreased beyond these operating temperature limits, the turbine may suffer from melting or freezing of the blades. In this study a minimum operating temperature limit for turbine is defined as 240 K for all calculations. If the minimum operating temperature of turbine is changed, how system is affected from this alteration is investigated by using HSNSD system performance metric. Other system parameters such as TES tank length, radius and, volume of the cavern are held constant in this study.

As is seen from Figure 4.29, if the turbine can be designed to withstand 233K, the minimum inlet air temperature can be accepted as approximately 550K; hence the temperature of air coming from the cavern can be acceptable to 550K to enter the

turbine after passing through the TES tank. Consequently, HSNSD value decreases as the turbine withstands lower temperature.

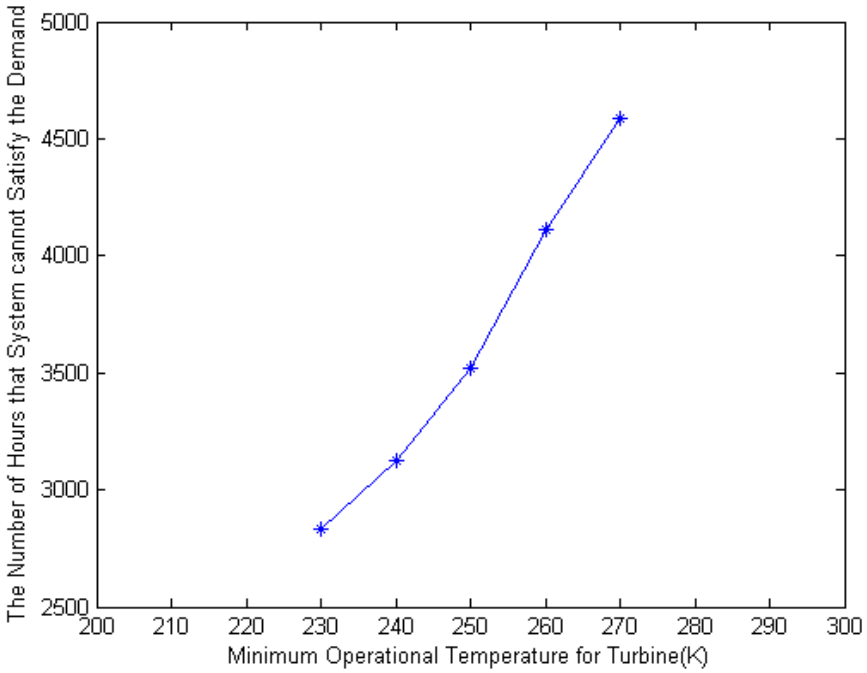

Figure 4.29 Hourly system not satisfy demand vs. minimum turbine operation temperature

4.6.5 Changes in the Initial Fullness of Air Storage Cavern

In this study, all calculations are done assuming the air storage cavern is initially full until this section. If the initial capacity of the air storage cavern is different from its maximum level, how the system performance is affected is investigated with the performance metric HSNSD value. For 10^6 m^3 cavern volume and 13 kg/s mass flow rate of turbine, the HSNSD values are presented in Figure 4.30

As can be seen from Figure 4.30, HSNSD is not changed up to a certain ratio of fullness. After that point, the pressure of the cavern starts to reach its minimum value in some hours of the year. Hence the HSNSD value starts to increase. For the given condition it does not make a strong difference whether initially the cavern is at 70 bar or 45 bar according to HSNSD values. However if the volume of the cavern, mass

flow rate of the air goes to turbine or demand and supply profile are changed, HSNSD value may be significantly affected.

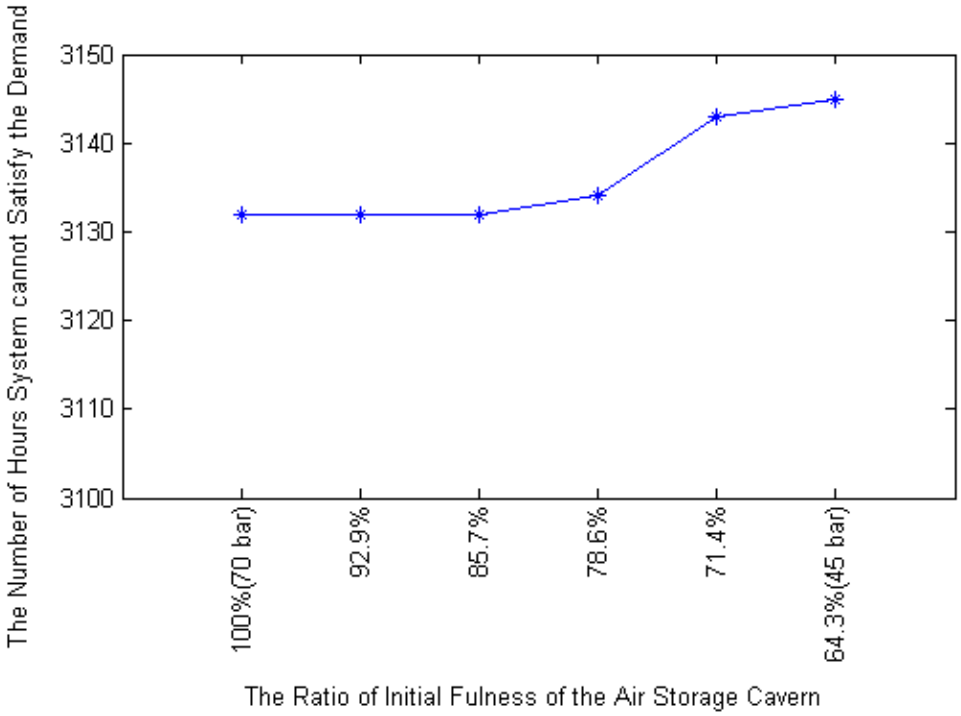

Figure 4.30 Hourly system not satisfy demand vs. initial fullness ratio of the tank

CHAPTER 5

SUMMARY AND CONCLUSIONS

5.1 Summary of the Study

In the Chapter 1, background information about the needs of renewable energy for the present and the future are given. Conceptual information about renewable energy storage, some types of renewable energy storage systems and, advanced adiabatic compressed air energy storage system (AA-CAES), which is the focus of the study, are introduced. Studies about AA-CAES system in the literature are explained and the main objectives of the study are given. Finally, the organization of the work is presented.

In the Chapter 2, the schematic of an AA-CAES model is given and system components are introduced. The governing equations for compression, expansion, heat storage and related assumptions based on these stages are presented. One of the most important parts of the study which is the verification of packed bed thermal energy storage model with existing experimental results is given. Finally, governing equations and related assumptions for air storage stage of AA-CAES model is introduced.

In the Chapter 3, a methodology for sizing and assessment of wind integrated AA-CAES system is introduced. First, a specific location where AA-CAES plant is built is determined and wind farms power production and energy demand profile belonging to the selected site are gathered. An hourly comparison between energy production and energy demand data is made and according to sign of a difference between demand and production, energy storage or energy consumption profiles are

obtained. By using these profiles, maximum cascade compression and expansion durations are determined. The sizing of packed bed thermal energy storage tank and minimum volume of the air storage cavern are calculated according to the maximum cascade compression and expansion periods respectively. System limitations such as maximum and minimum pressure limits of the cavern, and pressure loss in the packed bed TES are introduced under different conditions of the system. Finally several parametric studies about system design parameters with sizing are explained.

In the Chapter 4, the application of the sizing and assessment methodology of a wind integrated AA-CAES system is applied to the Datça Peninsula in Turkey. According to the maximum cascade compression and expansion periods, different sizes of the packed bed thermal energy storage tanks are obtained and evaluated. According to selected TES tank size, minimum cavern volume requirement is obtained. Several parametric studies about system design parameters and limits with sizing are done and assessments of these parametric studies are given.

5.2 Conclusions

In the application of methodology to Datça Peninsula, 7 different length and radius pairs are presented to evaluate their performance. Except L=10m and R=10.2m, any of the 6 cases yields similar performance and the final size may be selected based on other considerations such as costs or size limitations in terms of length and radius. Without considering cost and size limitations of the TES tank, 40 m length and 5.4 m radius of TES tank is the reasonable choice among the other TES size pairs given in Chapter 4 by evaluating the only system performance. In order to consume stored wind farm's excess energy, a minimum 2.1×10^5 m^3 volume of the cavern should be needed to store the air within the pressure limits according to 40 m length and 5.4 m radius. For these sizes, the sizing ratio (R_s) is calculated as 5×10^{-3}. For the sizing ratio value which is smaller than 5×10^{-3}, the performance of the system is limited by the size of TES tank. In the same way, for the sizing ratio value which is greater than 5×10^{-3}, the performance of the system is limited by the air storage cavern. If the

volume of the air storage cavern is approximately 10^6 m^3 air storage cavern does not affected the pressure limits of the system for the mass flow rate of 13 kg/s and if the cavern is initially full. The mass flow rate of the turbines for Datça should be 13 kg/s at most in order to get highest efficiency of the system. For this design 1545 out of 4710 hours when the Datça Peninsula demand exceeds the supply from the wind farm is totally met under these conditions. For all expansion periods, the total power production from AA-CAES is the 2.065 x10^4 GWh for the conditions that are: initially full cavern, 13 kg/s turbine mass flow rate and 40m length 5.4 m radius TES tank. Total excess energy in the compression period is calculated 3.26 x10^4 GWh. As a result of this, the round trip efficiency is calculated as 63.35% which has the similar round trip efficiency compared to other concept AA-CAES systems (60%-70%) [39], [40] from equation (5.1.1) for a one year period.

$$\eta_{RTE} = \frac{Turbine\ Energy\ Output}{Compressor\ Energy\ Input} \tag{5.1.1}$$

In Table 10, the system performance results are given.

Table 10 System Performance Results

Size of the TES Tank	L=40 m, R=5.4 m
Minimum Volume Requirement	2.1x10^5 m^3
Mass Flow Rate of the System	13 kg/s
Total Power Production	2.065x10^4 GWh
The Number of Hours Demand is Completely Satisfied	1545 hours
Initial Fullness of the Cavern	100%
Round Trip Efficiency	63.3%

5.3 Future Works

In this study, a methodology developed for sizing and assessing a wind integrated advanced adiabatic compressed air energy storage system (AA-CAES). The following tasks can be applied to this system to enlarge the area of usage and investigate possible methods to increase the system performance.

- An application of AA-CAES system to the grid according to level of the price of the electricity.
- An application of AA-CAES system to concentrating solar power systems.
- An application of AA-CAES system for combining both wind and solar powers.
- An application of two compressors, two turbines and two heat storage tank to investigate system performance.
- An application of phase change thermal energy storage materials to AA-CAES system.
- Determine TES size according to a parameter other than the maximum cascade compression or expansion period.
- Determine the universal Rs value that can be applied to every AA-CAES systems to predict the system performance.

REFERENCES

[1] "World Energy Outlook 2012," pp. 1–3, 2012.

[2] "BP Energy Outlook 2030," vol. 0383, no. January, pp. 16–17, 2012.

[3] T. Barker, "Climate Change 2007 : An Assessment of the Intergovernmental Panel on Climate Change," no. November, p. 44, 2007.

[4] TUBITAK, "Türkiye'de Termik Santrallar ve Sanayi Tesislerinden Gelen Karbondioksit Emisyonu Envanterinin Çıkartılması ve Karbondioksitin Yeraltı Jeolojik Ortamlarda Depolanma Potansiyelinin Belirlenmesi," 2009. [Online]. Available: http://www.eie.gov.tr/projeler/projeler_tanimli4.aspx#top [Accessed: 24-Jan-2014].

[5] H. Saygın and F. Çetin, "Recent Developments in Renewable Energy Policies of Turkey," p. 2, 2009.

[6] K. Y. C. Cheung, S. T. H. Cheung, R. G. N. De Silva, and J. J. Woo, "Large-Scale Energy Storage Systems," p. 3, 2003.

[7] H. Ibrahim, A. Ilinca, and J. Perron, "Energy Storage Systems—Characteristics and Comparisons," *Renew. Sustain. Energy Rev.*, vol. 12, no. 5, p. 1223, Jun. 2008.

[8] S. D. Lim, A. P. Mazzoleni, J. Park, P. I. Ro, B. Quinlan, and N. Carolina, "Conceptual design of ocean compressed air energy storage system," 2012.

[9] F. D. S. Steta, "Modeling of an Advanced Adiabatic Compressed Air Energy Storage Unit and an Optimal Model-Based Operation Strategy for its Integration into Power Markets," Swiss Federal Institute of Technology (ETH) Zurich, 2010.

[10] A. Sharma, V. V. Tyagi, C. R. Chen, and D. Buddhi, “Review on thermal energy storage with phase change materials and applications,” *Renew. Sustain. Energy Rev.*, vol. 13, no. 2, pp. 318–345, Feb. 2009.

[11] M. Haider and H. Walter, “High temperature thermal energy storage systems based on latent and thermo-chemical heat storage,” no. 1029166, 2011.

[12] “Energy Storage: Compressed Air (CAES).” [Online]. Available: http://climatetechwiki.org/technology/jiqweb-caes. [Accessed: 05-Jan-2014].

[13] S. LEMOFOUE, “Investigation and optimisation of hybrid electricity storage systems based on compressed air and supercapacitors,” vol. 3628, p. 11, 2006.

[14] Y. M. Kim, “Novel Concepts of Compressed Air Energy Storage and Thermo-electric Energy Storage,” vol. 5525, 2012.

[15] Y. Zhang, K. Yang, X. Li, and J. Xu, “The thermodynamic effect of thermal energy storage on compressed air energy storage system,” *Renew. Energy*, vol. 50, pp. 227–235, Feb. 2013.

[16] S. Zunft, C. Jakiel, M. Koller, and C. Bullough, “Adiabatic Compressed Air Energy Storage for the Grid Integration of Wind Power,” no. October, pp. 26–28, 2006.

[17] C. Bullough, C. Gatzen, C. Jakiel, M. Koller, A. Nowi, S. Zunft, M. A. N. T. Ag, and D.- Oberhausen, “Advanced Adiabatic Compressed Air Energy Storage for the Integration of Wind Energy,” no. November, pp. 22–25, 2004.

[18] M. Beeman, “Design and Evaluation of an Advanced Adiabatic Compressed Air Energy Storage System at the Michigan-Utah Mine,” 2010.

[19] Y.-M. Kim, J.-H. Lee, S.-J. Kim, and D. Favrat, “Potential and Evolution of Compressed Air Energy Storage: Energy and Exergy Analyses,” *Entropy*, vol. 14, no. 12, pp. 1501–1521, Aug. 2012.

[20] G. Grazzini and A. Milazzo, “A Thermodynamic Analysis of Multistage Adiabatic CAES,” *Proc. IEEE*, vol. 100, no. 2, pp. 461–472, Feb. 2012.

[21] M. A. Riaz, “Feasibility of compressed air energy storage to store wind on monthly and daily basis,” 2010.

[22] L. Doerte, S. W. Tamme, R. Wörner, and A. Zunft, “特约文章 Advances in thermal energy storage development at the German Aerospace Center (DLR),” no. l, 2012.

[23] S. Zunft, R. Tamme, U. Hartwig, and A. Ternedde, “Thermal Energy Storage Technologies for Advanced Adiabatic Compressed Air Energy Storages (AA-CAES),” in *STORE Storage for Renewable Energies AixenProvence France 2021102003*, 2003.

[24] M. Klafki, S. Zunft, S. Pazzi, and P. Moser, “Status and Technical Challenges of Advanced Compressed Air Energy Storage (CAES) Technology Motivation for Large-Scale Energy Storage,” pp. 1–8, 2009.

[25] F. Schmidt and J. Willmott, *Thermal Energy Storage and Regeneration*. .

[26] B. Xu, P.-W. Li, and C. L. Chan, “Extending the validity of lumped capacitance method for large Biot number in thermal storage application,” *Sol. Energy*, vol. 86, no. 6, pp. 1709–1724, Jun. 2012.

[27] M. Tesfay and M. Venkatesan, “Simulation of Thermocline Thermal Energy Storage System Using C,” vol. 3, no. 2, pp. 354–364, 2013.

[28] K. G. Allen, “Performance characteristics of packed bed thermal energy storage for solar thermal power plants by,” no. March, 2010.

[29] W. Karaki, P. Li, J. Van Lew, M. M. Valmiki, C. Chan, and J. Stephens, “Experimental Investigation of Thermal Storage Processes in a Thermocline Storage Tank,” pp. 1–8, 2011.

[30] “Xceltherm-600 Synthetic Oil Properties.” [Online]. Available: http://www.radcoind.com/products/industrial-energy/xceltherm-600 engineering/. [Accessed: 08-Feb-2014].

[31] R. S. Subramanian, “Flow through Packed Beds and Fluidized Beds,” pp. 1–6, 2001.

[32] “Air Liquide Gas Encyclopedia.” [Online]. Available: http://encyclopedia.airliquide.com/Encyclopedia.asp?GasID=73. [Accessed: 06-Jan-2014].

[33] R. E. Sonntag, C. Borgnakke, and G. J. Van Wylen, *Fundamentals of thermodynamics*. 2009, pp. 1–14.

[34] “Huntorf Air Storage Gas Turbine Power Plant.” BROWN BOVERI & CIE.

[35] R. D. Moutoux, “Wind Integrated Compressed Air Energy Storage In Colorado,” 2007.

[36] “Karst ve Mağara,” 2012. [Online]. Available: http://www.mta.gov.tr/v2.0/daire-baskanliklari/jed. [Accessed: 08-Feb-2014].

[37] “Enercon Product Overview,” pp. 2–24.

[38] “Dares Windfarm”. [Online]. Available: http://www.demirer.com.tr/santral/dares/indexeng.html. [Accessed: 08-Feb-2014].

[39] M. Budt, D. Wolf, and R. Span, “Modeling a Low-temperature Compressed Air Energy Storage with Modelica,” pp. 791–800, Nov. 2012.

[40] L. Nielsen, “Dynamic Simulation of an Innovative Compressed Air Energy Storage Plant - Detailed Modelling of the Storage Cavern,” vol. 4, no. 8, 2009.

APPENDIX A

METHODOLOGY FOR SIZING TES TANK FLOW CHART

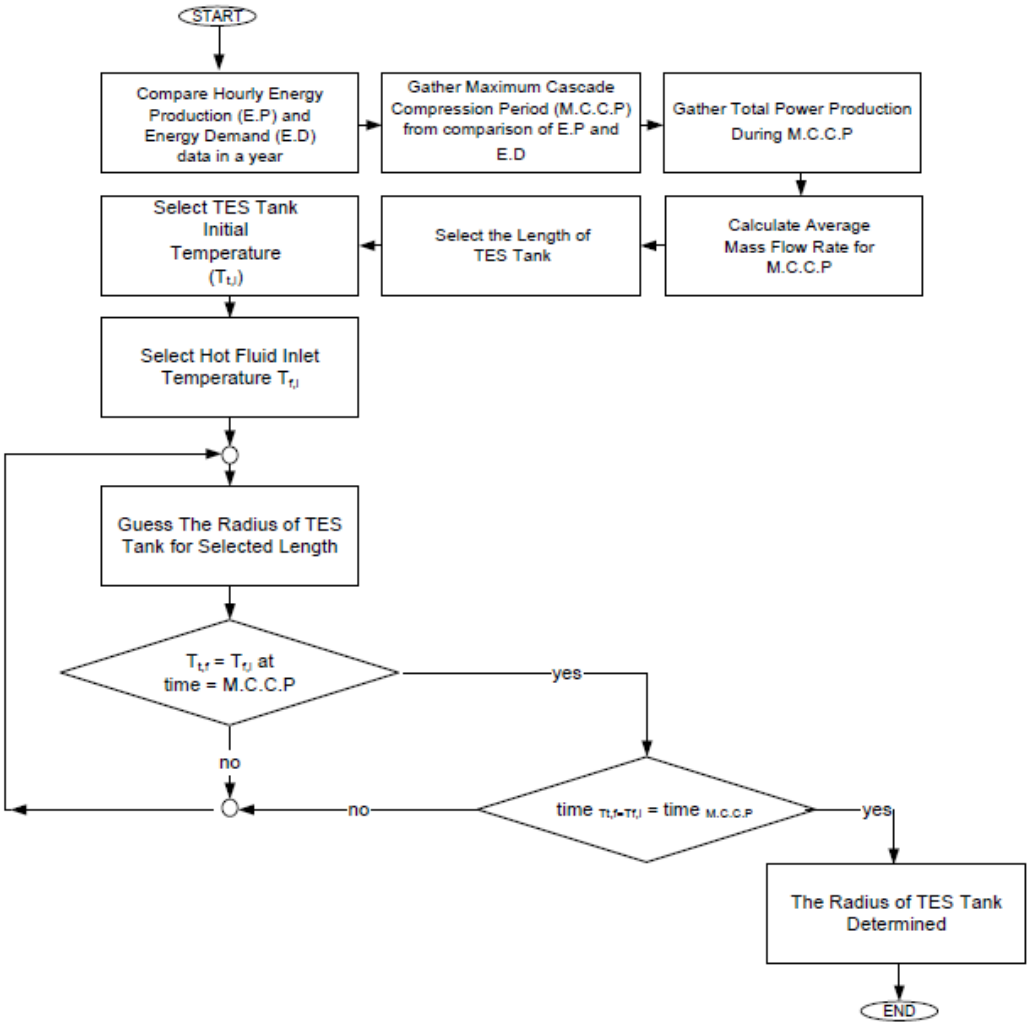

Figure A.1 Sizing TES tank flow chart

APPENDIX B

METHODOLOGY FOR SIZING MINIMUM VOLUME OF THE AIR STORAGE CAVERN FLOW CHART

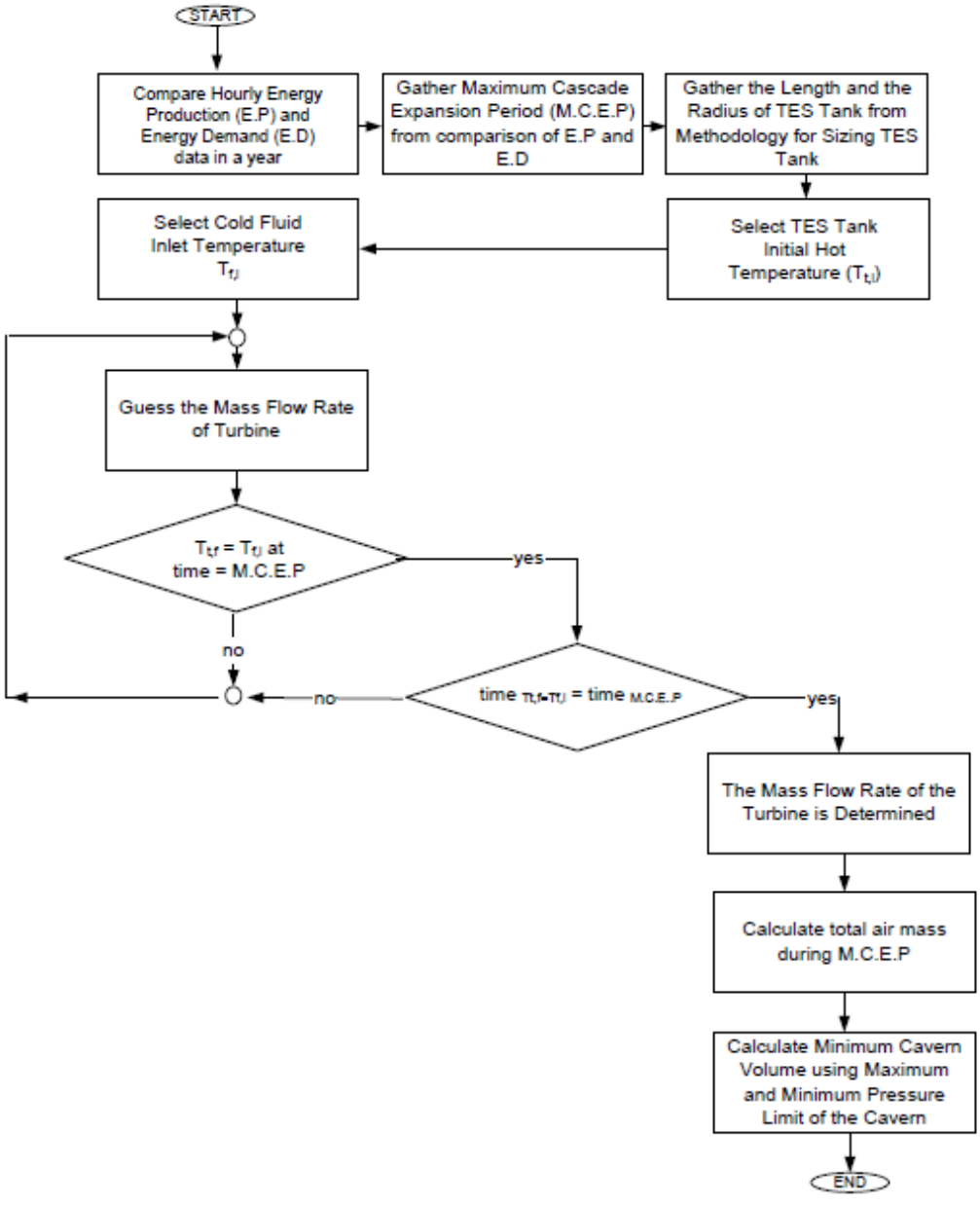

Figure B.1 Sizing minimum volume of air storage cavern flow chart

APPENDIX C

METHODOLOGY FOR ASSESSING AA-CAES SYSTEM FLOW CHART

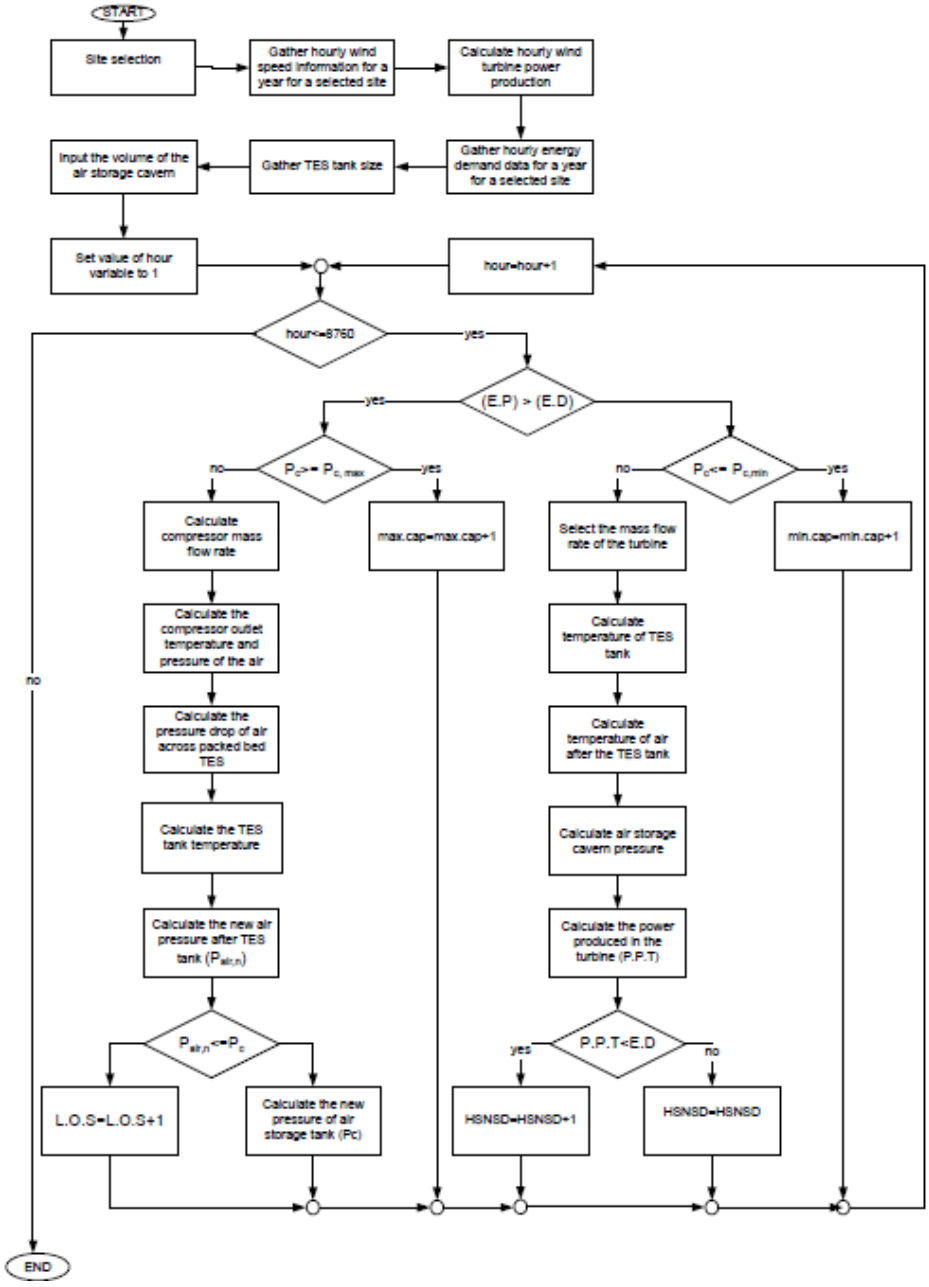

Figure C.1 General assessing methodology for AA-CAES